

Modelling degradation of medical implants made of biodegradable polymers

Thesis submitted for the degree of Doctor of
Philosophy

At the University of Leicester

by

Xinpu Chen

Department of Engineering

University of Leicester

12/27/2016

Abstract

THESIS:

Modelling degradation of medical implants made of biodegradable polymers

AUTHOR:

Xinpu Chen

Bioresorbable polymer is widely used inside the human body as resorbable medical devices such as fixation screws, plates, sutures, and tissue engineering scaffolds. The most important feature for such devices is that they ‘disappear’ after serving the temporary function that is surgically required. The current design for these devices is still based on trial and error. The degrading process is complex and many factors were involved. This makes the design optimisation very hard. The degradation rate for such devices varies from months to years, making the experimental work expensive and time-consuming. Mathematical modelling could be used in the early stages of designing, and would give an indication of certain degradation behaviours without doing experiments first. The existing mathematical models developed by the Leicester group were used to successfully capture the trend of average molecular weight, degree of crystallisation, and Young’s modulus. However, the previous models still have many gaps to fully capture the underlying chemistry and physics of polymer degradation. Some of the models are also over-complicated to be used in practical designs. This thesis presents several new developments and simplifications to the previous models. These include the separation of long and short polymer chains in the rate equation for polymer chain scission, adding the effect of water diffusion and providing a list of analytical solutions for simple but commonly used situations. A complete set of governing equations are provided by integrating the new rate equation with previously developed equations for crystallization, oligomer diffusion and short chain diffusion. A major issue in the development of biodegradable devices is that it is extremely time consuming and expensive to obtain experimental data for degradation rate because the degradation can take up to several years. The thesis presents a demonstration on how the mathematical model, together with the finite element method, can be used to project degradation rate from one device, for which experimental data are available, to another which is under design. Finally the effective cavity theory for change in Young's modulus and degradation detection using mode analysis, previously developed by the Leicester group, are simplified to make them much more straightforward to use by end users.

Acknowledgements

I would like to use this opportunity to thank my supervisor, Jingzhe Pan. He provided all the help I needed even through the most inconvenient times. I had many problems during this PhD study, and I am grateful that he did not give up on me and still trusted in me.

Also, I would like to thank my girlfriend who helped me through the most challenging times and for being with me when most needed.

Contents

Abstract	i
Acknowledgements	ii
List of Figures	vii
List of Tables	xii
Chapter 1: Introduction	1
1.1 Biodegradable polymers	1
1.2 Medical implants made of biodegradable polymers.....	2
1.3 The need for computer modelling in implant design.....	4
Chapter 2: Mechanisms of degradation of biodegradable implants.....	5
2.1 Factors that control the degradation rate	5
2.2 Hydrolysis reaction.....	6
2.3 Crystallinity	7
2.4 Oligomer production	8
2.5 Non-uniform degradation.....	9
2.6 Non-uniform Young's modulus distribution.....	10
Chapter 3: A review of mathematical models for polymer degradation.....	12
3.1 Existing models for the degradation of biodegradation polymers.....	12
3.2 Previous work on modelling by the Leicester group.....	13
3.3 Remaining issues in modelling biomedical device degradation.....	16
3.4 Purpose and structure of this thesis	17
Chapter 4: Master equations for amorphous polymers, analytical solutions and a parametric study of the mathematical model	19
4.1 Degradation equations for amorphous polymers.....	19
4.1.1 Previous mathematical models developed by the Leicester group	19
4.1.2 Further development to the equation of degradation rate	23
4.2 Analytical solutions and cross-checking with numerical solutions.....	26
4.2.1 Analytical solutions	26

4.2.2 Numerical solution of the master equation	30
4.2.3 Cross-checking analytical solutions with the corresponding numerical solutions	34
4.3 A parameterisation study of the master equation	38
4.3.1 Effect of \bar{k}_2/k_1	38
4.3.2 Effect of \bar{C}_0	40
4.3.3 Effect of α and β	41
4.3.4 Effect of χ_1 and χ_2	43
4.4 Conclusions	46
Chapter 5: Degradation model including crystallisation, oligomer diffusion and water diffusion	48
5.1 Introduction	48
5.2 Degradation equations for semi-crystalline polymers	49
5.2.1 Equations for degree of crystallinity	49
5.2.2 Equations for rate of chain scission	50
5.2.3 Equations for number-average molecular weight	52
5.3 Diffusion equations and a collection of governing equations for semi-crystalline polymers	53
5.3.1 Diffusion equation for short chains	54
5.3.2 Collection of the governing equations for semi-crystalline polymers	57
5.4 Non-dimensionalisation and degradation map	61
5.4.1 Non-dimensionalisation of governing equations	62
5.4.2 Degradation map	64
5.4.3 Effect of other factors on the degradation map	68
5.5 Conclusion	72
Chapter 6: Cross-reading of the degradation rates of different devices made of the same polymer and the effect of water diffusion	73
6.1 The need for a cross-reading method	73

6.2 A finite element model for interference screw	75
6.3 Cross-reading with a coronary stent	82
6.4 Effect of water diffusion.....	93
6.4.1 Degradation equations for semi-crystalline polymers adding in water diffusion.....	93
6.4.2 Effect of water diffusion for 2D square plate	95
6.4.3 A finite element model for interference screw with water diffusion counted	106
6.5 Conclusion.....	115
Chapter 7: A simplified Effective Cavity Theory	116
7.1 Introduction	116
7.2 Previous Effective Cavity Theory	117
7.2.1 Numerical model by Gleadall, et al. (2015)	117
7.2.2 Analytical model by Samami (2016).....	121
7.3 Simplified Effective Cavity Theory	123
7.3.1 Analysis the Young's modulus change due to chain scission using the simplified model	124
7.3.2 Effect of crystallinity on Young's modulus using the simplified model.	126
7.3.3 Analysing Young's modulus change for semi-crystalline polymer during degradation using the simplified model.....	128
7.4 Using experimental data to check the reliability of the Simplified model.....	130
7.5 A full equation list of the mathematical model for polymer degradation adding in a simulation of mechanical properties.....	134
7.6 Conclusion.....	136
Chapter 8: Detection of degradation using vibration analysis	137
8.1 Introduction	137
8.2 Vibration analysis and damage detection.....	138
8.3 Detection of degradation for a plate model using beam element study	139

8.3.1 The plate model has been used	139
8.3.2 1D beam element model for degradation detection	141
8.4 Local degradation detection – using a 3D cube as a unit of biodegradable implant device	147
8.5 Conclusions	156
Chapter 9: Major conclusion and future work	158
9.1 Conclusion	158
9.2 Further work	160
References	163
Appendix	169

List of Figures

Figure 1: Flow chart of C++ program for calculating numerical solution.....	33
Figure 2: Normalised average molecular weight reduction trend during degradation for: (A) equation (4-26); (B) equation (4-34); and (C) numerical integration of equation (4-22).....	35
Figure 3: Compare analytical solution with numerical solution for special cases: (a) pure non-catalysed hydrolysis reaction for early stage; (b) pure non-catalysed hydrolysis reaction; (c) pure auto-catalysed hydrolysis reaction for early stage; (d) pure auto-catalysed hydrolysis reaction.	37
Figure 4: Average molecular weight reduction trend during degradation calculated using different parameters.....	39
Figure 5: Effect of \bar{C}_0 on the degradation behaviour for pure autocatalytic hydrolysis in cases (A) $\bar{C}_0 = 10^{-10}C_{chain^0}/C_{e^0}$, (B) $\bar{C}_0 = 0.1C_{chain^0}/C_{e^0}$, (C) $\bar{C}_0 = 0.5C_{chain^0}/C_{e^0}$, (D) $\bar{C}_0 = C_{chain^0}/C_{e^0}$ and (E) $\bar{C}_0 = 0.01$. $k_1 = 0$ and $\bar{k}_2 = 1$	40
Figure 6: Calculated average molecular weight reduction trend during degradation for two individual sets of parameters	42
Figure 7: Calculated short chains production by chain scissions during degradation for two individual sets of parameters	42
Figure 8: Calculated average molecular weight reduction trend during degradation for two individual sets of parameters showing they give the same prediction for samples with a thickness of 0.3mm.	44
Figure 9: Calculated average molecular weight reduction trend during degradation for two individual sets of parameters identical to those used in Fig. 8 showing they give different predictions for samples with a thickness of 2mm.	44
Figure 10: Short chain diffusion in a plate showing distributions of short chain concentration over thickness of the plate at different stages of degradation.	55
Figure 11: Removing or depositing short chains due to difference in the diffusion flux J on either sides of a small section.	56
Figure 12: Molecular weight (vertical axis) averaged across the plate at $\bar{t} = 27$ as a function of $\bar{D}_{polymer}$ (horizontal axis). $\bar{k}_1 = 0.001$	73
Figure 14: Degradation map showing different behaviours of degradation of an infinitively large plate controlled by $\bar{D}_{polymer}$ and \bar{k}_1 . Other parameters used in the	

calculation are $\alpha = 1$, $\beta = 1$, $\chi_1 = 0$, $\chi_2 = 1$, $m = 4$, $n = 0.5$, $\overline{D}_{pore} = 1000 \overline{D}_{polymer}$,
 $N_{dp0} = 2307$ and $C_{ol0} = 0$ 67

Figure 15: Effect of crystallisation on degradation map. The solid lines show the four zones for semi-crystalline polymers while the dash lines are for amorphous polymers..... 69

Figure 16: Degradation map obtained using $\alpha = 28$ and $\beta = 2$ with all other parameters identical to that for Fig. 14. 70

Figure 17: Degradation map for solid cylinder using the same parameters as those used for the large plate in Fig. 14..... 71

Figure 18: A cross-sectional view of the interference screw with mesh (length unit mm). 76

Figure 19: Interference screw – average molecular weight distribution at two different degradation times: (a) week 7, (b) week 28. 77

Figure 20: Interference screw – degree of crystallinity distribution at two different degradation times: (a) week 7, (b) week 28. 78

Figure 21: Using a mathematical model to fit interference screw experimental data of (a) molecular weight and (b) degree of crystallinity. 79

Figure 22: Using mathematical model to fit (a) average molecular weight and (b) degree of crystallinity screw experimental data for all parameters listed in Table 1 Cases A, B, C, and D, respectively. 81

Figure 23: Biomedical stent (a) before deformation, (b) after deformation, (c) Molecular weight distribution of the whole stent, at week 16 using parameter listed in Table 1 Case D (all length units in mm) (COMSOL database was applied to obtain the geometry).. 85

Figure 24: Partial mesh of the stent highlighted part in Fig. 23 (c) (all length units in mm).. 86

Figure 25: Distributions of 1/12 of the stent viewed along longitudinal axis for (a) average molecular weight and (b) degree of crystallinity under different degradation times: weeks 5 and 15, which used the parameters listed in Table 1 Case D. 88

Figure 26: Distributions of 1/12 of the stent viewed along longitudinal axis for (a) average molecular weight and (b) degree of crystallinity under different degradation times: weeks 8 and 32, which used the parameters listed in Table 1 Case C. 90

Figure 27: Predicted biomedical stent degradation behaviour (a) average molecular weight (b) degree of crystallinity, for different sets of parameters listed in Table 1.	92
Figure 28: 2D square plate model with side lengths of 1mm.	95
Figure 29: Average molecular weight and water uptake distribution for 2D plate with side length 1mm.	99
Figure 30: Average molecular weight and water uptake distribution for 2D plate with side length 5mm.	102
Figure 31: Normalised average molecular weight reduction with time for the 2D plate with and without counting the effect of water diffusion with side length of (a) 1mm and (b) 5mm.	103
Figure 32: Water diffusion against time for 2D plate with side length of (a) 1mm and (b) 5mm.	105
Figure 33: (a) average molecular weight (b) degree of crystalline and (c) water uptake distribution for the interference screw model counting the effect of water diffusion at weeks 7 and 28.	109
Figure 34: Counting water diffusion in the interference screw model and comparing the result for (a) average molecular weight and (b) degree of crystallinity.	111
Figure 35: Best fitting of the mathematical model counting water diffusion for (a) average molecule weight and (b) degree of crystallinity.	113
Figure 36: Average molecule weight reduction for storage assuming the atmosphere contains 0.5% to 4% of water.	114
Figure 37: Apply individual scissions to the amorphous polymer. Shape of the effective cavity suggested by Gleadall, et al. (2015) in the previous Effective Cavity Theory	118
Figure 38: Use FEA model to analysis the effect of the effective cavity to Young's modulus in cubic matrix by Gleadall, et al. (2015) (length unit in nm).	119
Figure 39: Use FEA model to analysis the effect of changing in crystallinity to Young's modulus (Gleadall, et al., 2015) (length unit in nm).	120
Figure 40: Semi-crystalline polymer matrix which contains effective cavity and crystal particle (Gleadall, et al., 2015).	121
Figure 42: Semi-crystalline polymer which contains two inhomogeneities particles: effective cavity and crystal (Samami, et al., 2016).	122
Figure 43: The FEA model with mesh for a spherical effective cavity in a cubic matrix which stand for amorphous polymer (length unit in nm).	125

Figure 44: Effect of the volume fraction of spherical effective cavity on normalised Young's modulus during degradation with a best fit of exponential line	126
Figure 45: Use FEA model to analysis changing in crystallinity to Young's modulus in cubic matrix by Gleadall, et al. (2015) (length unit in nm).	127
Figure 46: Effect of the volume fraction of crystal particle on normalised Young's modulus during degradation with a best fit of exponential line (Gleadall, et al., 2015)	128
Figure 49: Five degradation experimental data listed in Table 2 were used to check the reliability of the simplified Effective Cavity Theory, previous model fitting was also included: (a) Weir, et al. (2004), (b) Tsuji, et al. (2000), (c) and (d) Duek, et al. (1999), and (d) Lam, et al. (1994).....	133
Figure 50: (a) 2D plate used in Samami's paper for degradation detection model (b) Young's modulus distribution for the 2D plate during degradation along centre x direction (Samami and Pan, 2015)	140
Figure 51: 1D beam modal of the degrading plate.....	141
Figure 52: First mode shape achieved from beam element study using commercial software COMSOL (a) normalised mode shape displacement, (b) normalised curvature, (c) normalised absolute difference between the intact beam mode shape curvature (week 0) and degraded beam mode shape curvature, along beam shown in Fig. 51 at various degradation times.	143
Figure 53: Check convergence of the model using (a) normalised curvature at week 0 and week 12 (b) normalised absolute difference of curvature at week 12, with 100 and 600 elements respectively.	145
Figure 54: Maximum distinction of normalised absolute curvature difference against maximum percentage drop of Young's modulus from the surface to the centre of the plate on different degradation stages at weeks 3, 6, 9, and 12.....	146
Figure 55: (a) a 3D cube model (b) a centre part of the cube model (c) convert the centre part of the cube into a 1D beam model.	147
Figure 56: Normalised average molecule weight reduction over time for the whole cube model.	148
Figure 57: Distribution of normalised average molecular weight over the cross-section of the cube at week 20.	149

Figure 58: Distributions of (a) normalised average molecule weight, (b) number of scissions, (c) volume degree of crystallinity, (d) Young's modulus, along the beam shown in Fig. 55 at different degradation times..... 150

Figure 59: First mode shape of (a) normalised mode shape displacement, (b) normalised curvature, (c) normalised absolute difference between the intact beam mode shape curvature (week 0) and degraded beam mode shape curvature, along beam showed in Fig. 55 at various degradation times. 152

Figure 60: First mode shape of normalized absolute difference between the intact beam mode shape curvature (week 0) and degraded beam mode shape curvature at varies degradation times and when diffusion coefficient is 10^{-22} 153

Figure 61: Max distinction of normalized absolute curvature difference against max percentage drop of Young's modulus from the surface to centre of the plate at different degradation times for diffusion coefficient taking as 10^{-14} m^2/s and 10^{-22} m^2/s respectively, dish line and solid line are the best fitting straight lines for each set of data. 155

List of Tables

Table 1: Four sets of parameters that could fit the same interference screw experimental data.	80
Table 2: Experimental set-ups, initial measurements, and calculations for the five individual sets of experimental data that were used in the simplified Effective Cavity Theory.	130
Table 3: Parameters for the molecular weight distribution calculation for the cube model.....	148

Chapter 1: Introduction

This PhD thesis provides studies of mathematical modelling of biodegradable polymer degradation behaviours. This chapter will provide a brief background of such biodegradable polymers and their real-world applications.

1.1 Biodegradable polymers

Biodegradable polymers have been used widely inside the human body for the last few decades. It is predicted that the usage of these devices in the future will increase tremendously. The characteristic of not needing a second surgery is attractive enough, not to mention its good mechanical properties, fantastic biocompatibility, and thermo-elasticity. Currently, biodegradable polymer such as polyglycolide (PGA), polylactide (PLA), and their copolymers (PLGA) are the most popular ones. Each of these polymers has unique performance attributes and they have been used in different fields depending on these distinctive characteristics. PGA is the simplest linear, aliphatic polyester. It has the fastest average degradation rate among the above commonly used polymers. The average degradation time is between four and six months (Miller, et al., 1977). It is a semi-crystalline polymer containing 45% to 55% of initial volume degree of crystallinity. The melting point is between 224 °C and 226 °C and glass transition temperature is between 36 °C and 40 °C (Miller, et al., 1977). Initially, PGA was introduced to medical use in the 1960s as sutures. Shortly after that, PLA, a synthetic degradable material with more hydrophobic and a slower degradation rate, was brought into the market. Two particular forms of PLA, poly(L-lactic acid) or PLLA and poly(D-lactic acid) or PDLA, were suggested to be useful in medical applications. Both are semi-crystalline polymers with a volume degree of crystallinity up to 40%, a melting point of 170 °C to 195 °C, and a glass-transition temperature from 50 °C to 60 °C (Karst and Yang, 2006). PLLA is a stereoregular polymer, found to be of increasing mechanical strength and toughness. Therefore, it would be solved better as sutures and in other applications which need high physical strength such as orthopaedic implants. Poly-DL-lactide (PDLLA) is the optically inactive racemic form, which is usually amorphous. Based on its nature of having lower tensile strength and faster degradation, drug delivery devices are its most suitable use. A mix of PLLA and PDLA

blends has characteristics different to any of its copolymers such as crystal structure, melting point, and glass-transition, and these characteristics are influenced by the percentage of the blends. A 50/50 PLLA/PDLA blend can form into a stereocomplex. Due to the stereocomplex crystallites structure, this PLLA and PDLA complex polymer have higher tensile strength and Young's modulus compare to both pure polymers before blend. Furthermore, the glass-transition temperature and the melting point are also both higher than those of pure PLLA and PDLA. In which we have the glass-transition temperature for the 50/50 PLLA/PDLA blend is between 65 °C to 72 °C and melting point is between 220 °C to 230 °C (Karst and Yang, 2006). Polydioxanone is another commonly used degradable polymer which where commercially introduced in 1981. Polydioxanone can be used as an alternative to PGA and PLA for unloaded orthopaedic applications. Because it's a semi-crystalline polymer and it has a low melting temperature and slower degradation rate, polydioxanone made orthopaedic devices will slowly delivery drugs over one year period. This is necessary when the tissue needs a long time to heal, slowly releasing of drug will lead to a continually support of healing in tissue (Buchanan, 2008).

1.2 Medical implants made of biodegradable polymers

In October 2010, Professor Anthony Gershlick implanted a PLA stent into a heart patient at the University Hospitals of Leicester NHS Trust. This was the first case of using a fully biodegradable stent in the UK. Every year, tens of thousands of people suffer from heart disease caused by narrowed artery or thrombus. Implanting a stent is a much safer and minimally invasive surgical procedure to solve such an issue. The stent would be injected into the patient's artery from other parts of the body, for example, the leg. It will follow the artery to the lesion part. A balloon is then implanted to expand the stent into position. The stent will expand and support the narrowed artery, which will obtain normal blood flow. However, most of the commonly used stents have a base of unabsorbable material, which will be permanently left inside the body. An elevated risk of bio-incompatibility remains. Therefore, a biodegradable stent is strongly necessary. The biodegradable stent used in the University Hospitals of Leicester had been designed to extend the narrowed artery, restoring the blood flow and providing support while the opened area heals. Once no longer required, the stent

slowly dissolves into carbon dioxide and water, over a period of two years. During the degradation, the drug layer contained in the stent releases the drug and attenuates the response of injured tissue that has been caused by the high-pressure deployment of the stent. The benefit of it will be that there is no permanent implant left behind, allowing the artery to be more functionally normal.

After being used as sutures in the 1970s, many other medical implants made of biodegradable polymer were quickly developed. Biodegradable polymers made screws and plates, which were used for bone fixation. About 10% of the bone fractures in UK need internal fixation devices such as screws, pins, and plates. They are needed to supply physical strength when the bone is weak; therefore, the materials used as implants need to be physically strong to support human daily activities such as walking or lifting. For that reason, metal used to be chosen as the material for these kinds of implants. However, the disadvantage of metal-made implants is obvious. Broken bones need support at the beginning, but they heal over time. At a certain point, the bone will be fully healed and the implants no longer required. For some implants, a second surgery can be performed to remove them, but for others, a second surgery is difficult and risky. Therefore, patients have been forced to carry these “no longer needed” implants for the rest of their lives, bearing the risk of bio-incompatibility and the pain that may be caused by it. Even if a second surgery has been performed, there is still risk of infection and other complications, and a second invasion will be a huge damage to the body. The introduction of biodegradable polymer solved the issue of needed secondary surgery and the permanent residence of implants. Biodegradable polymer-made implants first provide broken bones with the support they require through surgery. As time goes by, the bone heals and slowly takes control as the implant slowly degrades into carbon dioxide and water. Finally, the implant disappears and the healed bone takes back full control. In the full process, no second surgery is needed and no implant remains. Furthermore, drug-loaded implants can slowly release the drug into the needed area to help heal the bone and surrounding tissue.

Biodegradable polymers are also used as scaffolds for tissue engineering. In this intensive application, porous foam scaffolds have been made to let the tissue grow around it inside and outside the human body. As tissue grows, the scaffold degrades slowly; finally, there is nothing remaining of the original scaffold. Currently, tissue engineering has been used for growing tissues such as bone, skin, and cartilage. More

complex tissues, such as organ tissues, are the focus of upcoming research. As growing organ tissues become more realistic, patients could benefit from exchanging the failing organ for their own tissue-grown organ. This would make organ donation and transplantation unnecessary, and makes the organ obtaining easier. In the next decades, tissue regeneration may be one of the most important scientific developments.

1.3 The need for computer modelling in implant design

In all the above applications, the biodegradable devices firstly provide some temporary functions, then degrade and let the body take over control slowly. Finally, the implant devices fully degrade into carbon dioxide and water, thus disappearing. Two crucial factors that need to be considered during the process are degradation rate and mechanical property. For an implant device, it is important to predict how long it will take to fully degrade and disappear, and it is important to monitor the mechanical property during degradation to make sure the device can always supply the function that is needed before the body can heal and take over control. However, the development of such devices is still dominated by trial-and-error. Degradation takes from weeks to years, depending on applications. Testing fresh design ideas for the devices requires long-term *in vitro* and *in vivo* experiments and, finally, human clinical trials. Therefore, the development of designs is both expensive and time-consuming. Consequently, virtual testing using computer modelling is particularly helpful. Although experimental tests will still be necessary and play a dominant role in the future design, using computer modelling in the early design stage can significantly accelerate development and avoid unnecessary experiments. The following chapter gives a brief introduction of degradation mechanisms.

Chapter 2: Mechanisms of degradation of biodegradable implants

This chapter gives a brief introduction of degradation mechanisms.

2.1 Factors that control the degradation rate

After serving their function, biodegradable medical devices disappear and hand back full control to the body. Degradation rate is the most important feature. Therefore, most of this PhD thesis is focused on degradation rate. Furthermore, modelling polymer degradation also leads to the study of drug release. Many biodegradable devices would contain drugs that would slowly be released into the human body for certain treatment, such as drug-eluting coronary stents and tissue-engineering scaffolds. Broadly speaking, the degradation rate of a polymeric device is affected by:

- Type and properties of the raw polymer;
- Manufacturing and sterilisation conditions;
- *In vivo* environment of the device; and
- Shape and size of the device.

Each of these factors contains many other variables; therefore, the degradation rate depends on an extensive list of variables. It is too complicated to relate the degradation rate of the device back to all these factors, and there are currently no computer models possible to incorporate all these factors. In particular, the *in vivo* nature of device degradation is not yet fully understood. Therefore, the work presented will only focus on the shape and size effect on the degradation rate, and aims to help designs of degradable devices to have an easier understanding of the mathematical model.

The mechanisms of biodegradation are complicated which include hydrolysis reaction, crystallisation, and diffusion. The complicated behaviour makes the optimal device design very difficult and the capture of the degradation trend not straightforward. A breakdown review of these mechanisms is listed below.

2.2 Hydrolysis reaction

Hundreds or thousands of polymers repeat units, also called monomers, are formed into polymer long chains. The degradable devices are considered to be constituted by these long chains after the manufacturing process. PLA (polylactide) is an aliphatic polyester, which consists of three carbon atoms, four hydrogen atoms, and two oxygen atoms. An oxygen atom for one polymer repeat unit bonds to a carbon atom for the next polymer repeat unit through an ester (Karst and Yang., 2006). Water modulus attacks these ester bonds after diffusing into the amorphous polymer region. Diffusion rate of water modulus is much higher than the degradation rate or the diffusion rate of short polymer chains into the surrounding environment (Li et al., 2000), which will be discussed below. Therefore, water can be assumed to be abundant everywhere in the amorphous region, even at the very beginning of the degradation. Water modulus attack ester bonds cause one long polymer chain to break into two new shorter polymer chains. Each of the two newly formed polymer chain contains a new end, which are alcohol end and carboxylic acid end respectively (Galeska et al., 2005). The carboxylic acid end group has a high degree of dissociation. When the number of scissions increases the carboxylic acid end group increases; therefore, local acidity increases (Cameron and Kamvari-Moghaddam., 2008). This behaviour catalysts the hydrolysis reaction and will play a leading rule in some of the degradation.

In experimental analysis, molecular weight was often used as a measurement factor to study the average number of polymer repeat units in every individual polymer chains. The measurements were often taking place by gel permeation chromatography (GPC). The aim for GPC is to find the distribution of the molecular weight. This has been done by measuring time needed for polymer chains to pass through a column of porous beads, which was controlled by the molecular weight. The distribution of molecular weight could be found by form the given molecular weight range into factions of polymer chains, which would be getting from the GPC result. However, chains that contain small numbers of the repeating unit can be difficult to measure and are beyond the scope of GPC. Therefore, excluding chains below a certain length for modulus weight calculations would be necessary for theoretical degradation analysis such as computer modelling. Furthermore, short chains could diffuse out of the polymer, hence will not be counted in the GPC analysis (Joshi and Himmelstein, 1991). Number

average molecular weight and weight average molecular weight are mostly likely the two factors that would be measured and be included in the literature review. Therefore, it makes sense to use these two factors in computation modelling to validate the model by compare the model results to the literature measurements. The number average molecular weight indicated the average mass of each individual polymer chain, which could be achieved by dividing the total mass of all polymer chains to the total number of chains. Number average molecular weight decreases very quickly at the beginning of the degradation, as the number of chains increases and no short chains, which need to be eliminated from the measure or calculation, are produced yet. The ratio of weight average molecular weight over number average weight gives the polydispersity of the polymer, which indicates how broad the polymer chain distribution is. Number average molecular weight over the mass of one repeat unit gives the degree of polymerisation.

2.3 Crystallinity

Polymer chains are considered under random configuration in amorphous polymers. They overlap with each other and form into an inattentive region. On the other hand, there could be some region where polymer chains align next to each other, which gives the most stable atomic positions. Such regaining of packed polymer chains is referred to as crystallisation (Grizzi et al., 1995). A single collection of aligned polymer chains is referred as a crystallite. One polymer chains can overlapping to a few other polymer chains, which would be impossible for them to all straighten out and form into a single crystal. Therefore, a 100% crystallised polymer will not exist (Li et al., 1990). Compared to amorphous polymers, crystallites have a higher value of stiffness and better mechanical properties, because the chains packing together increase the overall interatomic attraction. However, it is hard for water molecules to diffuse into a crystalline region. Therefore, crystalline regions are generally considered to resist hydrolysis and degradation of crystalline polymers is much slower than amorphous polymers. Crystalline region of a biodegradation polymer device can affect its over and local mechanical property and over all degradation rate, therefore it is necessary to understand and predict how it change during degradation. Small polymer chains or monomers can move around inside of polymer devices, and one often finds that they

are easily combined with other chain ends and grow into a new crystallite or combine with the existing crystallite chain ends and increase the volume fraction of crystallinity. For that reason, the volume fraction of crystallinity can increase as well as decrease during degradation, whereas the number average molecular weight trend could only decrease. That could also explain the phenomenon seen from some experimental data, which is that the Young's modulus of the polymer increases at the beginning of the degradation. The crystallite can also increase by scissions. Every scission has a chance to cause the newly produced chain ends to fold back and forward to form into a new crystallite. This is known as chain cleavage-induced crystallisation.

2.4 Oligomer production

Chain scission causes long polymer chains to break into smaller ones. When the chains are small enough, particularly less than eight repeat units, they will be referred to as oligomers. Oligomers have been assumed to have the ability to move around inside the polymer; it could form into crystallite, it could increase the local acidity, and could therefore lead to autocatalysis hydrolysis reaction, and it could be diffused out of the polymer. Although it has been mentioned that disassociation of carboxylic acid chain ends causes autocatalysis hydrolysis, Pan and his collaborators (2016) suggest that the contribution of short polymer carboxylic acid chain ends may dominate this process because of the high movability of the short chains. An advanced mathematical model has been developed to separate the long and short chains, which will be discussed later.

Scissions can happen in two forms. If all the scissions occur at the ester bonds next to the polymer chain ends, then each chain scission creates a monomer. This is known as end scission. If the chain scission occurs randomly along the polymer chains, then one scission could create an oligomer or, most likely, would break one long polymer chain into two smaller polymer chains. Therefore, random scission is much more efficient in reducing molecular weight than end scission, and end scission is more efficient in the generation of short chains than random scission. It can be observed from literature that for most of the cases average molecule weight reduces fast at the beginning of the degradation, which could not be explained by pure end scission. Also, literature demonstrate a usual weight loss at the end of degradation, which would not be able to explain by pure random scission because too few short chains have been created and

even fewer of them could be diffused out. Gleadall, et al. (2014) studied the existing data in the literature and concluded that the degradation of common biodegradable polymers is typically a combination of random and end scissions. Whereas, most of the scissions happens at chain ends, because it is easier for them to have water molecule around them. And the scission happens by chain ends produce most of the monomers responsible for weight loss. However, it is the few random scissions that cause the molecular weight reduction, especially at the beginning of degradation. In general, the production of short chains in random scission can be empirically related to number of chain scissions (Han, et al., 2010), whereas, in end scission, the number of ester units of the short chains should be equal to the number of scissions.

2.5 Non-uniform degradation

This thesis assumes that the degradation mechanism is caused by two main hydrolysis reactions – non-catalytic reaction and autocatalytic reaction. In the first stage of degradation, water molecules attack ester bonds causing scission; this reaction happens naturally and no catalytic is required. Long polymer chains have been chopped into shorter chains, some of them small enough to diffuse out (less than eight units of polymerisation). Scission breaks the polymer chains into two end groups – hydroxyl alcohol group and carboxylic acid end group. The carboxylic acid end group has a high rate of dissociation, which produces H^+ . H^+ works as a catalytic, which can cause more scissions and increase the degradation. This process is called autocatalytic reaction. Autocatalytic reaction is the main cause of the non-uniform degradation. Production of H^+ increases the local acidity, causing some part of the polymer to degrade faster than other parts. The short polymer chains which contains acid end groups could be diffused out when its near to the surface of a device. Which will lower the local acidity and decrease the hydrolysis reaction. Whereas, in the middle part of the device, short chains cannot diffuse out as fast as the surface, local acidity is still high compared to the surface, and autocatalytic reaction is taking a big part. Therefore, the centre of the device degrades faster than the surface, which may cause a holey structure toward the end of the degradation. Two main factors have significant control of the non-uniform degradation. One is the size of the device. A thicker device causes short chains in the centre of the device to be harder or take longer to diffuse out. Consequently, local

acidity is higher and causes more scission and faster degradation. From the literature, we know that a thicker device degrades faster than a thinner one. Therefore, local high acidity can also lead to faster degradation for the whole device. This is called the size effect. The second factor is the diffusion coefficient. A higher diffusion coefficient causes short chains to diffuse out of the device more easily and lower the local acidity. In contrast, a smaller diffusion coefficient makes it less easy for the short chains to diffuse out and local acidity is high. However, short chains in or near enough to the surface can still diffuse out, which causes the device to generate a thin layer on the surface. In this thin layer degradation is slow, due to short chains diffusing out and low local acidity. This thin wall phenomenon has been found in many degradation modelling cases. In this chapter, the effect of diffusion coefficient on the degradation detection will again be studied.

2.6 Non-uniform Young's modulus distribution

Non-uniform degradation leads to non-uniform distribution of average molecule weight and number of scissions. From the previous computation models developed by Leicester group, a direct link between the number of scissions and local Young's modulus has been found. Therefore, a distribution of Young's modulus can be calculated that relates to locations at various degradation times, as long as we have the data of average molecule weight distribution or number of scissions distribution from the literature or by achieving them from a degradation model. In the literature, most of the experimental data of average molecule weight and important material properties, like Young's modulus, have been achieved by taking an average over the whole device or sample. That is because some of the medical implants, like the coronary stents, are normally a quite small size. Measurement of the different degradation behaviour across the polymer is difficult by applying normal experimental method. However, local distribution of important material behaviours, for example Young's modulus, is vital for designing such medical devices. For example, in the thin wall phenomenon, the thin wall layer in the surface may have a very high Young's modulus value but the centre of the device may already be nearly holey. The average Young's modulus may still be in an acceptable range, but the device is way past its mechanical capacity. Non-uniform Young's modulus distribution can be implanted into vibration analysis.

Vibration analysis will be used as an alternative method which could provide a detection of the different distribution behaviour of the material properties, therefore detecting the degradation.

Chapter 3: A review of mathematical models for polymer degradation

This chapter provides a brief list of existing models for biodegradable polymer degradation. A literature review of the mathematical models developed by the Leicester group will also be presented. The remaining issues in the mathematical modelling of degradation and the purpose and the structure of this thesis are given at the end of this chapter.

3.1 Existing models for the degradation of biodegradation polymers

Chain scission mathematical models were the first models to be developed for degradation modelling, by Pitt and his collaborators in 1981 and 1987. The 1981 and 1987 models were developed for autocatalytic and non-catalytic hydrolysis reaction individually. Linear relationship was considered between the concentration of carboxylic acid chain end group in the autocatalytic model. Later on, Siparsky, et al. (1998) and Lyu, et al. (2007) proved that the autocatalytic model is linearly related to the concentration of H^+ , which is produced after disassociation of acid chain end groups. H^+ works as catalyst rather than chain ends. Then, the autocatalytic hydrolysis model was modified based on the equilibrium condition for acid chain end disassociation. The first simulation of full molecular weight distribution model was developed by Batycky, et al. (1997) and Antheunis, et al. (2009). Again, autocatalytic and non-catalytic hydrolysis reactions were considered separately in the models. The group at the University of Leicester then combined both non-catalytic and autocatalytic hydrolysis models into a single model. The model that combines both hydrolysis mechanisms has been successfully used to fit many sets of experimental data, whereas the model for each individual mechanism can only be used to fit particular cases.

A diffusion model was first introduced by Joshi and Himmelstein (1991), which gives the basic physicochemical properties for degradable polymer systems that predicts controlled release of bioactive agents. The concentration of different species controls

the diffusion coefficient. From the NMR measurements, Gao and Fagerness (1995) could present another expression of diffusion coefficient model which is concentration dependent. In their expressions, concentration of water, drug, and polymer are all been linked to the change of diffusion coefficients. Including Gao and Fagerness' expression into the previous hydrolysis reaction model, a good fit can be found between the model predictions for polymer degradation and the corresponding experimental data. However, the diffusion coefficients that used in the model are empirical and not available for another polymer system. Another model developed by Peral, et al. (2009) presents degradation of solid devices. In which the degradation of this polymer matrix adds in count diffusion of water, monomers and oligomers. The autocatalytic hydrolysis reaction and increasing of crystallisation during degradation was not considered in this model. However, the model did demonstrate the molecular weight distribution function through the device and over time.

3.2 Previous work on modelling by the Leicester group

Wang, et al. (2008) combined both models by Pitt and his collaborators (1981, 1987) on autocatalytic and non-catalytic hydrolysis reaction; therefore, a single model had been formed to follow both of these hydrolysis mechanisms. Wang also allowed the water-soluble small polymer chains to diffusion out of the device, which led to reduce of local acidity and concentration of catalyst and caused fewer scissions and a lower autocatalytic hydrolysis reaction. Non-dimension was applied to the model parameters to simplified the mathematical model. To understand the degradation is in non-catalytic hydrolysis, autocatalytic hydrolysis, or a combination of hydrolysis and oligomer diffusion condition, a degradation map was introduced. Finite element analysis was used to study the degradation model and solve the diffusion reaction equations. Strip and square meshes were used. The model was used to show how it can assist the design of sophisticated fixation devices. Wang also used the entropy spring theory to study the Young's modulus change in biodegradable polymers cause by hydrolysis reaction in amorphous polymers. Based on the assumption of isolated polymer chain scission, a computation simulation for hydrolysis reaction was created to study the effect of average molecular change on Young's modulus, in which during polymer deformation short polymer chains were considered not affect the entropy

change of a linear biodegradable polymer. Poly(L-lactic acid) and poly(D-lactic acid) experimental data from Tsuji's (2001) were used to prove the validation of this model. A good fit was shown. However, this model introduced by Wang only considered end scission.

Following the work of Wang, et al. (2008), Han and Pan (2009, 2010) extended his model and included increases in polymer crystallinity during degradation. Han and Pan (2009, 2010) also combined both mechanisms for end scission and random scission. In addition to the model considered both non-catalytic and autocatalytic hydrolysis, Han and Pan also add in the effect of temperature. Water-soluble short polymer chains diffuse out of the device is also considered. Han also developed a model to address the effect of temperature on degradation rate, following the studies on TCP/polyester composite materials degradation. Finally, from a swelling polymer matrix she presented an early stage study on drug release.

Ding (2011) also studied the effect of chain scissions on Young's modulus. In his method mathematical model was not used, but an atomistic study was introduced. A molecular model of two polymer crystals and an amorphous region in between was created, which used both molecular dynamics method and Monte Carlo steps. Random scission was considered to happen in the amorphous region of the model. The system was set to equilibrium and then applied different numbers of scission to it. From several virtual tensile tests, deformation in molecular dynamics simulation can be achieved. Semi-crystalline biodegradable polymer was assumed in his model. It was found that when the temperature is below glass transition temperature, Young's modulus reduces quickly for semi-crystalline polymer. The reason for that is the internal energy controls the Young's modulus of semi-crystalline polymer at such temperature. If the temperature was above the glass transition temperature, the Young's modulus is controlled by the entropy of the amorphous phase, therefore reduction slows down. This proved that the widely observed semi-crystalline biodegradable polymer degradation behaviours could be obtained by using this numerical study.

Gleadall (2015) simplified Han's (2009) model on simulation of crystallisation during degradation by assuming fast crystal growth. The model is much easier to use and is possible to follow by end users with little engineering or modelling background. The simplified crystallisation theory was combined with the previous degradation model

and used to provide further studies on the following factors that affect degradation: autocatalysis; random and end scission; initial molecular weight; and residual weight. This further understanding on the factors could help the biomedical device designer or degradation users who are not from an engineering-related background. Since the degradation mathematical model is still at an early stage, many factors are still unclear and the model is constantly developing; the research work should still be continuing finding out the effects of these factors on the degradation. Gleadall also developed a numerical Effective Cavity Theory, which provides a simulation of Young's modulus change during degradation. The improvement of his theory hugely reduced the computational demands and allowed the simulation for complex biodegradable polymers; also, it could capture the Young's modulus change for polymers below their glass transition temperatures. Furthermore, he combined the degradation model with this Effective Cavity Theory to allow mathematical degradation models to simulate one more crucial factor: Young's modulus for glassy polymers.

Different to Gleadall (2015), Samami, et al. (2016) provided an analytical solution to the Young's modulus calculation. The constitutive law for the degrading bioresorbable polymers introduced could also predict the change of mechanical properties other than Young's modulus, such as Poisson's ratio and ultimate tensile strength. In his theory, a semi-crystalline polymer was assumed to be formed continually by three inclusions that have different behaviours: cavity caused by each scission; new crystal as a solid inclusion; and amorphous polymers surrounding these two inclusions. The existing theories of such continuum solid were used to calculate the degrading polymer effective elastic properties. The porous materials scaling relations were used to predict the degrading polymer tensile strength. They were packed together to form into a constitutive law for the degrading polymers, and the validation of such constitutive law was provided by fitting experimental data. Samami, et al. (2016) also presented a numerical study to detect the degradation in degrading polymers using vibration analysis. It has been shown that the absolute mode shape curvature difference between the degrading polymer and the intact polymer could provide a relatively good indication for the location of the degradation. However, the measurement accuracy requirement is very high. Nevertheless, it is still a good indication of finding the local degradation.

3.3 Remaining issues in modelling biomedical device degradation

The degradation mathematical model is constantly developing by adding in more factors that have been proved to have a big effect and removing factors that could be simplified. The developed mathematical model eventually needs to be used for further understanding the degradation behaviour, therefore, helping to design the biodegradable medical devices. A designer of such devices will normally not have a strong background in engineering; therefore, a complicated method, especially the long list of parameters, will be hard for them to fully follow and ever harder for them to choose for each of these parameters.

The current degradation mathematical model does not consider the different contributions between the long and short carboxylic end groups, even though it is well-known that the carboxylic end group provides the extra hydrolytic ability that leads to auto-catalysis hydrolysis. One thing we know for sure is that the short carboxylic end groups could diffuse out of a device, which would reduce the auto-catalysis hydrolysis rate. Additionally, long carboxylic chains are considered to have low movability, so separation of them is necessary.

Indication of degradation behaviour is not clear. For designers who will use the degradation mathematical model, it is hard for them to tell what causes the degradation behaviour they have just achieved from the model – whether the degradation is more controlled by non-catalyst hydrolysis reaction or auto-catalyst hydrolysis reaction.

Faster water diffusion is always assumed in the current degradation mathematical model, but two parameters that would change that were never considered to be an effect, namely, the water diffusion coefficient and the thickness of the device. The water diffusion coefficient has little changing room but the thickness of the device could be an issue for water diffusion, as it can be 1/10 of a millimetre up to half a hundredth of a millimetre. Whether the biodegradable medical device is always water abounded is very important for degradation, as degradation is assumed to be kicked off by a water molecule attacking the ester bond.

The mathematical model was created to be use for designing purposes, but there is still not an easy method that could use the mathematical model. By using engineering technology, a simple design method could be suggested.

The storage conditions of biodegradable medical devices have never been considered in degradation mathematical model building. It is an important issue that needs to be added in because the atmosphere contains water vapour and this could cause the medical device to lose its function, which needs to be avoided. Mathematical simulation could provide an indication of whether a certain atmosphere condition would cause such problem.

Young's modulus change is a very import factor in understanding degradation. However, the analytical model presented by Samami, et al. (2016) is over-complicated and hard to follow for the degradation model end user who does not have an engineering-related background. Additionally, Gleadall, et al.'s (2015) model contains too many parameters, which will affect the, Effective Cavity Theory, which is not easy to follow. The same problem exists for the degradation detection model introduced by Samami, et al. (2016): it is also hard to follow and over-complicated.

Many experiments were carried out for biodegradation polymers, but in varying the degradation model by using such experimental data there was always information missing. For example, many experiments did not pre-measure the oligomer residents before degradation, which would (as has been confirmed) change the degradation behaviour. Other suggestions have been made in this thesis to the experimental work in order to improve the degradation model.

3.4 Purpose and structure of this thesis

The purpose of this thesis is to create a clearly displaced degradation mathematical model that contains the new development and to provide a step-by-step explanation and guidelines for using such a mathematical model in further designs. It contains many simplifications to the currently existing model. The subsequent structure of this thesis can be described as follows:

Chapter 4: Mathematical model for amorphous polymers with a development of separating long and short carboxylic chain ends.

Chapter 5: Mathematical model for semi-crystalline polymers with degradation map.

Chapter 6: Validation of the newly developed model by fitting experimental data and suggestion of designing method and storage condition.

Chapter 7: Simplified Young's modulus degradation model.

Chapter 8: Simplified degradation detection model.

Chapter 9: Major conclusions and recommendations for future work.

Chapter 4: Master equations for amorphous polymers, analytical solutions and a parametric study of the mathematical model

This chapter presents a new development to the mathematical model for polymer degradation based on previous work by the Leicester group. In the newly developed model, the carboxylic end groups on the short and long polymer chains are separated. Furthermore, seven analytical solutions are presented to show that the newly developed model can be reduced to previous models in the literature. A parametric study was carried out to understand the effect of different parameters on the degradation model. A large part of this chapter has been included in the book edited by Pan (Pan and Chen, Chapters 2 and 3, 2013). In which equations, figs and data fittings are contributed by writer.

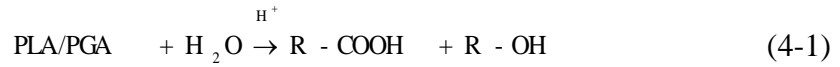
4.1 Degradation equations for amorphous polymers

All the assumptions, results, and conclusions in the current section are being considered under the amorphous phase. It is convenient to discuss degradation theory starting with amorphous polymers, as amorphous polymers include a major part of biodegradable polymers. Furthermore, all semi-crystalline polymers contain an amorphous phase. It is therefore logical to focus attention on amorphous polymers first.

4.1.1 Previous mathematical models developed by the Leicester group

Following by the mechanism of polymer degradation, hydrolysis reaction happens by water molecules attacking the ester bonds of the polymers, which causes the long polymer to cleave. Two end groups – hydroxyl alcohol (R–OH) and carboxylic acid (R–COOH) – are produced. The carboxylic acid end group has a high degree of dissociation, which will generate H^+ . H^+ works as a catalyst to the hydrolysis reaction, and will increase the rate of the reaction. For simplicity, the chemical structure of the

polymers and the actual reaction steps are ignored here. The hydrolysis reaction is phenomenologically described as

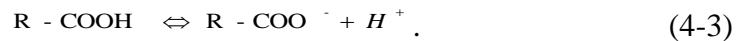


Using R_s to represent the total number of chain scissions per unit volume of the material, the changing rate of R_s can be written as (Wang, et al., 2008; Han and Pan, 2009):

$$\frac{dR_s}{dt} = k_1 C_e + k'_2 C_e C_{H^+} \quad (4-2)$$

in which C_e is the ester bonds concentration of the polymers, C_{H^+} represent the concentration of H^+ . The concentration of water molecules does not appear in the equation because it is assumed that they are abundant (Li, et al., 2000). The right-hand side first term of the equation $k_1 C_e$ is a hydrolysis reaction that is not catalysed by H^+ . The second term $k'_2 C_e C_{H^+}$ represents an auto-catalysed hydrolysis reaction. The first term is included to account for a range of factors such as potential lack of mobility of the $-\text{COOH}$ end groups or copolymer/polymer blend containing weak auto-catalysed species. The corresponding reaction constants k_1 and k'_2 can be tailored to reflect these complexities phenomenologically.

The carboxylic end groups can be disassociated into the following:



This reaction is fast and reversible. It can therefore be treated as being always at equilibrium with an equilibrium expression of

$$K_a = \frac{C_{H^+} C_{\text{COO}^-}}{C_{\text{COOH}}} \quad (4-4)$$

in which K_a is the equilibrium constant. K_a is known at specific temperatures. For example, PDLLA and PGA have $K_a = 1.349 * 10^{-4}$ ($pK_a = 3.87$) at 37 °C, because $C_{H^+} = C_{\text{COO}^-}$, equation (4-4) gives

$$C_{H^+} = [K_a C_{\text{COOH}}]^{1/2} \quad (4-5)$$

Input equation (4-5) into equation (4-2) gives the following expression for scission rate:

$$\frac{dR_s}{dt} = k_1 C_e + k_2 C_e [C_{COOH}]^{\frac{1}{2}} \quad (4-6)$$

in which a new reaction constant has been introduced: $k_2 = k_2' [K_a]^{-\frac{1}{2}}$.

The total number of short chain ester units which are produced from chain scission is referred to as R_{ol} . R_{ol} is related to the overall chain scission numbers R_s through the empirical relation listed below (Han, et al., 2010).

$$R_{ol} = \alpha C_{e0} \left(\frac{R_s}{C_{e0}} \right)^{\beta} \quad (4-7)$$

in which α and β are two parameters that controls the production of oligomers, which can switch between end scission and random scission, C_{e0} represent to initial long chain concentration of ester bonds.

Using C_{chain0} to indicate the total number of polymer chains existing at the beginning of degradation, each scission produces a $-COOH$ end group and we have

$$C_{COOH} = C_{chain0} + R_s \quad (4-8)$$

Again, using C_{e0} to represent the initial long chain concentration of ester bonds, the short chains are produced at the expense of C_{e0} . Using equation (4-7) gives

$$C_e = C_{e0} - R_{ol} = C_{e0} \left[1 - \alpha \left(\frac{R_s}{C_{e0}} \right)^{\beta} \right] \quad (4-9)$$

Submitting equation (4-8) and (4-9) into equation (4-6) gives

$$\frac{dR_s}{dt} = C_e \left\{ k_1 + k_2 [C_{COOH}]^{\frac{1}{2}} \right\} = C_{e0} \left[1 - \alpha \left(\frac{R_s}{C_{e0}} \right)^{\beta} \right] \left\{ k_1 + k_2 [C_{chain0} + R_s]^{\frac{1}{2}} \right\} \quad (4-10)$$

It is sometime convenient to use a normalised form of the above equation.

Defining

$$\bar{R}_s = \frac{R_s}{C_{e0}} \quad (4-11)$$

$$\bar{k}_2 = C_{e0}^{0.5} k_2 \quad (4-12)$$

equation (4-10) can then be rewritten as

$$\frac{d\bar{R}_s}{dt} = (1 - \alpha\bar{R}_s^\beta) \left[k_1 + k_2 (N_{dp0}^{-1} + \bar{R}_s)^{\frac{1}{2}} \right] \quad (4-13)$$

in which N_{dp0} is the degree of polymerisation given by

$$N_{dp0} = \frac{C_{e0}}{C_{chain0}} \quad (4-14)$$

The number averaged molecular weight M_n is the total weight of the polymer chains divided by the total number of chains, i.e. we have

$$M_n = \frac{C_{e0} M_{unit}}{C_{chain0} + R_s} \quad (4-15)$$

in which M_{unit} represents the molecular weight of a polymer repeating unit. Using M_{n0} to present the initial molecular weight of a polymer, equation (4-15) can be rewritten as a normalised form

$$\frac{\bar{M}_n}{M_{n0}} = \frac{M_n}{M_{n0}} = \frac{1}{1 + N_{dp0} \bar{R}_s} \quad (4-16)$$

When measuring the molecular weight, using gel permeation chromatography (GPC), for example, the short chains are too small to be detected. Furthermore, the short chains do not contribute to the mechanical properties of a polymer and including them in the number-averaged calculation distorts the true state of the polymer. It is, therefore, often necessary to exclude short chains from the calculation. Recalling that R_{ol} represents the total number of ester units of all the short chains and m represents the polymerisation average degree of the short chains, the number of short chains is given by R_{ol}/m . Averaged molecular weight excluding the short chains is then calculated as

$$M_n = \frac{(C_{e0} - R_{ol}) M_{unit}}{C_{chain0} + R_s - R_{ol}/m} \quad (4-17)$$

which can be normalised by M_{n0} as

$$\frac{\bar{M}_n}{M_{n0}} = \frac{M_n}{M_{n0}} = \frac{1 - \alpha\bar{R}_s^\beta}{1 + N_{dp0} \left(\bar{R}_s - \frac{\alpha}{m} \bar{R}_s^\beta \right)} \quad (4-18)$$

Equation (4-13) is the common rate of chain scission equation in the literature. It is not valid when diffusion of short polymer chains (less than eight units) needs to be added into the count. A further developed model was included in the next section, which separates the long and short polymer chains.

4.1.2 Further development to the equation of degradation rate

It is more appropriate to separate the carboxylic acid end groups into two types: 1) those of the long polymer chains that are not water soluble and cannot diffuse out of the device; 2) those of the short oligomers and monomers that are water soluble and can diffuse. The reason for that is that the two types of carboxylic acid end groups may behave differently in their capacity as catalyst for the hydrolysis reaction. Those of the long polymer chains may have limited mobility and do not fully contribute to the hydrolysis reaction. Furthermore, the two types of carboxylic acid end groups have different diffusion ability. The diffusion of the water-soluble chains out of a device reduces the acidity inside the polymer and reduces the degradation rate. For a device of a large size, such as a thick plate, the small chains near the surface can diffuse out quicker than those at the core of the device. The core therefore degrades faster than the surface shell and a thicker device degrades faster than a thin one (Li, et al., 1990). Therefore, oligomer diffusion and size effect are responsible for the heterogeneous degradation. This development was discovered by Pan and Chen (2013) and was included in Chapter 3 of their book.

To separate different contributions from chain ends on long and short chains, their contribution to C_{H^+} is split such that

$$C_{H^+} = \left[K_a \left(\chi_1 C_{COOH}^{long} + \chi_2 C_{COOH}^{short} \right) \right]^{\frac{1}{2}} \quad (4-19)$$

in which χ_1 and χ_2 are two partitioning parameters that take values between zero to one. For example, equation (4-19) is reduced to equation (4-5) by setting $\chi_1 = \chi_2 = 1$, and the contribution from the long chains can be switched off by setting $\chi_1 = 0$ and $\chi_2 = 1$.

and equation (4-2) becomes

$$\frac{dR_s}{dt} = k_1 C_e + k_2 C_e \left[K_a \left(\chi_1 C_{COOH}^{long} + \chi_2 C_{COOH}^{short} \right) \right]^{\frac{1}{2}} \quad (4-20)$$

in which a new reaction constant is introduced such that $k_2 = k'_2 [K_a]^{\frac{1}{2}}$.

Using C_{ol} to represent the total amount of ester units of oligomers and monomers (the short chains) per unit volume, the concentration of carboxylic end groups on the short chains can be estimated from C_{ol} as

$$C_{COOH}^{short} = \frac{C_{ol}}{m} \quad (4-21)$$

whereas m is the average degree of polymerisation of the short chains, which should be four, as we assume that oligomer chains are the chains of less than eight units.

It is important to recognise the difference between C_{ol} and R_{ol} . Firstly, C_{ol} is the number of oligomer ester unit per unit volume that still remains in the device, which includes the initial number of short chain (oligomer) ester units, which are referred to as C_{ol0} . Therefore, the C_{ol} value can change when short chains (oligomers) are diffused out of the device (not remaining in it anymore). Whereas R_{ol} is a historical accumulation of all the short chains ever produced.

The concentration of carboxylic end groups of the long chains increases with chain scission and decreases with the production of short chains; hence, we have

$$C_{COOH}^{long} = C_{chain\ 0} + R_s - \frac{R_{ol}}{m} \quad (4-22)$$

in which $C_{chain\ 0}$ is the concentration of polymer chain ends at the beginning of the degradation. R_{ol} is related to R_s through equation (4-7); therefore, equation (4-22) can be rewritten as

$$C_{COOH}^{long} = C_{chain\ 0} + R_s - C_{e0} \frac{\alpha}{m} \left(\frac{R_s}{C_{e0}} \right)^{\beta} \quad (4-23)$$

Combining equation (4-2), (4-19), (4-21), and (4-23) gives

$$\frac{dR_s}{dt} = k_1 C_e + k_2 C_e \left[\chi_1 \left(C_{chain\ 0} + R_s - C_{e0} \frac{\alpha}{m} \left(\frac{R_s}{C_{e0}} \right)^{\beta} \right) + \chi_2 \frac{C_{ol}}{m} \right]^n \quad (4-24)$$

in which n is the acid disassociation exponent, which should be 0.5 but can take other empirical values, and $k_2 = k_2' [K_a]^n$.

If the diffusion of the short chains is prohibited, we have

$$C_{ol} = C_{ol0} + R_{ol} = C_{ol0} + \alpha C_{e0} \left(\frac{R_s}{C_{e0}} \right)^\beta \quad (4-25)$$

$$C_e = C_{e0} - R_{ol} \quad (4-26)$$

Combining equations (4-24, 25, 26) gives

$$\frac{d\bar{R}_s}{dt} = \left(1 - \alpha \bar{R}_s^\beta \right) \left\{ k_1 + k_2 \left[\bar{C}_0 + \chi_1 \bar{R}_s + (\chi_2 - \chi_1) \frac{\alpha}{m} \bar{R}_s^\beta \right]^n \right\} \quad (4-27)$$

Equation (4-27) is the advanced non-dimensional master equation for chain scission. Whereas, $\bar{R}_s = R_s/C_{e0}$ represent the normalised total number of chain scissions by the number of ester unit at the beginning of the degradation.; \bar{C}_0 represent the condition of the polymer at the beginning of the degradation,

$$\bar{C}_0 = \frac{1}{C_{e0}} \left(\chi_1 C_{chain0} + \chi_2 \frac{C_{ol0}}{m} \right) \quad (4-28)$$

in which C_{ol0} is the initial total number of ester units of the short chains (monomers and oligomers) per unit volume, and C_{e0} is the initial number of ester units per unit volume; k_1 is the hydrolysis rate constant for non-catalytic reaction, and $\bar{k}_2 = C_{e0}^n k_2$ is the hydrolysis rate constant for autocatalytic reaction.

If assuming only the carboxylic end groups on the oligomers and monomers act as the catalyst (i.e. by setting $\chi_1 = 0$ and $\chi_2 = 1$), the equation (4-24) can be reduced to Pan and his collaborators' model (Han, 2011), which can fit many sets of experimental data in the literature. A parametric study of χ_1 and χ_2 was carried out to give a further understanding of long chain and short chain contributions to the degradation, which is presented later in this chapter.

4.2 Analytical solutions and cross-checking with numerical solutions

By applying special conditions into the master equation shown above, the long complex equation can be simplified into short equations that could have analytical solutions. Comparing the analytical solutions and the numerical solutions provides a cross-checking for the solutions. A C++ program was used to perform the necessary numerical calculation.

4.2.1 Analytical solutions

Case (a): In many studies, we are only interested in the early stage of the polymer degradation. At this stage, we assume that not many oligomers have yet been produced in the system. So, the total amount of oligomers produced R_{ol} is much smaller than the ester bond concentration C_{e0} , which means $\alpha \bar{R}_s^\beta \ll 1$. Furthermore, if we assume the hydrolysis is non-catalytic only, i.e. $k_1 = 1$, $\bar{k}_2 = 0$, then equation (4-27) can be reduced to

$$\frac{d\bar{R}_s}{dt} = k_1 \quad (4-29)$$

which gives

$$\bar{R}_s = k_1 t \quad (4-30)$$

Using equation (4-15) we have

$$M_n = \frac{M_{n0}}{1 + k_1 N_{adp0} t} \quad (4-31)$$

which can be rewritten as

$$\frac{1}{M_n} = \frac{1}{M_{n0}} + \frac{1}{M_{unit}} k_1 t \quad (4-32)$$

Case (b): Pure non-catalytic hydrolysis ($\bar{k}_2 = 0$) without the assumption of early stage degradation and $\beta = 1$, which is liner relationship.

The master eqn. (4-27) is reduced to

$$\frac{d\bar{R}_s}{dt} = k_1(1 - \alpha\bar{R}_s) \quad (4-33)$$

and its solution is

$$\bar{R}_s = \frac{1}{\alpha}(1 - e^{-\alpha k_1 t}) \quad (4-34)$$

Pure non-catalytic hydrolysis ($\bar{k}_2 = 0$) without the assumption of early stage degradation and $\beta = 2$, which is not a simple liner relationship.

The master eqn. (4-27) is reduced to

$$\frac{d\bar{R}_s}{dt} = k_1(1 - \alpha\bar{R}_s^2) \quad (4-35)$$

and the solution is

$$\bar{R}_s = \frac{1}{\sqrt{\alpha}} \frac{e^{2\sqrt{\alpha}k_1 t} - 1}{e^{2\sqrt{\alpha}k_1 t} + 1} \quad (4-36)$$

Case (c): On the other hand, if we assume that the hydrolysis is entirely autocatalytic ($k_1 = 0$) and for the early stage ($\alpha\bar{R}_s^\beta \ll 1$), $\beta = 1$, $\chi_1 = \chi_2 = 1$, and $n = 0.5$, then equation (4-27) can be reduced to

$$\frac{d\bar{R}_s}{dt} = k_2(N_{dp0}^{-1} + \bar{R}_s)^2 \quad (4-37)$$

which can be integrated to give

$$\bar{R}_s = \left[N_{dp0}^{-\frac{1}{2}} + \frac{1}{2}k_2 t \right]^2 - N_{dp0}^{-1} \quad (4-38)$$

Using equation (4-38) in equation (4-16) gives

$$M_n = \frac{M_{n0}}{\left(1 + \frac{1}{2} N \frac{1}{dp_0} k_2 t\right)^2} \quad (4-39)$$

which can be rewritten as

$$\left(\frac{1}{M_n}\right)^{\frac{1}{2}} = \left(\frac{1}{M_{n0}}\right)^{\frac{1}{2}} + \frac{1}{2} \left(\frac{1}{M_{unit}}\right)^{\frac{1}{2}} k_2 t. \quad (4-40)$$

Case (d): Pure autocatalytic hydrolysis ($k_1 = 0$) without the assumption of early stage degradation, $\beta = 1$ and $n = 0.5$.

The master equation (4-27) is reduced to

$$\frac{d\bar{R}_s}{dt} = \bar{k}_2 (1 - \alpha \bar{R}_s) [\bar{C}_0 + A \bar{R}_s]^{0.5} \quad (4-41)$$

and its solution is

$$\bar{R}_s = \frac{H^2 (1 + Ge^{-\sqrt{\alpha H k_2 t}})^2}{A \alpha (1 - Ge^{-\sqrt{\alpha H k_2 t}})^2} - \frac{\bar{C}_0}{A} \quad (4-42)$$

in which

$$A = \chi_1 + (\chi_2 - \chi_1) \frac{\alpha}{m}, \quad H = \sqrt{(\bar{C}_0 \alpha + A)} \quad \text{and} \quad G = \frac{\sqrt{\alpha \bar{C}_0} - H}{\sqrt{\alpha \bar{C}_0} + H} \quad (4-43)$$

In the literature, equations (4-34) and (4-40) are often used to determine whether a polymer degrades by autocatalytic hydrolysis reaction (Lyu, et al., 2007). In a degradation experiment, M_n is measured as a function of time using a set of samples. Using the measured data, $1/M_n$ and $(1/M_n)^{1/2}$ are plotted against time t . If $1/M_n$ versus time forms a straight line, then it is concluded that the hydrolysis is non-catalytic and k_1 can be calculated from the gradient of the line. On the other hand, if $(1/M_n)^{1/2}$ versus time forms a straight line, it is then concluded that the hydrolysis is autocatalytic and k_2 can be calculated from the gradient of the line. It is, however, often found that the two equations can only fit the very early stage of the measured experimental data.

Case (e): Early stage degradation ($\alpha \bar{R}_s^\beta \ll 1$), pure autocatalytic hydrolysis ($k_1 = 0$), either $\beta = 1$ or $\chi_1 = \chi_2 = 1$, and $n = 1$.

In this case, equation (4-27) can be simplified as

$$\frac{d\bar{R}_s}{dt} = \bar{k}_2 [\bar{C}_0 + A \bar{R}_s] \quad (4-44)$$

where

$$A = \chi_1 + (\chi_2 - \chi_1) \frac{\alpha}{m} \quad (4-45)$$

Equation (4-27) can be integrated to give

$$\bar{R}_s = \frac{1}{A} \bar{C}_0 (e^{A \bar{k}_2 t} - 1) \quad (4-46)$$

In the case that no separation is made between carboxylic end groups on the long and short chains ($\chi_1 = \chi_2 = 1$), solution (4-46) leads to

$$\ln(M_n) = \ln(M_{n0}) - k'_2 C_{e0} K_a t . \quad (4-47)$$

which is used in some of the literature.

Case (f): Early stage degradation ($\alpha \bar{R}_s^\beta \ll 1$), pure autocatalytic hydrolysis ($k_1 = 0$), either $\beta = 1$ or $\chi_1 = \chi_2 = 1$, and $n \neq 1$.

In this case, equation (4-27) can be simplified as

$$\frac{d\bar{R}_s}{dt} = \bar{k}_2 [\bar{C}_0 + A \bar{R}_s]^n \quad (4-48)$$

where

$$A = \chi_1 + (\chi_2 - \chi_1) \frac{\alpha}{m} \quad (4-45)$$

Equation (4-27) can be integrated to give

$$\bar{R}_s = \frac{1}{A} \left[(\bar{C}_0)^{1-n} + A(1-n) \bar{k}_2 t \right]^{\frac{1}{1-n}} - \frac{\bar{C}_0}{A} \quad (4-46)$$

If $\chi_1 = \chi_2 = 1$, and $n = 0.5$, then the above solution is reduced to equation (4-38).

Case (g): Early stage degradation ($\alpha \bar{R}_s^\beta \ll 1$), pure autocatalytic hydrolysis ($k_1 = 0$), only the short chains act as catalyst ($\chi_1 = 0$ and $\chi_2 = 1$), no residual oligomers at the beginning of the degradation ($\bar{C}_0 = 0$) and $n\beta \neq 1$.

In this case, the master equation (4-27) is reduced to

$$\frac{d\bar{R}_s}{dt} = \bar{k}_2 \left[\frac{\alpha \bar{R}_s^\beta}{m} \right]^n \quad (4-47)$$

which can be integrated to give

$$\bar{R}_s = \left[(1 - n\beta) \bar{k}_2 \left(\frac{\alpha}{m} \right)^n t \right]^{\frac{1}{1-n\beta}} \quad (4-48)$$

It can be concluded that $n\beta < 1$ otherwise the function is not defined.

4.2.2 Numerical solution of the master equation

4.2.2.1 Numerical algorithm for solving the master equation

By integrate the master equation (4-27), numerical solution could be found. By setting a pair of model parameters (i.e. α , β , \bar{C}_0 , n , \bar{k}_2 , k_1 and χ_1 , χ_2) the right-hand side of equation (4-27) is actually a function of \bar{R}_s . Whereas

$$\left(1 - \alpha \bar{R}_s^\beta \right) \left[k_1 + \bar{k}_2 \left(N_{adp\ 0}^{-1} + \bar{R}_s \right)^{\frac{1}{2}} \right] = f(\bar{R}_s) \quad (4-49)$$

Therefore

$$\frac{d\bar{R}_s}{dt} = f(\bar{R}_s) \quad (4-50)$$

We also know that $t = 0$, $\bar{R}_s = 0$ is the initial condition for the master equation.

Applying the definition of differentiation, we have

$$\frac{d\bar{R}_s}{dt} \approx \frac{\bar{R}_s(t + \Delta t) - \bar{R}_s(t)}{\Delta t} \approx f(\bar{R}_s) \quad (4-51)$$

Whereas Δt is a small length of time. Rearrange equation (4-51) a little bit and we have

$$\bar{R}_s(t + \Delta t) = \bar{R}_s(t) + \Delta t \times f(\bar{R}_s) \quad (4-52)$$

This can then be used to calculate the new \bar{R}_s after a small step of Δt and achieve a relationship between \bar{R}_s and t (Pan and Chen, Chapter 2, 2013).

4.2.2.2 A C++ program to perform this calculation

Set the libraries need to be used in the programme (`#include <stdio.h>`, `#include <math.h>` and `#include <stdlib.h>`). Give function prototype of two subroutines *function_of_ \bar{R}_s* and *calculate_ \bar{M}_n* , which will be used afterwards to calculate $f(\bar{R}_s)$ and \bar{M}_n , respectively. Set the main function. Give initial conditions ($t = 0$) as, $C_{e0} = 17300 \text{ mol/m}^3$, $C_{chain0} = 17.3 \text{ mol/m}^3$,

$$N_{dp0} = \frac{C_{e0}}{C_{chain0}} = \frac{17300 \text{ mol / m}^3}{17.3 \text{ mol / m}^3} = 1000, \bar{R}_s = 0, \bar{R}_{ol} = 0, \bar{M}_n = 1. \text{ Set inputs } m, n,$$

$\alpha, \beta, k_1, k_2, \bar{R}_s_MAX$ and N , and input values for them. In the program, a parameter \bar{R}_s_MAX has been introduced, which is shown as the maximum value of \bar{R}_s .

Δt is achieved by splitting \bar{R}_s_MAX into N numbers of equal parts (N is a parameter that usually takes a large number) and divide that by $f(\bar{R}_s)$, whereas

$$\Delta t = \frac{\bar{R}_s_MAX}{N} / f(\bar{R}_s), t = t + \Delta t. \text{ By doing this, } \Delta t \text{ is related to } \bar{R}_s_MAX, \text{ which is}$$

more appropriate and more general to get, and also easier to check convergence. The small \bar{R}_s_MAX has been split; the bigger that N is, the smaller Δt will be achieved. Therefore, to reduce Δt to check convergence, we only need to increase the number of N . However, normally to achieve a converged Δt , ultimately, millions of calculations ($N=1000000$) are needed. Therefore, we will get millions of sets of data. However, in reality, we only need a few sets of data (100 or 200 sets) to show the trend of outputs. Therefore, selecting data from all calculations is necessary. Here, inducts parameter *count* and *read_data.count* were set to 0 initially, and *read_data* was given a number that is the number of calculations we do before recording data. When *count = read_data*, we record the data out as one of our selected data, otherwise *count = count + 1*. By doing this, data that has been recorded can be reduced to an

appropriate number of sets for analysing. Set up a while loop, and give the argument as $\bar{R}_s \leq \bar{R}_{s_MAX}$. If the argument is false, end the program; if the argument is true,

calculate $f(\bar{R}_s)$, $\Delta t = \frac{\bar{R}_s - MAX}{N} / f(\bar{R}_s)$, $t = t + \Delta t$, $\bar{R}_s = \bar{R}_s + \Delta t \times f(\bar{R}_s)$.

Calculate \bar{R}_{ol} using equation (4-7), whereas $\bar{R}_{ol} = R_{ol}/C_{e^0}$. Calculate \bar{M}_n using equation (4-18), which is the equation for not excluding the short chains. Set up a *read_data* value to record data. Normally, the *read_data* value will be relevant to the number of N , $\frac{N}{read_data} = 100$ or 200 or sometimes bigger if necessary. *count* has been set to 0 initially before the while loop. If $count \neq read_data$, $count + 1$. If $count = read_data$ then record outputs t , \bar{R}_s , \bar{R}_{ol} , and \bar{M}_n into the “output” file and set *count* to 0. Please note that it is important to set *count* as 0 initially before the while loop. Otherwise, if it has been set in the loop, the loop will force *count* to be 0 every time when the loop runs. However, we only need *count* reset to 0 when $count = read_data$. If \bar{M}_n is close to zero then stop, close file “output”, and end the program. Otherwise, go back to the while loop and repeat the above procedure using the current value of \bar{R}_s .

4.2.2.3 Flow chart of the program

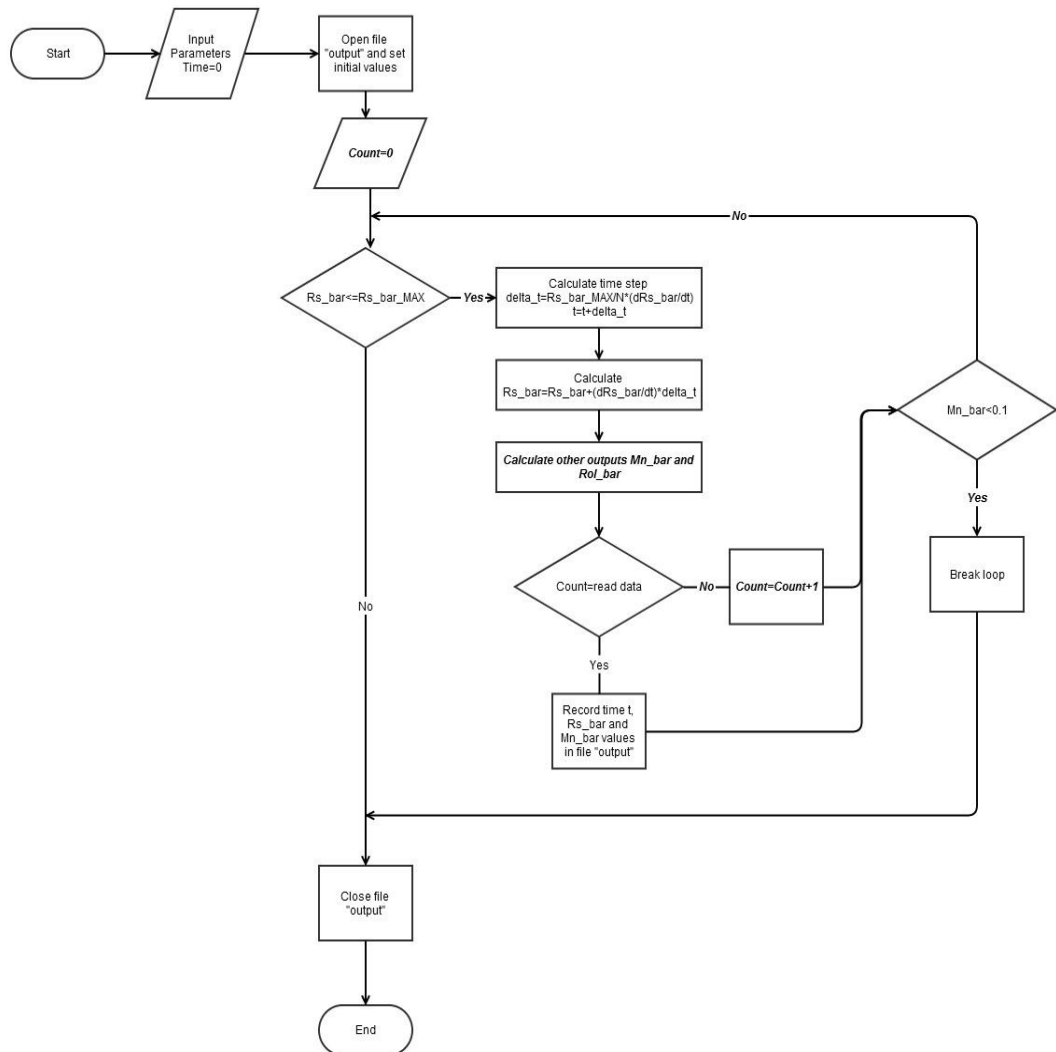


Figure 1: Flow chart of C++ program for calculating numerical solution

The actual program is shown in appendix.

4.2.2.4 A list of all the variable and array names of the computer program

Input parameters:

- 1) m - average degree of polymerisation of the short chains;
- 2) n - acid disassociation exponent of $-\text{COOH}$ groups;
- 3) α, β – empirical parameters for short chain production, dimensionless;

- 4) k_1, k_2_bar - hydrolysis rate constant for non-catalytic and autocatalytic reaction respectively;
- 5) $R_s_bar_MAX$ - maximum \bar{R}_s value that can be achieved;
- 6) N - number of equal parts into which \bar{R}_s_MAX will be split.

Output parameters:

- 1) t - time of degradation;
- 2) R_s_bar - normalised total number of chain scissions per unit volume;
- 3) R_{ol_bar} - normalised total number of oligomer units that have been produced per unit volume;
- 4) M_n_bar - normalised average molecule weight per unit volume.

Working variables and arrays:

- 1) $function_of_R_s_bar$ - function to calculate $f(\bar{R}_s)$;
- 2) $calculate_M_n_bar$ - function to calculate \bar{M}_n ;
- 3) $delta_t$ - small time step;
- 4) $Ce0$ - initial value for the ester bond concentration;
- 5) $Cchain0$ - initial value for the number of polymer chains;
- 6) $Ndp0$ - initial degree of polymerisation;
- 7) $count$ - used to count the number of calculations;
- 8) $read_data$ - used to select and record data.

4.2.3 Cross-checking analytical solutions with the corresponding numerical solutions

Fig. 2 provides an example of the numerical solution for M_n/M_{n0} versus time using $\alpha = 0.4, \beta = 1, m = 4, N_{dp0} = 1000, k_1 = 5 \times 10^{-5}/week, \bar{k}_2 = 5 \times 10^{-3}/week$, these parameters has been taken from (Han *et al.*, 2010) which has been used to successfully fitted experimental data. The time step used in the calculation is

$$\Delta t = \frac{\overline{R_s - MAX}}{N} / f(\overline{R_s}) = \frac{0.1}{10000000} / f(\overline{R_s})$$
 . The molecular weight was calculated using equation (4-18) (Fig. 2, case C). The analytical solutions given by equations (4-32) and (4-40) are also shown in the figure using the values of $k_1 = 5 \times 10^{-4} / \text{week}$ (Fig. 2, case A), and $\bar{k}_2 = 5 \times 10^{-3} / \text{week}$ (Fig. 2, case B), respectively.

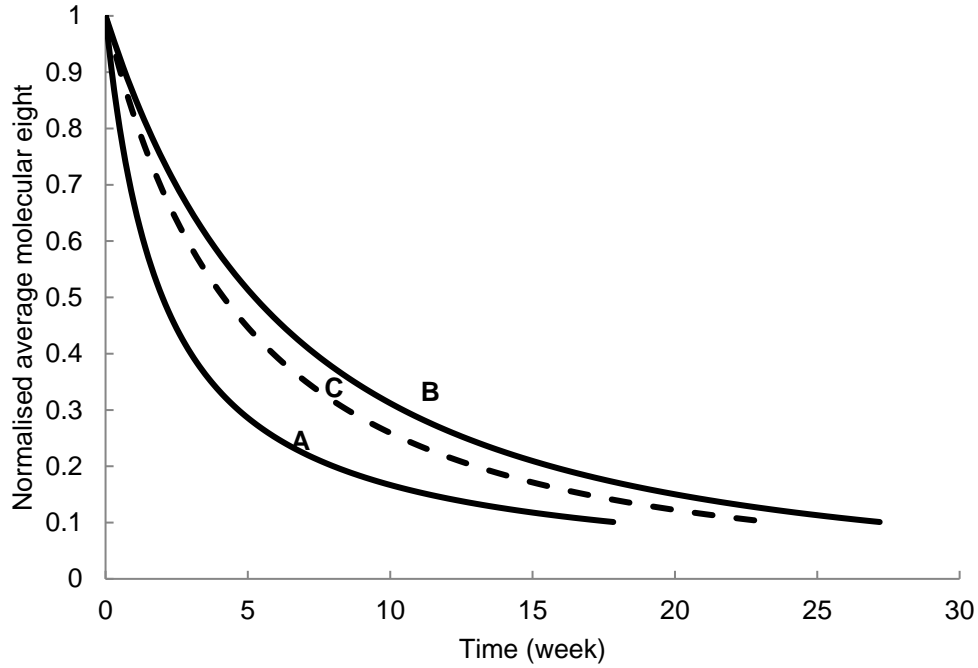
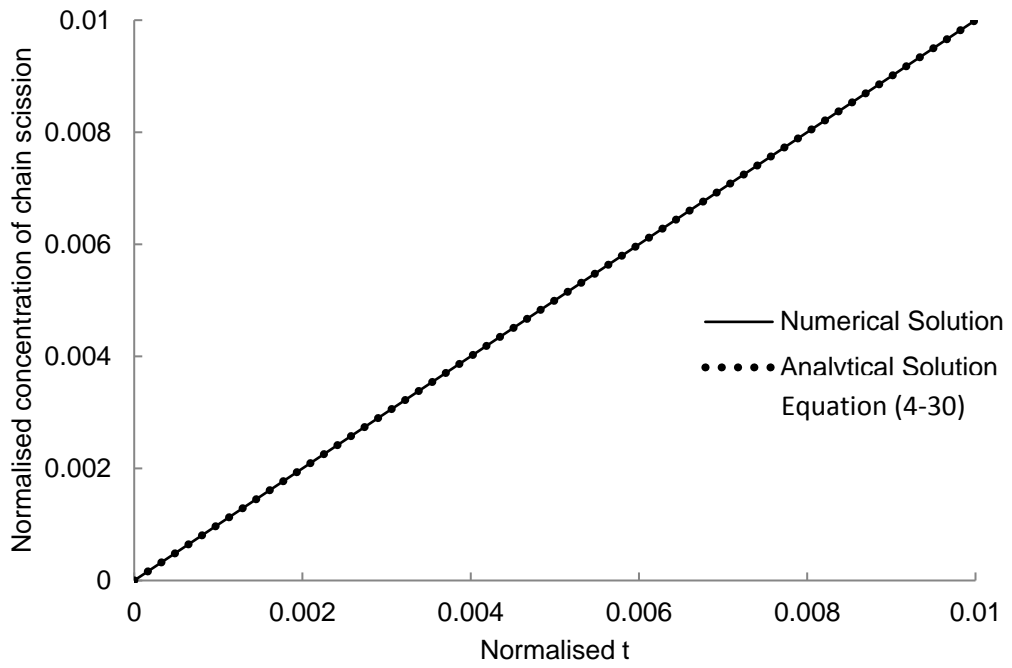


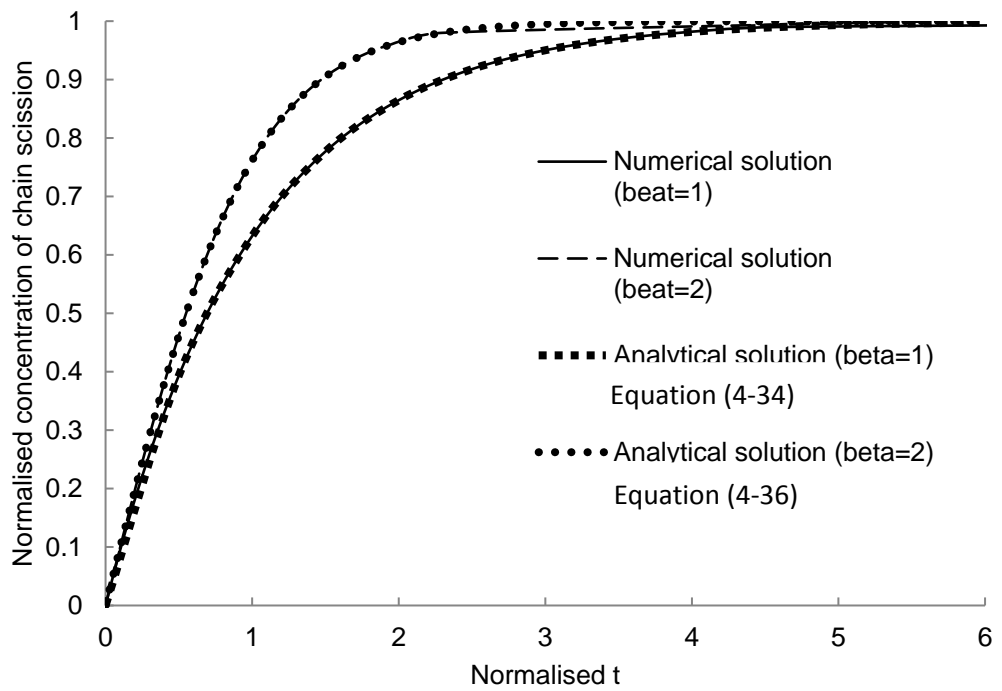
Figure 2: Normalised average molecular weight reduction trend during degradation for: (A) equation (4-26); (B) equation (4-34); and (C) numerical integration of equation (4-22).

Fig. 3 shows the first four cases of analytical solutions listed in section 4.2.1 cross-checking with their corresponding numerical solution. It has been shown that all numerical solutions agree with their corresponding analytical solutions. This confirms the validation of the master equation for these particular cases, and increases the persuasion of the master equation.

Case (a): Pure non-catalysed hydrolysis reaction for early stage



Case (b): Pure non-catalysed hydrolysis reaction



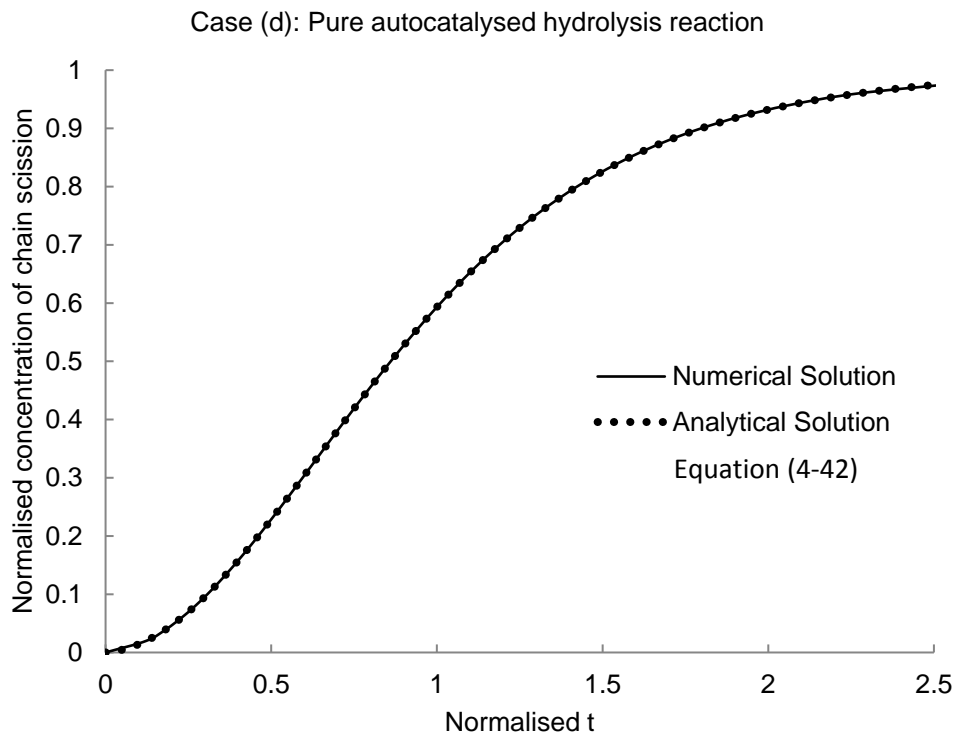
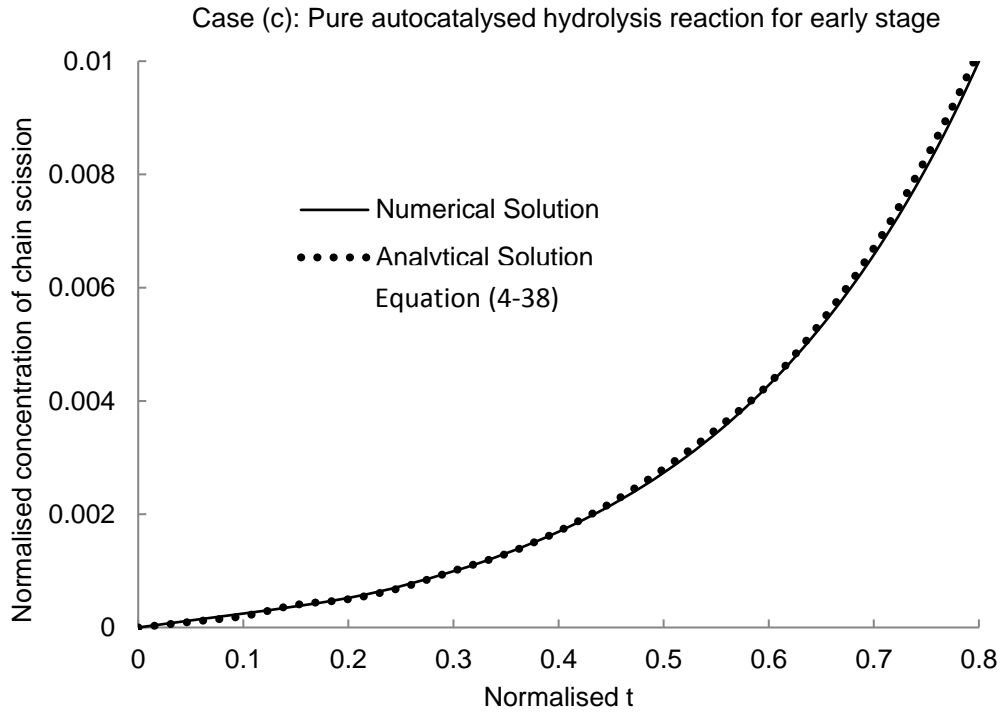


Figure 3: Cross-checking analytical solution with numerical solution for particular cases: (a) pure non-catalysed hydrolysis reaction for early stage; (b) pure non-catalysed hydrolysis reaction; (c) pure auto-catalysed hydrolysis reaction for early stage; (d) pure auto-catalysed hydrolysis reaction.

4.3 A parameterisation study of the master equation

Although the master equation is considered as a general model for amorphous polymer degradation, it is not a simple equation to solve yet, as it contains many value-uncertain parameters. To actually use the master equation in degradation modelling it is necessary to understand the effect of all parameters on the master equation itself and to the degradation model. Some of the parameters do not affect the degradation rate as much as others and the actual value of a few parameters can be fixed empirically to use in the fitting of the experimental data, which can then simplify the master equation and make the mathematical model easier to use for simulating degradation. As shown in the previous section, the advanced master equation of the rate of polymer chain scission is

$$\frac{d\bar{R}_s}{dt} = (1 - \alpha \bar{R}_s^\beta) \left\{ k_1 + \bar{k}_2 \left[\bar{C}_0 + \chi_1 \bar{R}_s + (\chi_2 - \chi_1) \frac{\alpha}{m} \bar{R}_s^\beta \right]^n \right\} \quad (4-27)$$

It contains five sets of parameters, which are:

- n - acid disassociation exponent of the $-\text{COOH}$ groups, which is usually taken as 0.5;
- α, β - oligomer production control parameters that can switch from end or random scissions;
- χ_1, χ_2 - partitioning parameters for the long and short chains to act as catalyst;
- \bar{C}_0 - initial condition of the polymer

$$\bar{C}_0 = \frac{1}{C_{e0}} \left(\chi_1 C_{chain\ 0} + \chi_2 \frac{C_{of0}}{m} \right) \quad (4-28)$$

- k_1, \bar{k}_2 - hydrolysis rate constant for non-catalytic reaction and autocatalytic reaction, respectively.

4.3.1 Effect of \bar{k}_2/k_1

The ratio of \bar{k}_2/k_1 stand for relative rate of autocatalytic hydrolysis with respect to non-catalytic hydrolysis. Fig. 4 gives the molecular weight calculation as functions of time using a range of different parameters. Curve A in the figure represents, in fact,

six different curves, all overlapping each other. This group of curves shares a common ratio of $\bar{k}_2/k_1 = 1$. The numerical calculation therefore shows that, for this ratio of \bar{k}_2/k_1 , changing the values of χ_1 , χ_2 , α , β , and n has no effect on the calculated molecular weight as a function of time. This is because these parameters are all related to autocatalytic hydrolysis, i.e. the second term in equation (4.2). The numerical analysis suggests that when \bar{k}_2/k_1 approaches unity the autocatalytic term can be ignored. Curves B and C in Fig. 4 were obtained using a common ratio of $\bar{k}_2/k_1 = 100$ and two different sets of values of χ_1 , χ_2 , α , β , and n . It can be observed that, at this ratio of \bar{k}_2/k_1 , changing the values of these parameters has a major effect on the results. This suggests that, at this ratio of \bar{k}_2/k_1 , the autocatalytic term in equation (4.2) dominates the hydrolysis reaction. In all the cases, it has been taken that $m = 4$, $\bar{C}_0 = 0$, and $N_{dp0} = 2307$.

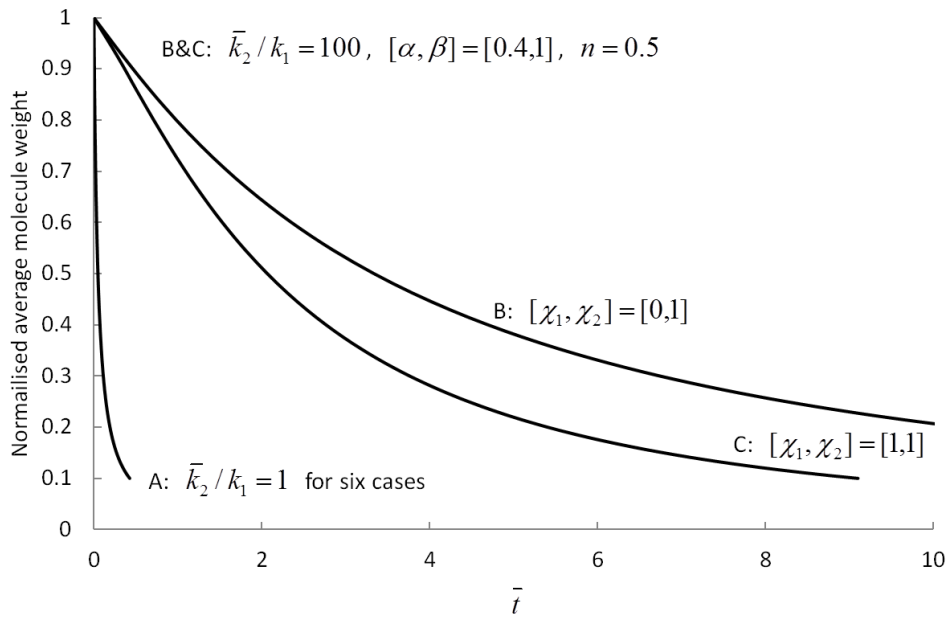


Figure 4: Average molecular weight reduction trend during degradation calculated using different parameters.

Curve A represents a set of six curves that overlap each other using $\bar{k}_2/k_1 = 1$, $[\alpha, \beta] = [0.4, 1], [28, 2], n = [0.1, 0.5]$ and $[\chi_1, \chi_2] = [0, 1], [1, 1]$. Curves B and C are for $\bar{k}_2/k_1 = 100$.

4.3.2 Effect of \bar{C}_0

Basically, \bar{C}_0 shows how many chains that contain the $-\text{COOH}$ end group have been used as catalyst initially. When only short chains work as a catalyst ($\chi_1 = 0, \chi_2 = 1$),

then $\bar{C}_0 = \frac{1}{C_{e0}} \left(\frac{C_{ol0}}{m} \right)$, which means that only the initial number of oligomer chains

in the device work as catalyst at the beginning of the degradation. Similarly, when long chain and short chain combine together to work as catalyst ($\chi_1 = 1, \chi_2 = 1$), then

$\bar{C}_0 = \frac{1}{C_{e0}} \left(C_{chain0} + \frac{C_{ol0}}{m} \right)$, which means that the sum of the initial number of polymer

chains and initial number of oligomer chains combine together to work as catalyst at the beginning of the degradation. Normally, when a medical device has been made,

we consider that it is been made by only long polymer chains, whereas $C_{ol0} = 0$.

However, in reality there are also cases where the device contains oligomer chains before degradation happens. The value of \bar{C}_0 can be measured before degradation.

Normally, we assume it to be 0 (when $\chi_1 = 0, \chi_2 = 1$ and $C_{ol0} = 0$). However, if that is not the case, the effect that different \bar{C}_0 has on the degradation behaviour is presented below.

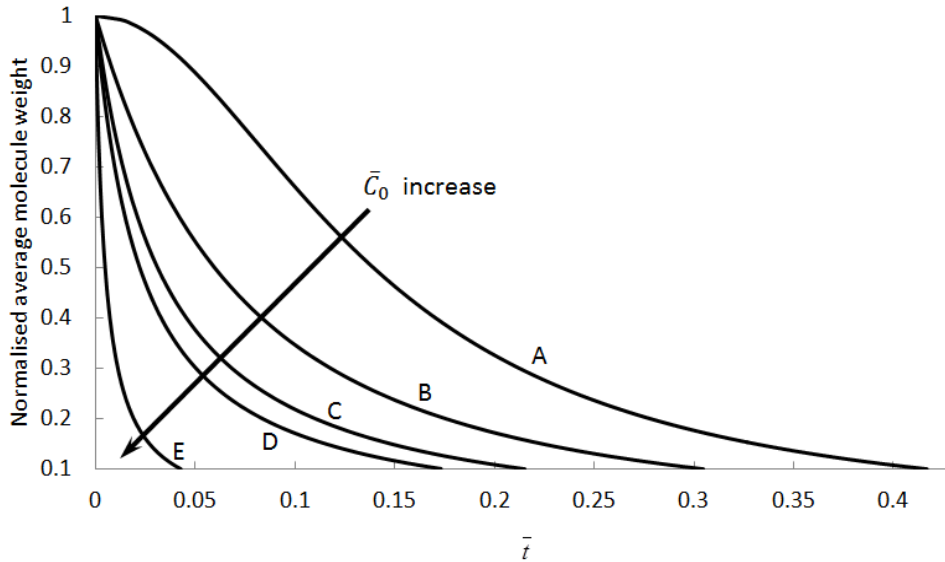


Figure 5: Effect of \bar{C}_0 on the degradation behaviour for pure autocatalytic hydrolysis in cases (A) $\bar{C}_0 = 10^{-10} C_{chain0}/C_{e0}$, (B) $\bar{C}_0 = 0.1 C_{chain0}/C_{e0}$, (C) $\bar{C}_0 = 0.5 C_{chain0}/C_{e0}$, (D) $\bar{C}_0 = C_{chain0}/C_{e0}$ and (E) $\bar{C}_0 = 0.01$. $k_1 = 0$ and $\bar{k}_2 = 1$.

Because the $-\text{COOH}$ end groups are relevant only if the hydrolysis is autocatalytic, let us focus on the case of pure autocatalytic hydrolysis by setting $k_1 = 0$ and $\bar{k}_2 = 1$. Fig. 5 shows that the calculation used a common set of parameters: $m = 4$, $N_{dp0} = 2307$, $\alpha = 0.4$, $\beta = 1$ and $n = 0.5$. If all the chain ends can act as catalysts, then $\bar{C}_0 = C_{chain0}/C_{e0}$, which is case D, shown in Fig. 5. Case A assumes an extremely small value of $\bar{C}_0 = 10^{-10}C_{chain0}/C_{e0}$. Cases B and C represent some moderate values of $\bar{C}_0 = 0.1C_{chain0}/C_{e0}$ and $\bar{C}_0 = 0.5C_{chain0}/C_{e0}$, respectively. Case E represents a very large value of $\bar{C}_0 = 0.01$, which means 1% of ester units act as catalysts for the hydrolysis reaction. It is very clear that an increasing value of \bar{C}_0 changes both the shape of the curve and the rate of the degradation. This is due to the initial catalyst helping the hydrolysis reaction produce more oligomers, which can also work as catalysts. Therefore, average molecule weight will drop hugely at the beginning of the degradation, even with just a small number of \bar{C}_0 .

4.3.3 Effect of α and β

To demonstrate this, Fig. 6 gives calculated average molecular weight reduction trend during degradation for two sets of parameters: case A uses $\alpha = 28$, $\beta = 2$, $k_1 = 1 \times 10^{-4}/\text{week}$ and $\bar{k}_2 = 0.01/\text{week}$ while case B uses $\alpha = 0.4$, $\beta = 1$, $k_1 = 1 \times 10^{-6}/\text{week}$ and $\bar{k}_2 = 0.01/\text{week}$. A common set of parameters - $m = 4$, $\bar{C}_0 = 0$, $N_{dp0} = 2307$, $\chi_1 = 0$, $\chi_2 = 1$ and $n = 0.5$ - were used. The ratios of \bar{k}_2/k_1 in the two cases are big enough for the hydrolysis reaction to be autocatalytic. Consequently, α and β are having a significant effect on the results, which is, however, missing from Fig. 6. The role played by α and β becomes clear in Fig. 7, which shows the calculated amount of short chains produced as functions of time for the two cases. It is apparent that the short chain production is very different for the two cases. It is therefore useful to remember that one cannot uniquely determine the values of α , β , k_1 and \bar{k}_2 from average molecular weight reduction trend during degradation alone. The information about short chain production has to be available in order to determine the values for α and β .

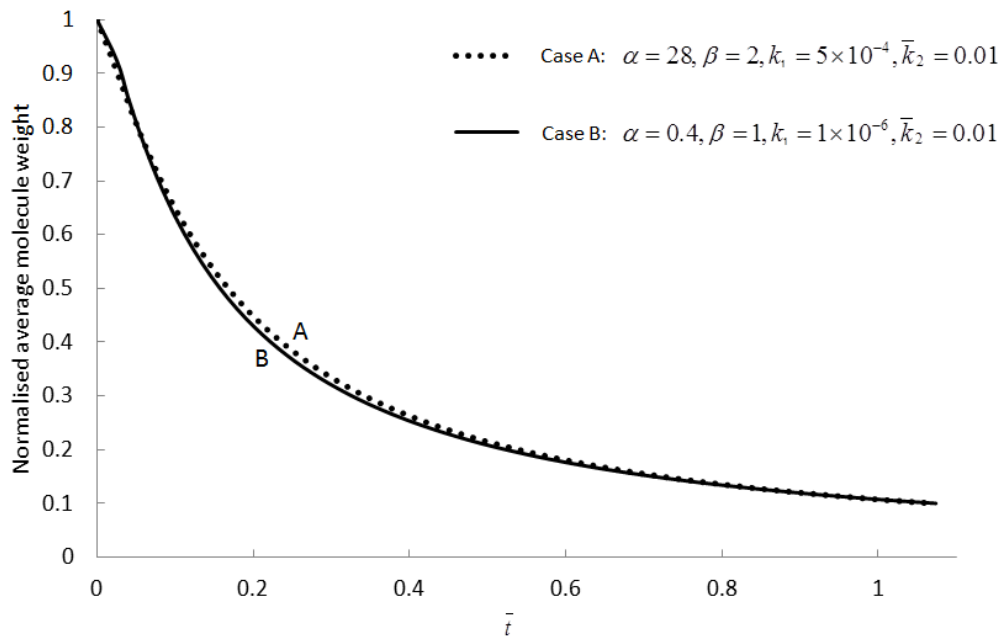


Figure 6: Calculated average molecular weight reduction trend during degradation for two individual sets of parameters

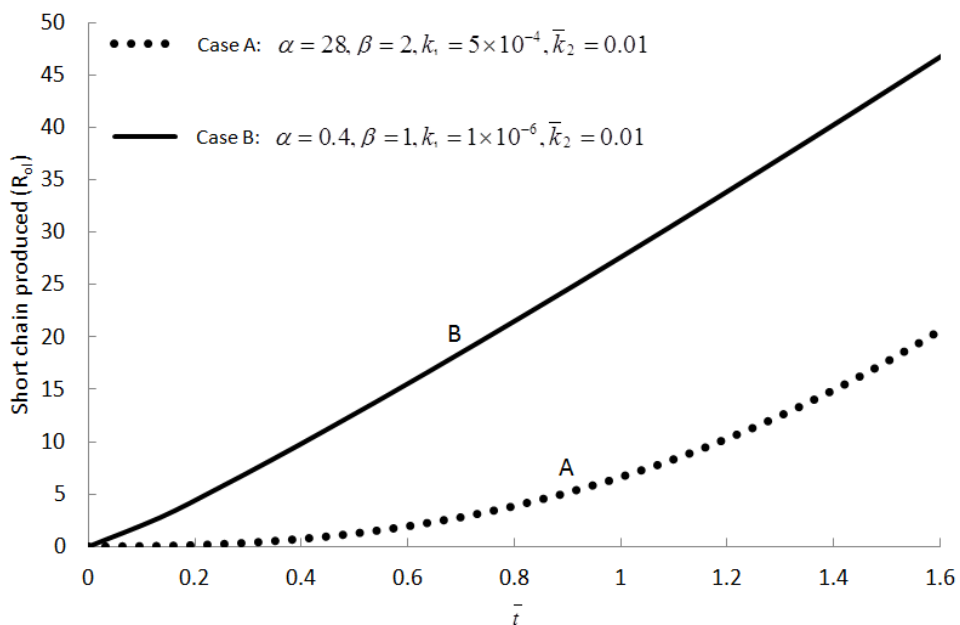


Figure 7: Calculated short chains production by chain scissions during degradation for two individual sets of parameters

4.3.4 Effect of χ_1 and χ_2

χ_1 and χ_2 are introduced in the model to partition the long and short chains. Their effect can be demonstrated by considering the short chain diffusion in the model. Therefore, apply different thickness of a same sample could be used to study the effect of long chain and short chain on degradation. Fig. 8 gives calculated average molecular weight reduction trend during degradation using two different sets of parameters: for case A $\chi_1 = 0, \chi_2 = 1, k_1 = 5 \times 10^{-4}/week$ and $\bar{k}_2 = 5 \times 10^{-5}/week$ and for case B $\chi_1 = 1, \chi_2 = 1, k_1 = 2 \times 10^{-5}/week$ and $\bar{k}_2 = 1.2 \times 10^{-4}/week$. A common set of parameters, $m = 4, \bar{C}_0 = 0, N_{dp0} = 2307, \alpha = 0.4, \beta = 1$ and $n = 0.5$, were used for both cases. The coefficient for short chain diffusion in non-degraded polymer is set as $D_{polymer} = 3.3 \times 10^{-14} m^2 /week$ for both cases. $D_{polymer}$ is the diffusion coefficient for amorphous polymer, which will be fully explained in the following chapters, in this section the parameter is necessary to set just as a constant value. It can be observed from Fig. 8 that the two sets of parameters give almost identical molecular weight as functions of time. These were, however, calculated using a sample thickness of 0.3mm. Fig. 9 shows the calculated results using the same sets of parameters but for a sample thickness of 2mm. Different molecular weight as functions of time can be observed. This demonstrates that in order to uniquely determine the values for χ_1 and χ_2 , one has to obtain experimental data using samples of different thicknesses.

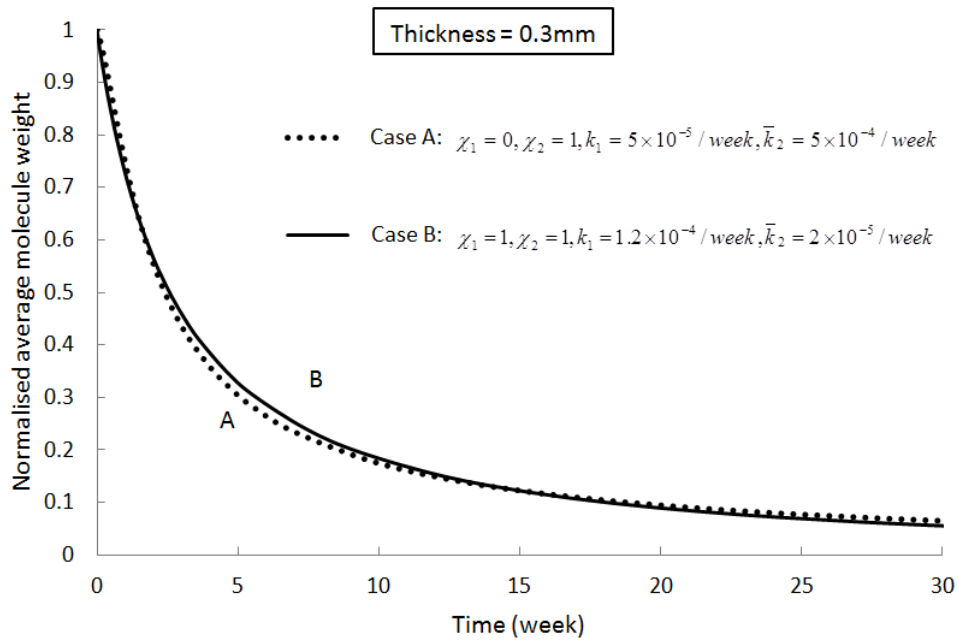


Figure 8: Calculated average molecular weight reduction trend during degradation for two individual sets of parameters showing they give the same prediction for samples with a thickness of 0.3mm.

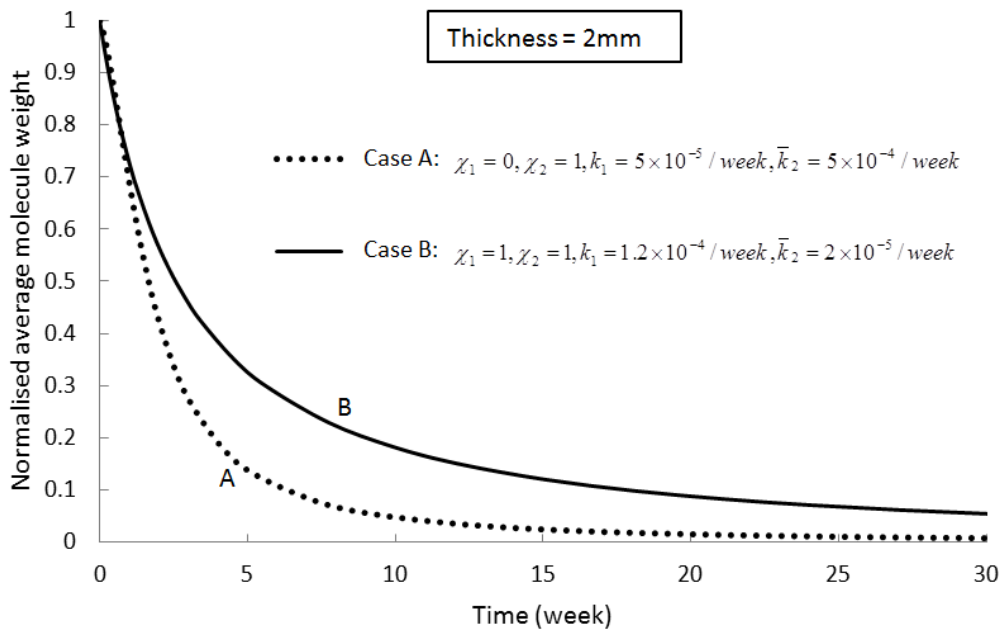


Figure 9: Calculated average molecular weight reduction trend during degradation for two individual sets of parameters identical to those used in Fig. 8 showing they give different predictions for samples with a thickness of 2mm.

From the parametric study, it can be observed that a unique set of parameters cannot be obtained using the average molecular weight test data alone. When one of two of the parameters was changed, the k_1 and \bar{k}_2 values could be changed accordingly to obtain the same trend of average molecular weight reduction as before (see Figs. 6 and 8). Thus, when fitting experimental data, more than one set of parameters can be used to match the same set of experimental data if the mathematical model is used to only simulate the average molecular weight reduction for the experiment. To obtain the uniqueness of a specific parameter, different experimental data need to be applied. For example, to obtain the values for α and β oligomer production data need to be fitted. To study whether short chain alone works as catalysis or long chain and short chain combine together work as catalysis, samples of different thickness need to be examined under exactly the same conditions. Unfortunately, for the current measurement method, oligomers are still very hard to detect, especially for monomers. To obtain oligomer production data experimentally we probably need to wait for a new measurement method to be developed. However, examining the different thicknesses of the sample could be a suggestion to the experimenters. If such experimental data could be found in future literature, the degradation mathematical model could be further developed based on it. Unfortunately, because of the complexities and time-consuming issue of the biodegradable polymers, not a huge amount of experiments has been carried out. Among them, many focused on the average molecular weight reduction; some also looked at other features such as crystallisation, water diffusion, and Young's modulus. It has been demonstrated that, even if the average molecular weight and crystallisation in the experimental data are used simultaneously, more than one set of parameters can still be found to fit this same set of experimental data. More details on this are given in Chapter 6.

Based on the above discussion, some parameters could be given a suggested value based on empirical recommendations. This can reduce the complexity of the formula, so the medical implant designers who wish to use this model as a pre-design tool could use it more easily. The suggested values are given as: 1) $\alpha = 28$ and $\beta = 2$, as random scission is more likely to happen during degradation; 2) $\chi_1 = 0$, $\chi_2 = 1$, as short chains have more move ability, so the contribution they make to the autocatalysis hydrolysis reaction would be considerably higher than that of long chains; 3) $n = 0.5$, as we consider the acid dissociation is in equilibrium; 4) $m = 4$, as the average DP of

oligomers. \bar{C}_0 could be obtained before degradation. That only leaves k_1 , \bar{k}_2 and diffusion coefficient $D_{polymer}$, which will be considered in the next chapter, could be played around with to fit the experimental data or obtain the required design conditions.

4.4 Conclusions

A development of separating long and short polymer chains has been made to the mathematical model that currently exists. This newly developed master equation adds in the different contributions that long and short –COOH chains make as catalyst. Different conditions could be applied to the master equation to reduce it to the previous mathematical equations that were presented in the literature. For example, by setting the two new parameters as $\chi_1 = 0$, $\chi_2 = 1$, the newly developed equation can be reduced to Pan and Han's model (Han, 2011), which has been successfully used to fit many experimental data. Seven cases of analytical solutions were achieved by applying different special conditions. The analytical solutions could be found in the literature under, it has been assumed, the same conditions. It proves that the master equation is the most advanced degradation mathematical equation that covers the majority of factors that affect the degradation. The master equation is more persuasive after successfully cross-checking the numerical solution to its corresponding analytical solution for four particular cases.

To be able to create a user-friendly environment for the medical implant designer who will use the mathematical model, a parametric study has been carried out in this chapter under the assumption of the amorphous phase. A suggested value has been given to some of the parameters in the master equation: $\chi_1 = 0$, $\chi_2 = 1$, (only short chains work as catalyst in degradation); $\alpha, \beta = 28, 2$ (random chain scission); $n = 0.5$ (treat acid disassociation of the carboxylic end groups as equilibrium); $m = 4$ (as the average DP of oligomers). \bar{C}_0 can be measured before degradation. That leaves only \bar{k}_2, k_1 to play around with in the master equation. Diffusion coefficient $D_{polymer}$ was added into the count in the next chapter. Instead of struggling to choose values to a long list of parameters, the designers now only need to adjust three parameters to fit experimental data or achieve the required condition. Moreover, in the case of a known

diffusion rate, the only thing need to do is to give different values of the two parameters to obtain the required data.

The designer who is using the mathematical model is recommended to first try the parameter values listed above. By inputting different \bar{k}_2, k_1 value, the model should be able to fit corresponding experimental data. Although all parameters can take different values under different conditions, it has been proved that by inputting different \bar{k}_2, k_1 the shift caused by changing other parameters can be covered. Furthermore, a suggestion of experimental procedure has been made. Degradation experimental data for the same implant under two different thicknesses would be crucial to find the unique set of parameters for the implant material. This is under the assumption that each biodegradable polymer has a unique set of parameters from which emerges their unique material properties.

Chapter 5: Degradation model including crystallisation, oligomer diffusion and water diffusion

This chapter presents the complete set of governing equations for polymer degradation including crystallisation, oligomer diffusion, and water diffusion for semi-crystalline polymers. These equations are solved to reproduce the degradation maps that were initially proposed by Wang, et al. (2008).

5.1 Introduction

The amorphous phase is very important in the study of biodegradable polymer degradation. However, many biodegradable medical devices currently in use have been produced from semi-crystalline polymers such as poly(L-lactide) (PLLA) and poly(glycolide) (PGA). In such semi-crystalline polymers, amorphous is only one part of the whole construction. We assume that a degrading semi-crystalline polymer has four constituent parts: amorphous long chains, which are not diffusible but can crystallise following cleavage; short chains, which can diffuse out of a device; crystallites, which can exist before degradation or be formed during degradation; water molecules, which cause the polymer chains to cleave. The amorphous phase has been studied in the previous chapter, but crystallites behave very differently to the amorphous polymers. It has been assumed that crystallites are much harder to degrade than in the amorphous phase (Zong, et al., 1999) due to the fact of water molecules being very hard to diffuse into crystallites. Additionally, picked crystallites also have much more mechanical properties than the amorphous polymers. A wide range of research has found that as semi-crystalline degrades, total degree of crystallinity could increase and the total mechanical property of the polymer often increase at the beginning of the degradation as well. This raise has been assumed to be caused by the increase of the degree of crystallinity (Zong, et al., 1999; Tsuji and Ikada, 2000; Tsuji and Muramatsu, 2001). Therefore, studying the growth of degree of crystallinity is very important. In the first part of this chapter, equations of degree of crystallinity and its related rate of chain scission equation have been presented. Additionally, an

oligomer diffusion equation has been included in order to understand the heterogeneous degradation of polymeric devices.

5.2 Degradation equations for semi-crystalline polymers

This section mainly provides a literature review of degradation mathematical equations for semi-crystalline polymers.

5.2.1 Equations for degree of crystallinity

The most widely used classical crystallisation theory was inducted by Avrami (1939, 1940, 1941), and it has been shown to be generally valid for semi-crystalline polymers. In his theory, a concept of extended degree of crystallinity was introduced and a relationship was established between the actual and extended degree of crystallinity. The so-called extended degree of crystallinity is an imaginary volume per unit volume of material that assumes that the crystals can grow freely and could overlap with each other. Therefore, the volume can be bigger than the unity, whereas the actual degree of crystallinity per unit of material volume should never be larger than one. With the assumption that ‘the most probable overlapping fraction is equal to the volume of the existing crystals’, the relationship between the actual and extended degree of crystallinity was presented by Avrami as follows:

$$\frac{dX_c}{dX_{ext}} = 1 - X_c \quad (5-1)$$

in which X_{ext} is the extended volume degree of crystallinity, which is fairly easy to calculate due to crystals growing freely in this imaginary region and every broken chain acting as a potential site of crystallisation. Gleadall (2012) presented a model to calculate the extended degree of crystallinity based on the assumption that a ‘crystallite grows to its full size much faster than chain scission’, also referred to as fast crystal growth. An extended degree of crystallinity could be simply related to number of scission times the average volume of crystallites. Not all chain scissions can lead to crystallites. Using p as a probability that a scission can cause growth of crystallinity

and v_c as average volume of the crystallites, the extended degree of crystallinity can be calculated as follows:

$$X_{ext} = v_c \times (pR_s) = k_c \bar{R}_s \quad (5-2)$$

k_c is new constant which gives

$$k_c = pv_c C_{e0} \quad (5-3)$$

This relationship between actual and extended degree of crystallinity was established purely on a probability argument; no crystal growth mechanism was considered. Therefore, it is necessary to modify it empirically to be able to fit experimental data. For example, the degree of crystallinity in polymers would never reach or near unity, as the amorphous phase still often takes a big count, even in semi-crystalline polymers. So a maximum limit of X_c can be introduced as $X_{c\max}$. An empirical impingement exponent λ is also frequently used in the literature. So the relationship between the actual and extended degree of crystallinity can be shown as (Pan, Chapter 4, 2013):

$$\frac{dX_c}{dX_{ext}} = [X_{c\max} - X_c]^\lambda \quad (5-4)$$

If $\lambda = 1$ and adding equation (5-2), the integration of equation (5-4) gives

$$X_c = X_{c\max} - (X_{c\max} - X_{c0})e^{-k_c \bar{R}_s} \quad (5-5)$$

in which X_{c0} is the degree of crystallinity at the beginning of degradation. If $\lambda \neq 1$ then the integration of equation (5-4) gives

$$X_c = X_{c\max} - \left[(\lambda - 1)k_c \bar{R}_s + (X_{c\max} - X_{c0})^{1-\lambda} \right]^{\frac{1}{1-\lambda}} \quad (5-6)$$

5.2.2 Equations for rate of chain scission

Based on the non-hydrophilicity character, the growth of degree of crystallinity can affect the rate of chain scission thus affecting the degradation rate. Therefore, it is necessary to link the growth of degree of crystallinity back to the rate of chain scission. However, the master equation (4-24) presented in Chapter 4 is a rate of chain scission

equation for amorphous polymers. By using superscript *amp* to represent the amorphous phase, the rate equation can be rewritten as follows:

$$\begin{aligned} \frac{dR_s^{amp}}{dt} &= k_1 C_e^{amp} + k_2' C_e^{amp} C_{H^+}^{amp} \\ &= k_1 C_e^{amp} + k_2 C_e^{amp} \left[\chi_1 \left(C_{\text{chain } 0}^{amp} + R_s^{amp} - \frac{R_{ol}^{amp}}{m} \right) + \chi_2 \frac{C_{ol}^{amp}}{m} \right]^n \end{aligned} \quad (5-7)$$

in which all symbols in equation (5-7) defined previously are now with an assumption of all the concentrations defined over the volume of the amorphous phase of a semi-crystalline polymer. The volume of the amorphous phase decreases with time as the crystalline phase increases in such semi-crystalline polymers. It is more convenient to replace the variables to the ones that define over the whole semi-crystalline polymer volume. For example, using R_s to represent number of scissions over the whole semi-crystalline polymer per unit volume, we have

$$R_s^{am} = \frac{R_s}{1 - X_c} \quad (5-8)$$

Whereas X_c is the volume of crystalline phase per unit volume of the semi-crystalline polymer. Differentiating the equation can give

$$\frac{dR_s}{dt} = (1 - X_c) \frac{dR_s^{am}}{dt} - R_s^{am} \frac{dX_c}{dt} \quad (5-9)$$

The right-hand side second term can be dropped as dX_c / dt has no control for the chain scission rate. Therefore, equation (5-9) now becomes:

$$\frac{dR_s}{dt} = (1 - X_c) \frac{dR_s^{am}}{dt} \quad (5-10)$$

If applying the similar transformation as equation (5-8) to all the other symbols in equation (5-7) and applying them into equation (5-10), the rate of scission equation over the whole volume of the semi-crystalline polymer can now be rewritten as (Han and Pan, 2009):

$$\frac{dR_s}{dt} = C_{e0} \psi(R_s) \left\{ k_1 + k_2 C_{e0}^n \left[\left(\chi_1 \varphi(R_s) + \frac{\chi_2}{m} \left(\frac{C_{ol}}{C_{e0}} \right) \right) \frac{1}{1 - X_c} \right]^n \right\} \quad (5-11)$$

in which

$$\psi(R_s) = 1 - \alpha \left(\frac{R_s}{C_{e0}} \right)^\beta - \frac{\omega}{C_{e0}} (X_c - X_{c0}) \quad (5-12)$$

$$\varphi(R_s) = \frac{C_{\text{chain } 0}}{C_{e0}} + \frac{R_s}{C_{e0}} - \frac{\alpha}{m} \left(\frac{R_s}{C_{e0}} \right)^\beta \quad (5-13)$$

C_{e0} represents the number of ester units of amorphous long chains per unit volume of the semi-crystalline polymer at the beginning of degradation, ω is the number of ester units per unit volume of the crystalline phase, and X_{c0} is the initial degree of crystallinity.

All variables in equation (5-11, 12, 13) are now defined over the whole volume of the semi-crystalline polymer.

5.2.3 Equations for number-average molecular weight

The semi-crystalline polymers number-average molecular weight can be calculated as all chains total weight of in amorphous and crystalline phases over the total number of polymer chains. If we assume all long chains and short chains are counted and there is no diffusion, then average molecular weight will be

$$M_n = \frac{(C_{e0} + \omega X_{c0}) M_{\text{unit}}}{N_{\text{chain } 0} + R_s} \quad (5-14)$$

The initial molecular weight is given by

$$M_{n0} = \frac{(C_{e0} + \omega X_{c0}) M_{\text{unit}}}{N_{\text{chain } 0}} \quad (5-15)$$

Equation (5-14) can be written into a normalised format as

$$\frac{\overline{M}_n}{M_{n0}} = \frac{M_n}{M_{n0}} = \frac{1}{1 + \frac{C_{e0}}{N_{\text{chain } 0}} \frac{R_s}{M_{n0}}} \quad (5-16)$$

Equation (5-16) and equation (4-15) are similar, except that here C_{e0} is the initial number of ester units of long chains of the amorphous phase per unit of volume and

$N_{chain\ 0}$ is the total number of the entire polymer chains, including the crystalline phase. $C_{e0} / N_{chain\ 0}$ is therefore no longer the degree of polymerisation of the polymer (Pan, Chapter 4, 2013).

If not counting the short chains in an average molecular calculation then the equation is given as follows:

$$M_n = \frac{(C_{e0} + \omega X_{c0} - R_{ol})M_{unit}}{N_{chain\ 0} + R_s - (R_{ol}/m)} = \frac{\left[C_{e0} + \omega X_{c0} - \alpha C_{e0} \left(\frac{R_s}{C_{e0}} \right)^\beta \right] M_{unit}}{N_{chain\ 0} + R_s - \frac{\alpha}{m} C_{e0} \left(\frac{R_s}{C_{e0}} \right)^\beta} \quad (5-17)$$

Whereas the total number of long chain ester units and number of long chains both decrease with the production of short chains.

If assuming that there are no short chains initially, the initial molecular weight is given by equation (5-15). The molecular weight equation can be normalised as

$$\frac{\bar{M}_n}{M_{n0}} = \frac{M_n}{M_{n0}} = \frac{1 + \bar{\omega} X_{c0} - \alpha \bar{R}_s^\beta}{(1 + \bar{\omega} X_{c0}) \left[1 + \frac{C_{e0}}{N_{chain\ 0}} \left(\bar{R}_s - \frac{\alpha}{m} \bar{R}_s^\beta \right) \right]} \quad (5-18)$$

Whereas $\bar{\omega} = \omega / C_{e0}$, the number of ester units per unit volume of crystalline phase is normalised by C_{e0} ; $\bar{R}_s = R_s / C_{e0}$, the number of chain scissions per unit volume is normalised by C_{e0} . All other parameters were previously defined in this section.

5.3 Diffusion equations and a collection of governing equations for semi-crystalline polymers

In this section, diffusion equations of short polymer chains have been presented. Governing equations were then collected to form a completed mathematical model that can be used to simulate degradation for semi-crystalline polymers and fit experimental data. This section has been included in the book edited by Pan (Pan and Chen, Chapter 6, 2016).

In the previous chapters, it has been assumed that the diffusion of short chains is prohibited, and consequently

$$C_{ol} = C_{ol0} + R_{ol} \quad (4-25)$$

whereas C_{ol0} represents the concentration of residual short chains at the beginning of degradation. Equation (4-25) is no longer valid when the short chains can diffuse, therefore, C_{ol} in equation (5-11) will be subject to change by diffusion.

5.3.1 Diffusion equation for short chains

Wang, et al. (2008) and Han and Pan (2009) introduced a diffusion equation into the degradation model. Fig. 10 illustrates diffusion of the short chains using an infinitively large plate placed in an aqueous media as an example. In Fig. 10(a), a rectangular unit of the plate is isolated. The left and right surfaces are exposed to the aqueous media and all the other surfaces can be considered as symmetry plans. Because of symmetry, diffusion only been assumed to happen in x direction, which is the thickness direction. Fig. 10(b) shows the section highlighted in Fig. 10(a) and distributions of the short chains in the plate. At the beginning, the short chains are generated everywhere in the plate and dissolve into the media off the left and right surfaces. As chain scission proceeds, more and more short chains are generated while some of them diffuse into the aqueous media. The concentration of short chains at the core of the plate reaches a peak value at some inter-medium time of the degradation. Toward the end of the degradation, a large number of long chains have been turned into short ones and diffused out.

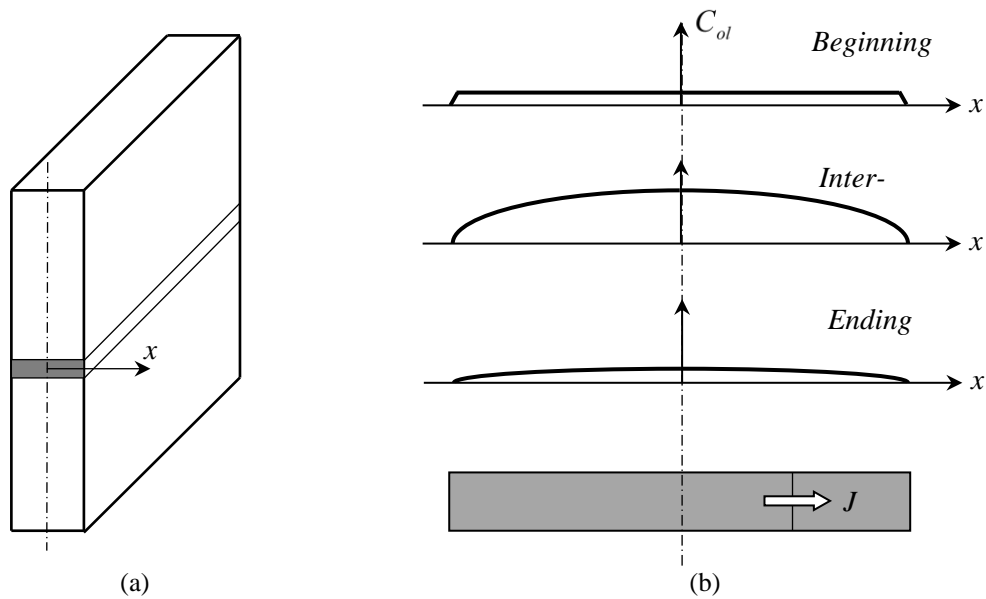


Figure 10: Short chain diffusion in a plate showing distributions of short chain concentration over thickness of the plate at different stages of degradation.

A diffusion flux, J , is defined as the number of ester units of short chains passing through unit area per unit time, as illustrated in Fig. 10(b). The driving force for the chain diffusion is the gradient of concentration, dC_{ol} / dx . Fick's diffusion law assumes that

$$J = -D \frac{dC_{ol}}{dx} \quad (5-19)$$

in which D is the diffusion coefficient. The minus sign is because chains diffuse from where their concentration is high to where it is low. Fick's law has been widely used because of its simplicity and its ability to capture the general trend observed in experiments. More sophisticated diffusion laws are sometime necessary, which no longer poses any problem because modern numerical methods, such as the finite element method, can deal with any diffusion law conveniently. Assuming D is isotropic and diffusion due to entropy and small deformation. Diffusion only happens in the direction of the thickness in this case.

At any location, x , the change in the concentration of short chains comes from two contributions: (a) production of short chains due to chain scissions at that location; and (b) deposit or removal of chains from this location by diffusion. (a) can be calculated by differentiating equation (4-7) as

$$\frac{dR_{ol}}{dt} = \alpha\beta \left(\frac{R_s}{C_{e0}} \right)^{\beta-1} \frac{dR_s}{dt} \quad (5-20)$$

To calculate (b) let us consider a small section, Δx , along the diffusion route, as illustrated in Fig. 11. In the figure, $J(x)$ and $J(x + \Delta x)$ represent diffusion flux entering and leaving the section, respectively. If $J(x) > J(x + \Delta x)$, then short chains are deposited on the small section and if $J(x) < J(x + \Delta x)$, then short chains are removed from the section, both of which lead to a change in the concentration of short chains in the section.

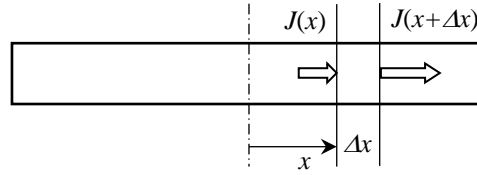


Figure 11: Removing or depositing short chains due to difference in the diffusion flux J on either sides of a small section.

The changing rate of the concentration can be calculated from the following statement of matter conservation:

$$J(x) - J(x + \Delta x) = \Delta x \times \left(\frac{dC_{ol}}{dt} \right)_{diffusion} \quad (5-21)$$

For a very small Δx , equation (5-21) can be written as

$$\left(\frac{dC_{ol}}{dt} \right)_{diffusion} = - \frac{dJ}{dx} \quad (5-22)$$

The total change in concentration is given by the summation of the short chain production due to chain scission and the change due to diffusion, i.e. we have

$$\frac{dC_{ol}}{dt} = \frac{dR_{ol}}{dt} - \frac{dJ}{dx} \quad (5-23)$$

Put equation (5-19) and (5-20) in equation (5-23) gives

$$\frac{dC_{ol}}{dt} = \alpha\beta \left(\frac{R_s}{C_{e0}} \right)^{\beta-1} \frac{dR_s}{dt} + \frac{d}{dx} \left(D \frac{dC_{ol}}{dx} \right) \quad (5-24)$$

For a general three-dimensional device, such as a screw or scaffold, using x_1 , x_2 , and x_3 to represent the three coordinates in the space, equation (5-18) can be expanded as

$$J_1 = -D \frac{\partial C_{ol}}{\partial x_1}, \quad J_2 = -D \frac{\partial C_{ol}}{\partial x_2}, \quad J_3 = -D \frac{\partial C_{ol}}{\partial x_3} \quad (5-25, 26, 27)$$

in which J_1 , J_2 and J_3 represent diffusion fluxes in the three directions, respectively.

Equation (5-23) can be expanded as

$$\frac{dC_{ol}}{dt} = \frac{dR_{ol}}{dt} - \left(\frac{\partial J_1}{\partial x_1} + \frac{\partial J_2}{\partial x_2} + \frac{\partial J_3}{\partial x_3} \right) \quad (5-28)$$

Substituting equations (5-20) and (5-25, 26, 27) into equation (5-28) gives

$$\frac{dC_{ol}}{dt} = \alpha\beta \left(\frac{R_s}{C_{e0}} \right)^{\beta-1} \frac{dR_s}{dt} + \frac{\partial}{\partial x_1} \left(D \frac{\partial C_{ol}}{\partial x_1} \right) + \frac{\partial}{\partial x_2} \left(D \frac{\partial C_{ol}}{\partial x_2} \right) + \frac{\partial}{\partial x_3} \left(D \frac{\partial C_{ol}}{\partial x_3} \right) \quad (5-29)$$

This type of equation is referred to as a reaction-diffusion equation in the literature.

5.3.2 Collection of the governing equations for semi-crystalline polymers

All mathematical equations that would need to be implanted into finite element software in order to provide the degradation simulation are listed below. The equations could be used to fit experimental data and provide further understanding of degradation behaviour. Only governing equations for semi-crystalline polymers have been listed below as they are commonly existing polymers, and amorphous polymers governing equations could be achieved from these equations by setting $X_c = 0$ and $X_{c\max} = 0$.

The governing equation for rate of chain scission for semi-crystalline polymers is

$$\frac{dR_s}{dt} = C_{e0} \psi(R_s) \left\{ k_1 + k_2 C_{e0}^n \left[\left(\chi_1 \varphi(R_s) + \frac{\chi_2}{m} \left(\frac{C_{ol}}{C_{e0}} \right) \right) \frac{1}{1 - X_c} \right]^n \right\} \quad (5-11)$$

in which

$$\psi(R_s) = 1 - \alpha \left(\frac{R_s}{C_{e0}} \right)^\beta - \frac{\omega}{C_{e0}} (X_c - X_{c0}) \quad (5-12)$$

$$\varphi(R_s) = \frac{C_{chain\ 0}}{C_{e0}} + \frac{R_s}{C_{e0}} - \frac{\alpha}{m} \left(\frac{R_s}{C_{e0}} \right)^\beta \quad (5-13)$$

Short chain diffusion equation is

$$\frac{dC_{ol}}{dt} = \alpha \beta \left(\frac{R_s}{C_{e0}} \right)^{\beta-1} \frac{dR_s}{dt} + \sum_{i=1}^3 \frac{\partial}{\partial x_i} \left(D \frac{\partial C_{ol}}{\partial x_i} \right) \quad (5-29)$$

Degree of crystallinity equations are

$$X_c = \begin{cases} X_{c\ max} - (X_{c\ max} - X_{c0}) e^{-k_c \left(\frac{R_s}{C_{e0}} \right)}, & \lambda = 1 \\ X_{c\ max} - \left[(\lambda - 1) k_c \left(\frac{R_s}{C_{e0}} \right) + (X_{c\ max} - X_{c0})^{1-\lambda} \right]^{\frac{1}{1-\lambda}}, & \lambda \neq 1 \end{cases} \quad (5-5, 5-6)$$

Equations (5-11) and (5-29) are subject to the following initial conditions: $R_s = 0$, $C_{ol} = C_{ol0}$ at $t = 0$, and boundary condition $C_{ol} = 0$ at device surface.

A semi-crystalline polymer which is under degradation can be considered for two-phase material made of a polymer phase and a porosity phase. According to Jiang, et al., the diffusion coefficient D can be related to porosity V_{pore} through

$$D = D_{matrix} + (1.3V_{pore}^2 - 0.3V_{pore}^3) (D_{pore} - D_{matrix}) \quad (5-30)$$

in which

$$V_{pore} = (1 - X_{c0}) \left[\alpha \left(\frac{R_s}{C_{e0}} \right)^\beta - \frac{C_{ol} - C_{ol0}}{C_{e0}} \right] \quad (5-31)$$

and D_{matrix} is diffusion coefficient of the semi-crystalline matrix. The semi-crystalline matrix can also be considered as a two-phase material made of an amorphous phase as well as a crystalline part. The crystalline part of the polymer has diffusion coefficient which is very small and could take as zero. Again, according to Jiang, et al., D_{matrix} can be calculated as

$$D_{matrix} = \left(1.3V_{am}^2 - 0.3V_{am}^3\right)D_{polymer} \quad (5-32)$$

whereas $D_{polymer}$ is diffusion coefficient of short chains in non-degraded amorphous polymer and

$$V_{am} = \frac{1 - V_{pore} - X_c}{1 - V_{pore}} \quad (5-33)$$

The average molecular weight at any location can be calculated using equation

$$\overline{M}_n = \frac{M_n}{M_{n0}} = \frac{1 + \overline{\omega} X_{c0} - \alpha \overline{R}_s^\beta}{(1 + \overline{\omega} X_{c0}) \left[1 + \frac{C_{e0}}{N_{chain\ 0}} \left(\overline{R}_s - \frac{\alpha}{m} \overline{R}_s^\beta \right) \right]} \quad (5-18)$$

in which $\overline{R}_s = R_s / C_{e0}$ and $\overline{\omega} = \omega / C_{e0}$.

For thin samples used in most degradation experiments, the diffusion of short chains only happens in one direction which is the thickness of the sample. In such cases, the governing equation can be solved either analytically, using a weighted residual method (Wang, et al., 2008), or numerically, using a finite difference method (Han and Pan, 2011). For general three-dimensional devices, however, the equations have to be solved by finite element method.

All the symbols used in the governing equations are grouped and listed below.

(I) Variables that depend on time t and location (x_1, x_2, x_3) and need to be found by solving the governing equations:

- R_s – number of chain scissions per unit volume;
- C_{ol} - number of ester units of short chains per unit volume;

- X_c – volume percentage of crystalline phase;
- M_n – number averaged molecular weight;

Only R_s and C_{ol} are independent variables.

(II) Parameters that describe polymer properties:

- C_{e0} – initial number of ester units of long chains in amorphous phase per unit volume;
- $C_{chain\ 0}$ – initial number of amorphous chains per unit volume;
- $N_{chain\ 0}$ – initial number of polymer chains, including the crystalline phase, per unit volume;
- $N_{dp\ 0}$ – initial average degree of polymerisation of amorphous polymers;
- $C_{ol\ 0}$ – initial number of ester units of residual short chains per unit volume;
- M_{n0} – initial number averaged molecular weight;
- X_{c0} – initial volume degree of crystallinity;
- $X_{c\ max}$ – maximum volume degree of crystallinity;
- ω – number of ester units of crystalline phase per unit volume.

(III) Empirical parameters:

- α , β – empirical parameters for short chain production;
- χ_1 , χ_2 – partitioning parameters for –COOH groups on long and short chains;
- m – average degree of polymerisation of short chains, usually set as four.

(VI) Kinetic parameters:

For amorphous polymers:

- n – exponent for acid dissociation of –COOH end groups, usually taken as 0.5
- k_1 – rate constant of non-catalytic reaction;

- k_2 – rate constant of autocatalytic reaction;
- $D_{polymer}$ – diffusion coefficient of short chains in non-degraded amorphous polymer;
- D_{pore} – diffusion coefficient of short chains in liquid-filled pores.

For semi-crystalline polymers, add:

- λ – impingement exponent for crystal growth;
- $k_c = p v_c C_{e0}$ – in which p is the probability for a cleaved chain to form a crystallite and v_c is the average size of the crystallites.

5.4 Non-dimensionalisation and degradation map

The governing equations were normalised. The non-dimensional equations were used to study the different behaviours of degradations through a ‘degradation map’, which was first developed by Wang, et al. (2008). However, Wang, et al. (2008) used an over-simplified model for degradation, which only assumed degradation through end scission. The purpose here is to use the newly developed equation to reconfirm the degradation map published previously. The concept of the degradation map is presented here as a recalculation of Wang’s work. Furthermore, the effect of other factors on the degradation map is also developed. This section has been included in the book edited by Pan (Pan and Chen, Chapter 6, 2016). In which equations, figs and data fittings are contributed by writer.

For a simple device, such as a plate or a pin, it is possible to graphically illustrate the conditions that lead to different behaviours of degradation using the degradation map. These conditions also indicate when the diffusion of the short chains can be ignored in the mathematical model. If the short chain diffusion can be ignored, then the analytical or numerical solutions provided in Chapter 4 can be used. The governing equations in Section 5.3 contain quite a few parameters. By performing a non-dimensionalisation exercise, it is possible to identify two non-dimensional groups of these parameters that control the degradation behaviour. The thickness of the plate, or the diameter of the

pin, is one of the key parameters in the analysis. However, it is often possible to identify a characteristic diffusion distance (the outer diameter of a screw, for example) to replace the plate thickness or pin diameter in the following analysis. This, then, allows the degradation map to be used for general devices as a rough guide on whether short chain diffusion can be ignored.

5.4.1 Non-dimensionalisation of governing equations

Considering a very large plate, as illustrated in Fig. 10, that has a thickness l and is made of an amorphous polymer, the governing equations (4-24) and (5-29) can be rearranged as following without changing them:

$$\frac{d\left(\frac{R_s}{C_{e0}}\right)}{d(tk_2C_{e0}^n)} = \psi(R_s) \left\{ \frac{k_1}{k_2C_{e0}^n} + \left[\chi_1\varphi(R_s) + \frac{\chi_2}{m} \left(\frac{C_{ol}}{C_{e0}}\right) \right]^n \right\} \quad (5-34)$$

and

$$\frac{d\left(\frac{C_{ol}}{C_{e0}}\right)}{d(tk_2C_{e0}^n)} = \alpha\beta \left(\frac{R_s}{C_{e0}}\right)^{\beta-1} \frac{d\left(\frac{R_s}{C_{e0}}\right)}{d(tk_2C_{e0}^n)} + \frac{\partial}{\partial\left(\frac{x}{l}\right)} \left\{ \frac{D}{l^2k_2C_{e0}^n} \frac{\partial\left(\frac{C_{ol}}{C_{e0}}\right)}{\partial\left(\frac{x}{l}\right)} \right\} \quad (5-35)$$

Whereas

$$\psi(R_s) = 1 - \alpha \left(\frac{R_s}{C_{e0}}\right)^\beta \quad (5-36)$$

and

$$\varphi(R_s) = \frac{C_{chain\ 0}}{C_{e0}} + \frac{R_s}{C_{e0}} - \frac{\alpha}{m} \left(\frac{R_s}{C_{e0}}\right)^\beta \quad (5-13)$$

Such rearrangement is not unique and can be chosen as different parameters to normalise the equations. Here, all the concentrations are normalised by C_{e0} and all the lengths are normalised by the thickness of the plate. These are rather obvious choices of normalisation. Furthermore, both sides of the equations are divided by $k_2C_{e0}^n$. This

is because we chose to use the rate of autocatalytic hydrolysis as a reference for the rates of diffusion and non-catalytic hydrolysis. This is a sensible choice because autocatalytic hydrolysis is assumed to always occur in the polymers that are considered in this thesis, while diffusion and non-catalytic hydrolysis may or may not be important, depending on the device and polymers.

Defining the following non-dimensional variables (Wang, et al., 2008)

$$\bar{R}_s = \frac{R_s}{C_{e0}}, \bar{C}_{ol} = \frac{C_{ol}}{C_{e0}}, \bar{t} = k_2 C_{e0}^n t, \bar{x} = \frac{x}{l} \quad (5-37, 38, 39, 40)$$

and kinetic parameters

$$\bar{k}_1 = \frac{k_1}{k_2 C_{e0}^n}, \quad (5-41)$$

$$\bar{D} = \bar{D}_{polymer} + (1.3V_{pore}^2 - 0.3V_{pore}^3)(\bar{D}_{pore} - \bar{D}_{polymer}) \quad (5-42)$$

in which

$$\bar{D}_{polymer} = \frac{D_{polymer}}{k_2 C_{e0}^n l^2}, \bar{D}_{pore} = \frac{D_{pore}}{k_2 C_{e0}^n l^2} \quad (5-43, 44)$$

the governing equations can be non-dimensionalised as

$$\frac{d\bar{R}_s}{d\bar{t}} = \psi(\bar{R}_s) \left\{ \bar{k}_1 + \left[\chi_1 \varphi(\bar{R}_s) + \frac{\chi_2 \bar{C}_{ol}}{m} \right]^n \right\} \quad (5-45)$$

and

$$\frac{d\bar{C}_{ol}}{d\bar{t}} = \alpha \beta \bar{R}_s^{\beta-1} \frac{d\bar{R}_s}{d\bar{t}} + \frac{\partial}{\partial \bar{x}} \left(\bar{D} \frac{\partial \bar{C}_{ol}}{\partial \bar{x}} \right) \quad (5-46)$$

There are four kinetic parameters in the non-dimensionalised equations: n , \bar{k}_1 , $\bar{D}_{polymer}$, and \bar{D}_{pore} . The acid dissociation exponent n usually takes the value of 0.5. \bar{D}_{pore} reflects the diffusion rate of short chains in liquid and can be set as a value much larger than $\bar{D}_{polymer}$. The remaining two parameters, $\bar{D}_{polymer}$ and \bar{k}_1 , control the degradation behaviour of the plate. \bar{k}_1 reflects the non-catalytic hydrolysis rate relative to the autocatalytic hydrolysis rate. The larger \bar{k}_1 is, the faster the non-catalytic hydrolysis is

in comparison with the autocatalytic hydrolysis. $\bar{D}_{polymer}$ reflects the diffusion rate of short chains in non-degraded polymer relative to the autocatalytic hydrolysis rate. It also includes the effect of the thickness of the plate. The effect of a faster diffusion, thinner plate, or slower autocatalytic hydrolysis is equivalent as long as $\bar{D}_{polymer}$ remains the same.

5.4.2 Degradation map

Considering a very large plate, as shown in Fig. 10, the effect of changing $\bar{D}_{polymer}$ on the degradation behaviour of the plate is computed by solving equations (5-44) and (5-45) numerically. Fig. 12 shows the effect of changing $\bar{D}_{polymer}$ on molecular weight \bar{M}_n at $\bar{t} = 27$ for a fixed value of $\bar{k}_1 = 0.001$.

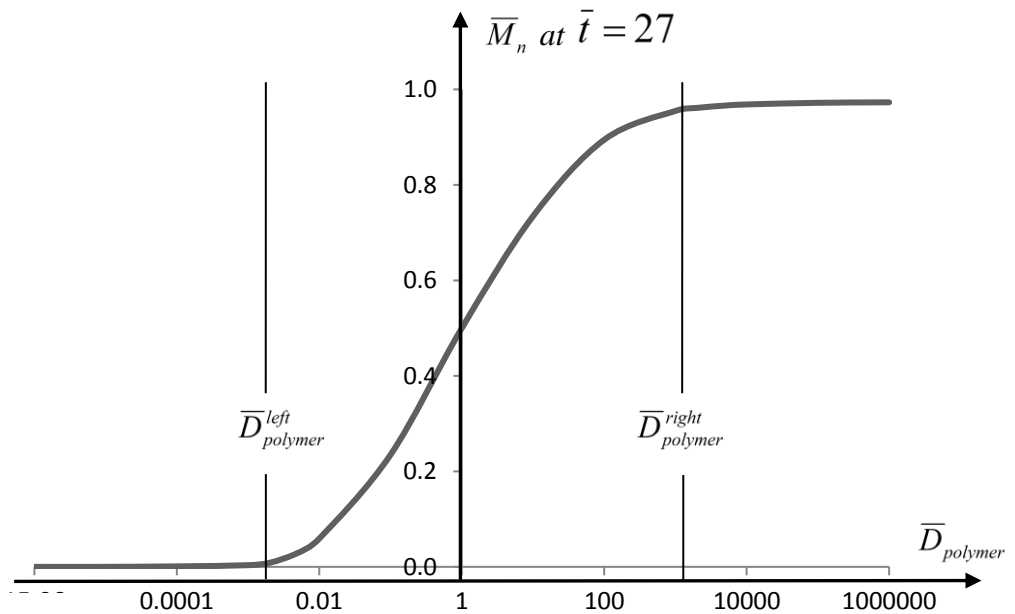


Figure 12: Molecular weight (vertical axis) averaged across the plate at $\bar{t} = 27$ as a function of $\bar{D}_{polymer}$ (horizontal axis). $\bar{k}_1 = 0.001$.

The choice of $\bar{t} = 27$ is arbitrary and will be discussed later. The average molecular weight in the plate is a function of x as marked in Fig. 10. The value of \bar{M}_n shown in Fig. 12 is calculated by averaging the molecular weight across the thickness of the

plate. Observing the very left section of the curve in Fig. 12, it can be seen that if $\bar{D}_{polymer}$ is very small, then \bar{M}_n has already reached zero at $\bar{t} = 27$. This means that if either the diffusion is very slow or the plate is very thick, degradation is fast because the short chains accumulate inside the plate and generate an acidic environment. Moving from the left to the right, as $\bar{D}_{polymer}$ gradually increases, so \bar{M}_n at $\bar{t} = 27$ also increases. This indicates that degradation is slowed down by the diffusion process. At the very right section, where either diffusion is very fast or the plate is very thin, the plate degrades very slowly because the short chains can leave the plate quickly. It is interesting to observe that \bar{M}_n does not change with $\bar{D}_{polymer}$ on either the very left section or the very right section. Two thresholds, referred to as $\bar{D}_{polymer}^{left}$ and $\bar{D}_{polymer}^{right}$, as shown in the figure, can be identified such that \bar{M}_n only changes with $\bar{D}_{polymer}$ if $\bar{D}_{polymer}^{left} < \bar{D}_{polymer} < \bar{D}_{polymer}^{right}$.

Choosing a different value for \bar{t} does not affect the values of $\bar{D}_{polymer}^{left}$ and $\bar{D}_{polymer}^{right}$. However, if \bar{t} is set at a too large a value, \bar{M}_n would be almost zero at this time for all values of $\bar{D}_{polymer}$. If \bar{t} is set at a too small a value, \bar{M}_n would not have changed very much at this time for all values of $\bar{D}_{polymer}$. Consequently, such choices of \bar{t} would make the identification of $\bar{D}_{polymer}^{left}$ and $\bar{D}_{polymer}^{right}$ difficult.

It is expected that the values of $\bar{D}_{polymer}^{left}$ and $\bar{D}_{polymer}^{right}$ depend on \bar{k}_1 . To account for the effect of \bar{k}_1 , the above calculation was repeated for a wide range of values of \bar{k}_1 and the numerical results are graphically presented using a degradation map, as shown in Fig. 14. The vertical axis of the map represents $\bar{D}_{polymer}$ and the horizontal axis represents \bar{k}_1 . The bottom part of the map represents the curve on the left side in Fig. 14 and the top part of the map represents the curve on the right side. For any fixed value of \bar{k}_1 , regions C, A, and B on the map correspond to the left flat section, the middle ascending section, and the right flat section of the curve, respectively. The boundary between regions C and A corresponds to $\bar{D}_{polymer}^{left}$ and the boundary between regions A and B corresponds to $\bar{D}_{polymer}^{right}$.

The top zone B represents where $\bar{D}_{polymer}$ is large, which means either diffusion is fast or the plate is very thin. Under these conditions, the short chains cannot remain inside the plate long enough to act as catalyst for the hydrolysis reaction. The polymer degrades at the non-catalytic rate and the degradation of the plate is uniform. Above the boundary between zones A and B , further increasing of $\bar{D}_{polymer}$ (by reducing the thickness, for example) cannot change the degradation rate. An interesting numerical result is that this boundary, i.e. $\bar{D}_{polymer}^{right}$, is very weakly affected by \bar{k}_1 and located at approximately $\bar{D}_{polymer}^{right} = 1000$. The absolute location of the boundary is, however, fuzzy because the curve in Fig. 14 shows a gradual transition between the two zones. Rearranging equation (5-42) gives

$$l_{th} = \sqrt{\frac{D_{polymer}}{D_{polymer}^{right} k_2 C_{e0}^n}} \approx \sqrt{\frac{D_{polymer}}{1000 k_2 C_{e0}^n}} \quad (5-46)$$

where l_{th} is a threshold for the thickness of the plate under which the degradation rate is no longer affected by the thickness. Equation (5-46) indicates that the faster the short chain diffusion or the slower the autocatalytic hydrolysis, the larger l_{th} becomes.

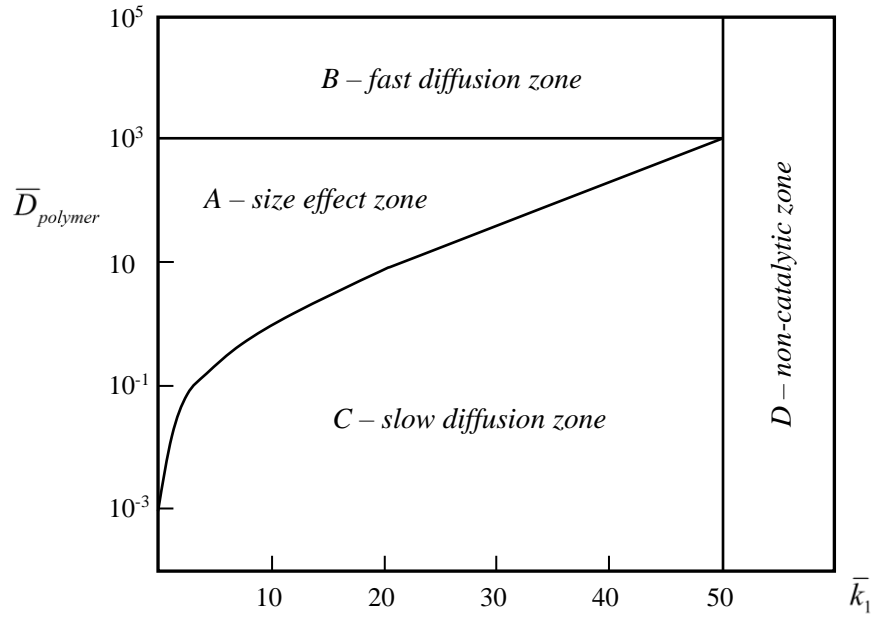


Figure 14: Degradation map showing different behaviours of degradation of an infinitely large plate controlled by $\bar{D}_{polymer}$ and \bar{k}_1 . Other parameters used in

the calculation are $\alpha = 1$, $\beta = 1$, $\chi_1 = 0$, $\chi_2 = 1$, $m = 4$, $n = 0.5$,

$$\bar{D}_{pore} = 1000 \bar{D}_{polymer}, N_{dp0} = 2307 \text{ and } C_{ol0} = 0.$$

Source: Original version obtained from Wang, et al. (2008). Recalculation has been done to provide the result.

In zone C, $\bar{D}_{polymer}$ is small, although the definition of “small” depends on \bar{k}_1 . In this zone, despite the fact that short chains near the surface of the plate diffuse into the aqueous media, the effect remains local to the surface layer throughout the lifetime of the plate and does not affect its overall degradation rate. Degradation of the plate is heterogeneous and a hard skin can be expected to form while the inside degrades faster due to the acidic environment. It is interesting to note that \bar{k}_1 has a significant effect on the upper boundary of this region. The larger the \bar{k}_1 , the easier it is for a plate to enter this zone from zone A.

The right zone D is where \bar{k}_1 is very large and the hydrolysis is dominantly non-catalytic. In this zone, diffusion of the short chains plays no role in the degradation rate; the plate degrades uniformly and the concept of a threshold thickness does not

exist. The numerical results show that the boundary between zone D and other zones is located at $\bar{k}_1 = 50$. Again, this absolute location is fuzzy because the numerical results show a gradual transition. Rearranging the equation (5-40) gives that $k_1 \geq 50 k_2 C_{e0}^n$ in zone D . $k_2 C_{e0}^n$ represents a rate of autocatalytic hydrolysis with a catalyst concentration of C_{e0} . Noticing that C_{e0} is the initial number of ester units of all the long chains, we have $C_{e0} \gg C_{ol}$, i.e. the usual amount of short chains available as catalyst is much smaller than C_{e0} . Therefore, $k_2 C_{e0}^n$ represents an unrealistically fast rate of autocatalytic hydrolysis. It is unlikely that a typical biodegradable polymer such as PLA or PGA falls into this zone.

In zones B , C , and D , there is no need to involve the diffusion equation in order to calculate the degradation rate. In the governing equations, one should set $C_{ol} = 0$ for zone B , $C_{ol} = R_{ol}$ for zone C , and $k_2 = 0$ for zone D . These conditions are covered in Chapter 4, above.

Zone A is where the diffusion of short chains and the hydrolysis reaction strongly interact with each other and the size effect on degradation rate is expected. Although the degradation map was calculated for a plate, the same principle applies for all sophisticated devices, such as screws or stents. Unfortunately, this is probably the zone into which most devices fall and the device design has to be carefully analysed, because changing the size has a major effect on its degradation rate.

The degradation map presented in Fig. 14 was firstly obtained by Wang, et al. (2008). It was recalculated using the updated version of the mathematical tool, and the calculation confirmed that the map was not affected by the updating of the mathematical model.

5.4.3 Effect of other factors on the degradation map

The degradation map shown in Fig. 14 was calculated using $\alpha = 1$, $\beta = 1$, $\chi_1 = 0$, $\chi_2 = 1$, $m = 4$, $n = 0.5$, $N_{dp0} = 2307$, $C_{ol0} = 0$, and $\bar{D}_{pore} = 1000 \bar{D}_{polymer}$. It was also assumed that the polymer is amorphous. The choice of some of these parameters will

lead to a big different for the degradation map, although the concept of the four zones is generally valid.

5.4.3.1 Effect of crystallisation induced by chain scission

Han and Pan (2009) compared degradation maps for amorphous (dash lines) and semi-crystalline polymers (solid lines), as reproduced in Fig. 15.

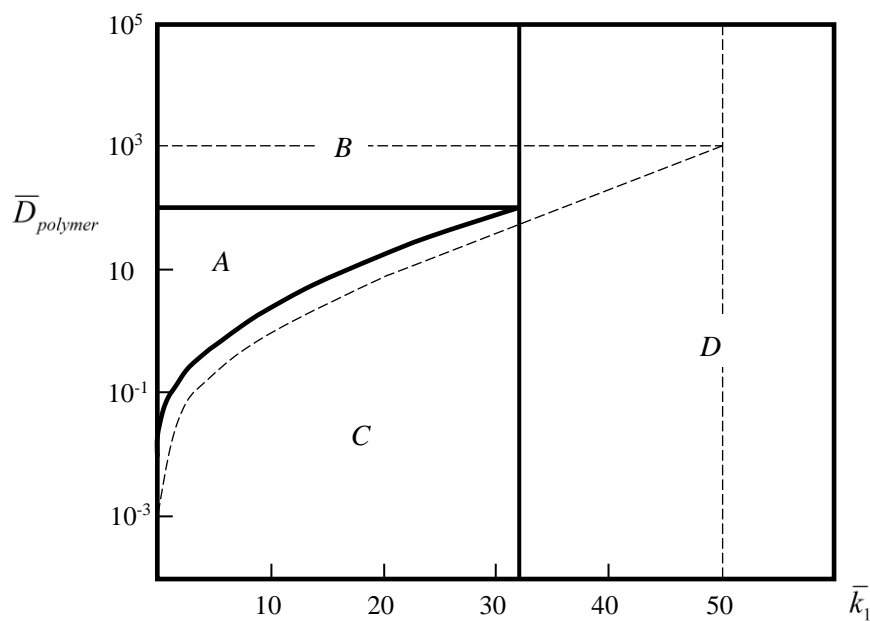


Figure 15: Effect of crystallisation on degradation map. The solid lines show the four zones for semi-crystalline polymers while the dash lines are for amorphous polymers.

Source: Han and Pan (2009).

Full details of the calculation can be found in the paper by Han and Pan (2009). It can be observed that zone A shrinks in all directions for semi-crystalline polymers. This indicates that it is more likely for semi-crystalline polymers to degrade uniformly than it is for amorphous polymers, i.e. semi-crystalline polymers are expected to show less size effect than amorphous ones. The underlying reason for this phenomenon is simple:

the crystalline phase resists degradation, which reduces the difference in degradation rate at different locations of a device.

5.4.3.2 Effect of α and β

As discussed in section 4.1, the values of α and β determine the amount of short chains produced by chain scissions through equation (4-7). For end scission, $\alpha = 1$ and $\beta = 1$. At this extreme, each scission produces a monomer and the chain scission is very efficient in producing short chains. For random scission, $\alpha = 28$ and $\beta = 2$, which reflects that the chain scission is rather ineffective in producing short chains. The real situation is between the two extremes. The degradation map is recalculated using $\alpha = 28$ and $\beta = 2$ and presented in Fig. 16. All the other parameters remain unchanged.

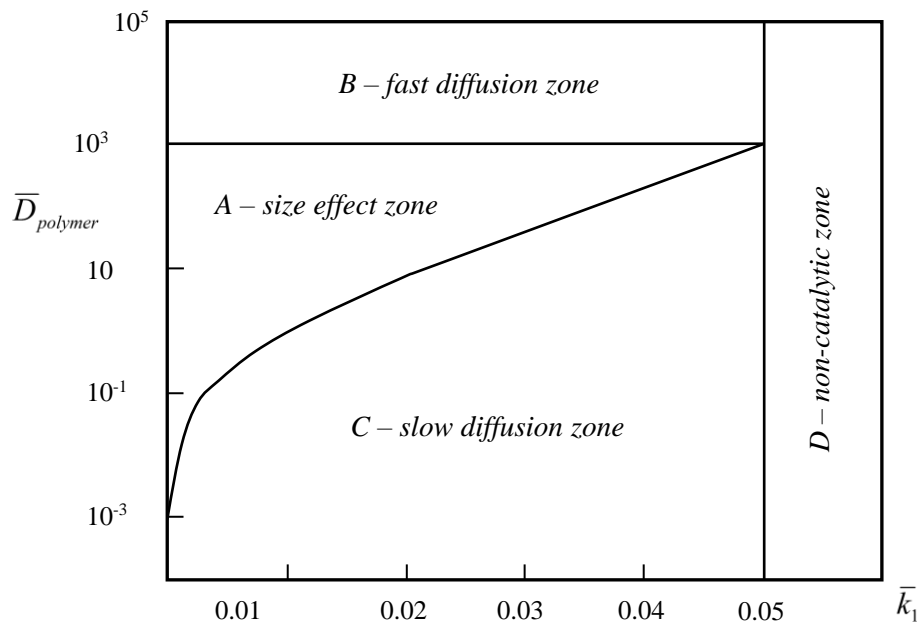


Figure 16: Degradation map obtained using $\alpha = 28$ and $\beta = 2$ with all other parameters identical to that for Fig. 14.

It can be observed that the degradation map for $\alpha = 28$ and $\beta = 2$ is identical in shape to that for $\alpha = 1$ and $\beta = 1$ except that the vertical boundary between zone D and other regions shifts to the left by three orders of magnitude. This means that if fewer short chains are produced, it is far more likely for a plate to degrade through non-catalytic hydrolysis.

5.4.3.3 Effect of device geometry

The degradation map can be calculated for devices of any sophisticated shape if the dimensions of the device scale by a single parameter. This parameter can be called the characteristic size of the device. In the case of the very large plate, its thickness is the characteristic size. For a sphere or a very long solid cylinder, the radius is the characteristic size. Replacing l in the definition of $\bar{D}_{polymer}$ in equation (5-42) with the characteristic size, a similar map can be calculated. Fig. 17 shows a degradation map for solid cylinders. All the parameters are the same as those for the map in Fig. 14. It can be observed from Fig. 17 that, the vertical boundary of zone D shifts to the left by half comparing with the map for the plate. This is because, for a solid cylinder, more material per unit volume is located at the surface, making it easier for the short chains to leave. Consequently, the cylinder behaves in a more non-catalytic manner in comparison with the plate.

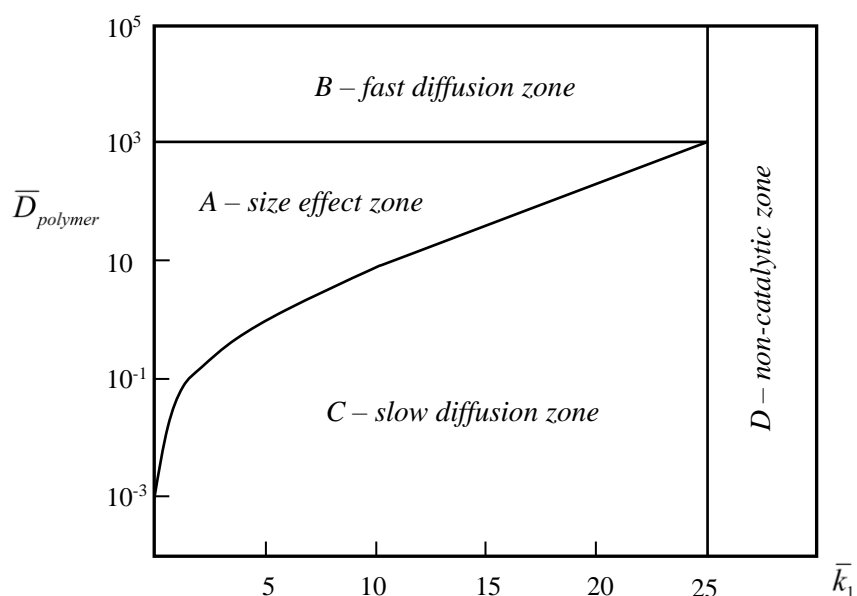


Figure 17: Degradation map for solid cylinder using the same parameters as those used for the large plate in Fig. 14.

5.5 Conclusion

A complete set of governing equations has been presented in this chapter, which includes crystallisation, oligomer diffusion, and their corresponding rate of scission equations. A previously presented degradation map (Wang, et al., 2008) was recalculated and proved to be valid even through the degradation model used was oversimplified. Furthermore, the studies on the effect of other factors on the degradation map had provided several other degradation maps, which could help to understand the behaviours of degradations under different conditions.

Chapter 6: Cross-reading of the degradation rates of different devices made of the same polymer and the effect of water diffusion

Degradation data, in particular that obtained from *in vivo* experiments, are very expensive and time-consuming to obtain. The mathematical model presented in Chapter 5 can be used to project degradation rate from one device to another, if they are made of the same polymer. This chapter demonstrates how the finite element method is applied to estimate the degradation rate of a newly designed device based on existing data of a different device. Also, the water diffusion effect was added in the second half of this chapter. A prediction of an interference screw for storage was made under different conditions of atmosphere.

6.1 The need for a cross-reading method

For biodegradable medical device designers, optimising the design of such devices is mostly achieved through trial-and-error. Experiments are unavoidable to fully understand the degradation behaviour, which is time-consuming and expensive. Because of the heterogeneous nature of degradation, design is never straightforward for these devices. For example, if more mechanical stiffness is required for the device, the designer cannot just increase the thickness of the device or use more materials, because a thicker device may lead to faster degradation due to autocatalytic hydrolysis reaction (Grizzi, et al., 1995), thus losing mechanical stiffness even quicker, which is against the design purpose. The available experimental cost of involving new materials into existing applications would be limited. As a result, materials which are well established in certain application were often used by companies to design new equipment for new applications or to optimise the prior designs of existing equipment (Buchanan, 2008). The polymers that are used in biodegradable medical devices are limited; therefore, most of the device designers would use the same or similar material to an existing device that has been experimentally tested. Furthermore, in some cases, the size or the shape of the existing device might need to be adjusted in order to meet other requirements. However, no matter how small the change is, the degradation

progress will not be fully understood unless an experiment was conducted. A tool that could predict the degradation rate would be very useful in the early stage of designing, even if it could just provide a range of prediction. A mathematical model could be introduced to achieve such goal.

The mathematical model presented in the previous chapters was successfully used to fit many experimental data. Specifically, a set of interference screw experimental data was fitted using the model that was presented in this chapter. However, there are still many factors that could affect the result of degradation – some we understand, some we may not fully understand. Therefore, the direct purpose of this chapter is very modest: the content will only consider and relate to the shape and size of the equipment design. The mathematical model is first used in fitting of the experimental data accumulated by the existing polymers and devices. Successfully fitted model parameters will then be kept the same for degradation analysis study for other devices which are made from the same material but with different designs (change of shape or size) under similar manufacturing conditions. A designer could intuitively obtain the estimated range of degradation rate and mechanical properties for the newly designed device. This type of computer modelling method is currently in use for many other engineering applications. For example, the approach is routinely used to calculate fatigue and the creep damage of engineering components for design modifications. For biodegradable medical devices, this modest level of computer modelling was already a leap forward from the trial-and-error approach that is currently practiced. Experimenting would still be necessary. A mathematical model would only be used as a tool at the first stage of designing by providing a predicted range of degradation behaviour. This would eliminate many unnecessary experiments and focus the resources on the ones that would be most likely to achieve the requirement.

In this chapter, the above method was used for cross-reading between an interference screw model and a biomedical stent model. Experimental data for the interference screw was presented by Schwash (1998). Assuming that a designer would like to use the same material and apply similar manufacturing conditions to design a biomedical stent, a range of molecular weight distribution and crystallisation could be calculated by applying the computer modelling. The designer can then decide whether the range covers what is required. If so, further experiments can then be carried out; if not, other changes may need to be made.

6.2 A finite element model for interference screw

Schwash (1998) presented the experimental data for interference screws. 25mm long and 9mm in diameter, that were used in a cruciate ligament. Hydrolytic degradation of the screw was performed *in vitro* in an iso-osmolar phosphate buffer solution (0.13 M, pH 7.4) at 37 °C. Experimental data for the interference screw made of PLA100-Sn was used here.

The mathematical model introduced in the previous chapters was used to fit the experimental data. Specifically, equations (5-5), (5-11), (5-18), and (5-28) were applied into commercial software COMSOL Multiphysics (license number 7074366) for the degradation calculation. Fig. 18 shows a cross-section mesh of the interference screw model used in COMSOL. The whole geometry contains 1,146 elements and 5,070 degrees of freedom were used, linear shape function was applied. The whole screw was assumed under an iso-osmolar phosphate buffer solution, so all surfaces were set as ‘no oligomer residue’, i.e. $C_{ol} = 0$. Parameters and variables used in this calculation are listed in Table 1, Case (A).

The pack of equations used in COMSOL is listed below.

Rate of chain scission of semi-crystalline polymer:

$$\frac{dR_s}{dt} = C_{e0} \psi(R_s) \left\{ k_1 + k_2 C_{e0}^n \left[\left(\chi_1 \varphi(R_s) + \frac{\chi_2}{m} \left(\frac{C_{ol}}{C_{e0}} \right) \right) \frac{1}{1 - X_c} \right]^n \right\} \quad (5-11)$$

in which

$$\psi(R_s) = 1 - \alpha \left(\frac{R_s}{C_{e0}} \right)^\beta - \frac{\omega}{C_{e0}} (X_c - X_{c0}) \quad (5-12)$$

$$\varphi(R_s) = \frac{C_{chain\ 0}}{C_{e0}} + \frac{R_s}{C_{e0}} - \frac{\alpha}{m} \left(\frac{R_s}{C_{e0}} \right)^\beta \quad (5-13)$$

Growth of crystallisation:

$$X_c = X_{c\ max} - (X_{c\ max} - X_{c0}) e^{-k_c \bar{R}_s} \quad (5-5)$$

Short chain diffusion equation:

$$\frac{dC_{ol}}{dt} = \alpha\beta \left(\frac{R_s}{C_{e0}} \right)^{\beta-1} \frac{dR_s}{dt} + \sum_{i=1}^3 \frac{\partial}{\partial x_i} \left(D \frac{\partial C_{ol}}{\partial x_i} \right) \quad (5-28)$$

Average molecular weight calculation equation:

$$\overline{M}_n = \frac{M_n}{M_{n0}} = \frac{1 + \overline{X}_{c0} - \alpha \overline{R}_s^\beta}{(1 + \overline{X}_{c0}) \left[1 + \frac{C_{e0}}{N_{\text{chain } 0}} \left(\overline{R}_s - \frac{\alpha}{m} \overline{R}_s^\beta \right) \right]} \quad (5-18)$$

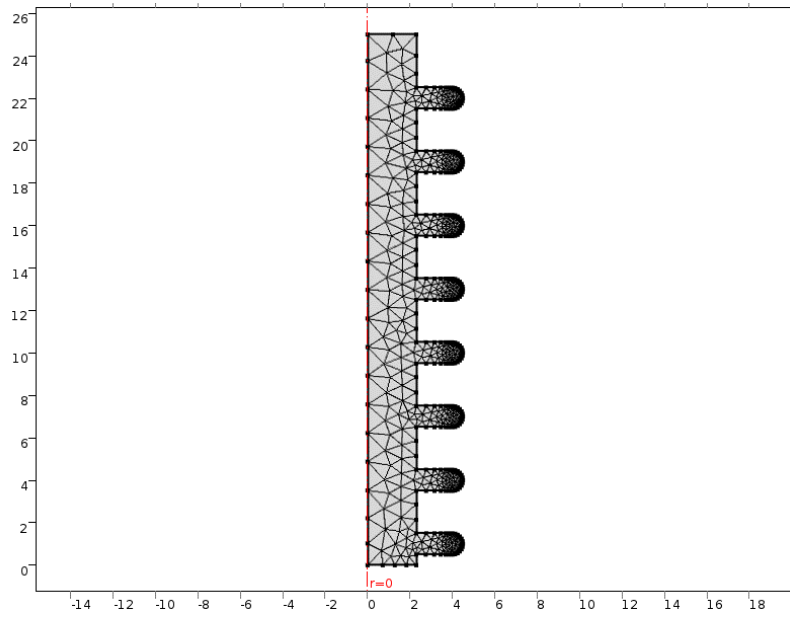
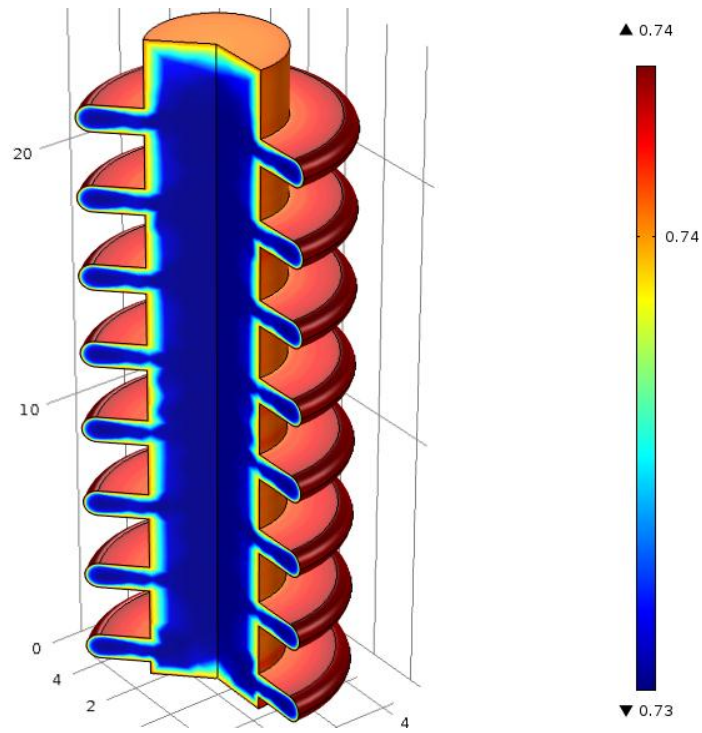
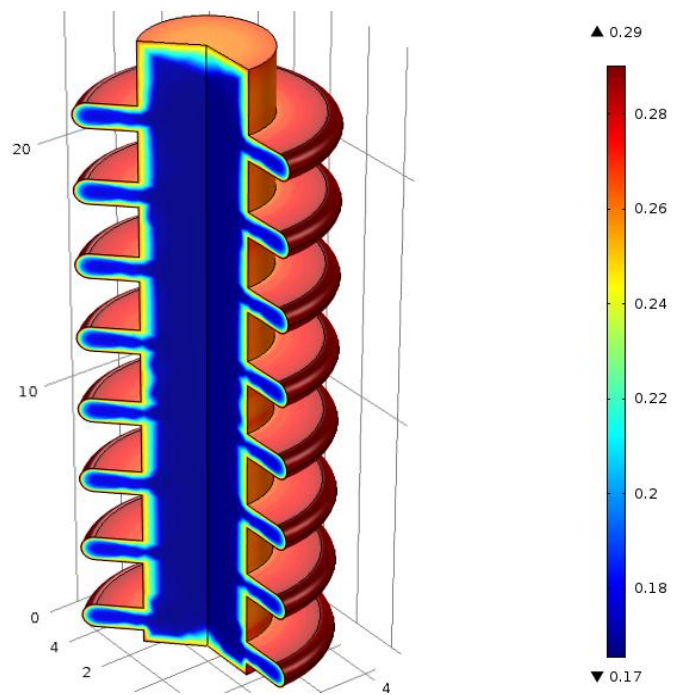


Figure 18: A cross-sectional view of the interference screw with mesh (length unit mm).

Normalised average molecular weight distribution and degree of crystallinity for two different degradation times – (a) week 7 and (b) week 28 – are shown in Fig. 19 and Fig. 20, respectively. The results appear to be fairly self-similar, in that the colour remains unchanged although the scale is varied. It can be observed that average molecular weight distribution difference between the surface and the core increases during degradation. That is because, as degradation progresses, the oligomers produced and stored inside of the screw cause the core area to degrade faster than the surface. A refining mesh was also used to check the convergence of the result. A refining mesh of 1,938 elements and 8,390 degrees of freedom gives the same degradation result; therefore, the result calculated can be proved as convergent.

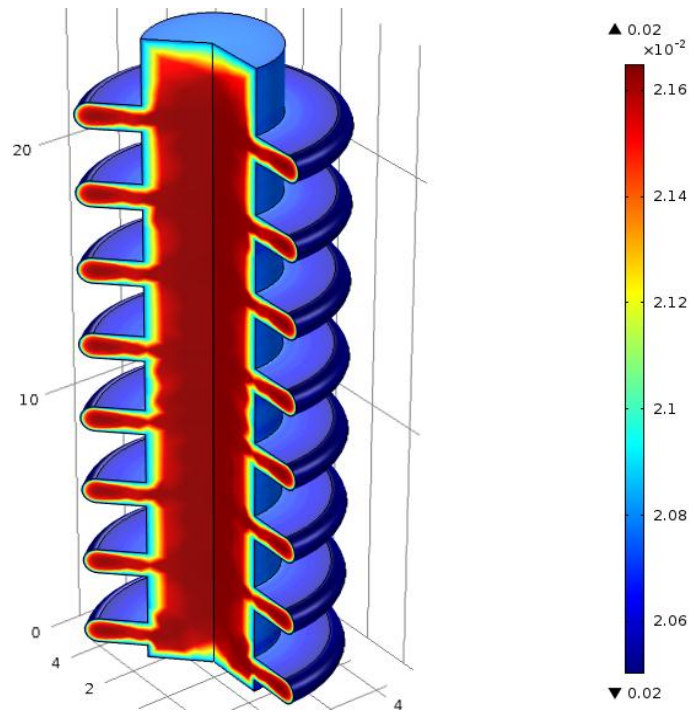


(a) week 7

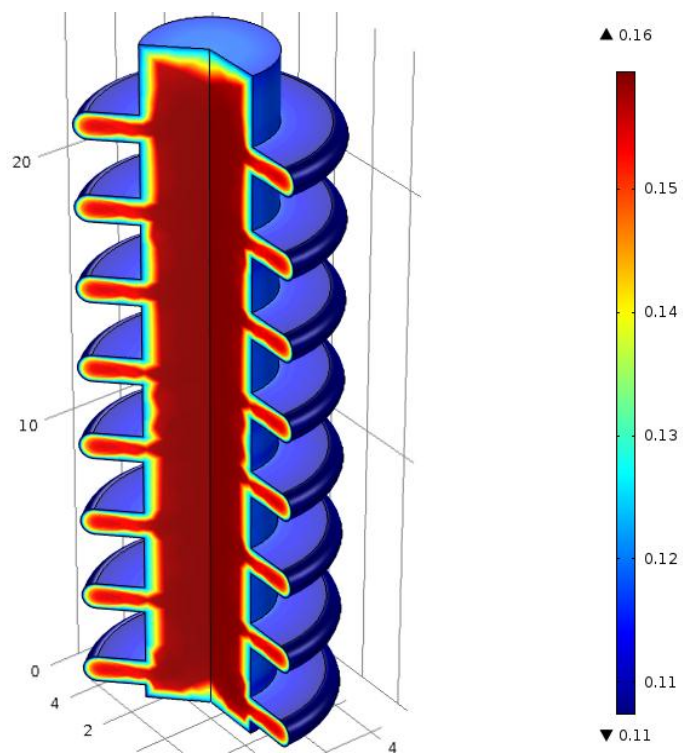


(b) week 28

Figure 19: Interference screw – average molecular weight distribution at two different degradation times: (a) week 7, (b) week 28.



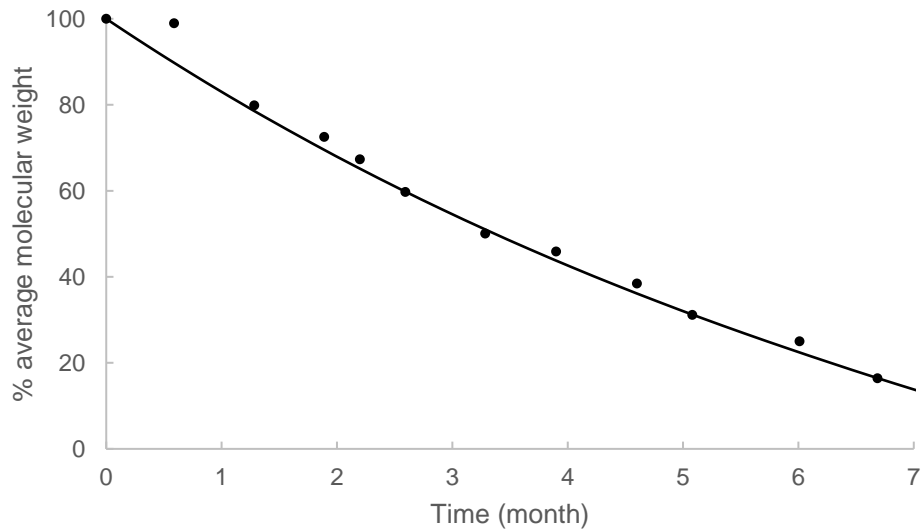
(a) week 7



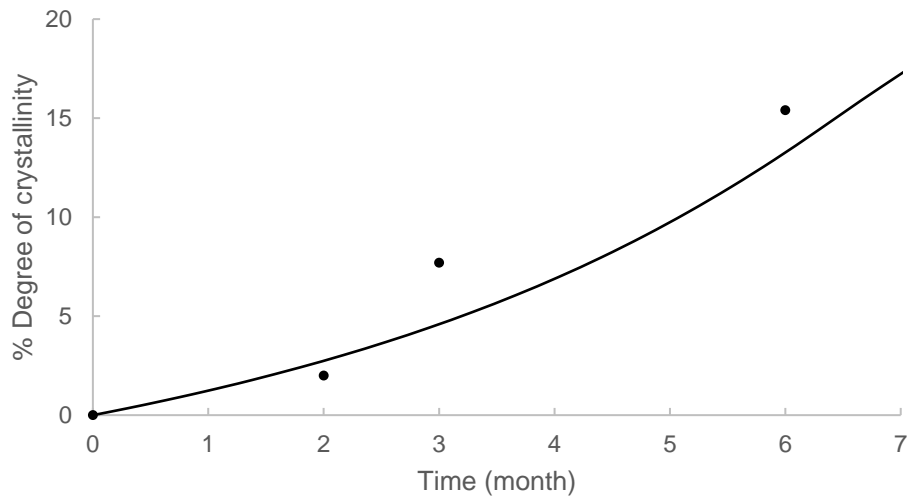
(b) week 28

Figure 20: Interference screw – degree of crystallinity distribution at two different degradation times: (a) week 7, (b) week 28.

The distribution of normalised average molecular weight distribution and degree of crystallinity was integrated through the entire geometry and divided by the whole volume for various degradation times. It is shown in Fig. 21 that the mathematical model can provide a good fitting to the experimental data for both (a) average molecular weight and (b) degree of crystallinity simultaneously. This also proves the validation of the mathematical model used.



(a)



— model fitting • Experimental data

(b)

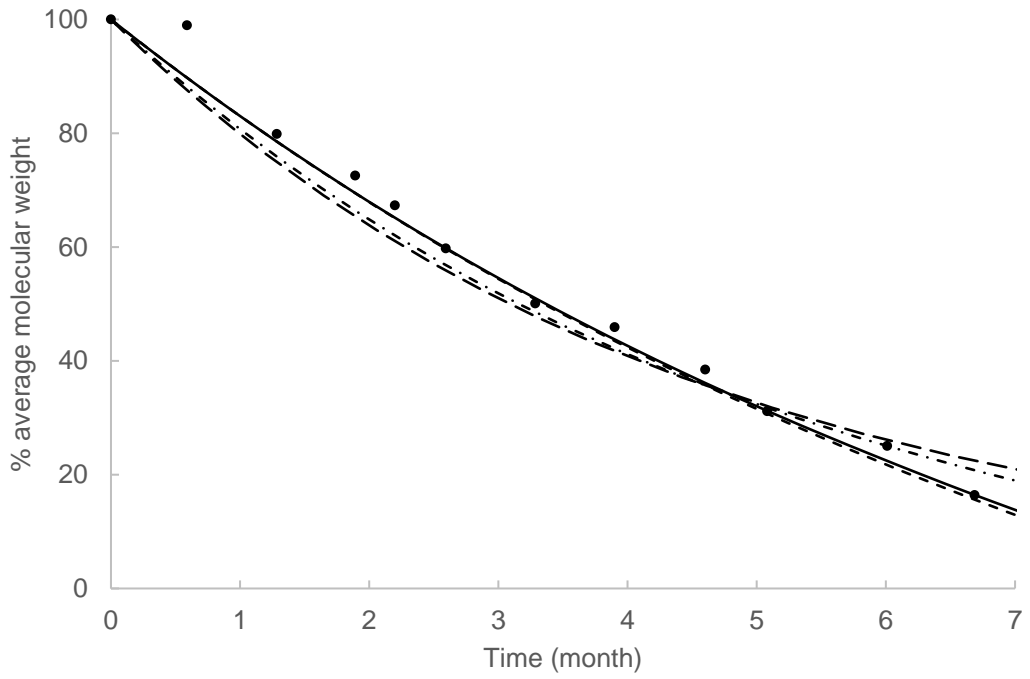
Figure 21: Using a mathematical model to fit interference screw experimental data of (a) molecular weight and (b) degree of crystallinity.

The parametric study of Chapter 4 presents that multiple sets of mathematical model parameters could be used to achieve the same set of degradation data. Based on this finding, four different sets of parameters were found, which could all fit the same interference screw experimental data shown in Fig. 22. Fig. 22 also shows that (a) average molecular weight and (b) degree of crystallinity experimental data can be fitted simultaneously to all four sets of parameters, which are listed in Table 1.

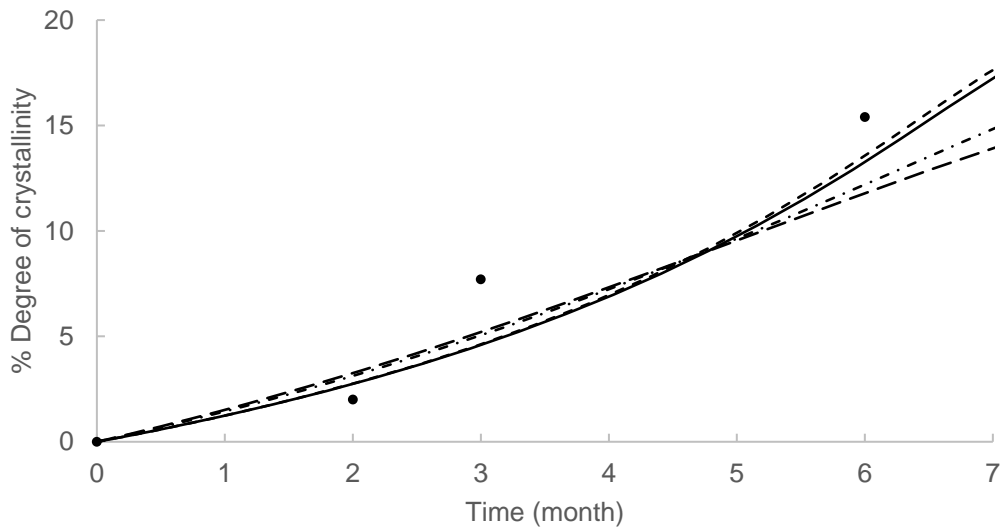
Case A	Case B	Case C	Case D
k_1 (1/day)	k_1 (1/day)	k_1 (1/day)	k_1 (1/day)
0.006	0.006	0.007	0.0005
$\bar{k}_2 = k_2/Ce_0^n$ (1/day)	$\bar{k}_2 = k_2/Ce_0^n$ (1/day)	$\bar{k}_2 = k_2/Ce_0^n$ (1/day)	$\bar{k}_2 = k_2/Ce_0^n$ (1/day)
2.3	2.3	10	0.007
χ_1	χ_1	χ_1	χ_1
0	0	0	1
$D_{polymer}$ (m^2/s)	$D_{polymer}$ (m^2/s)	$D_{polymer}$ (m^2/s)	$D_{polymer}$ (m^2/s)
10^{-14}	10^{-22}	10^{-10}	10^{-14}
D_{pore} (m^2/s)	D_{pore} (m^2/s)	D_{pore} (m^2/s)	D_{pore} (m^2/s)
10^{-11}	10^{-19}	10^{-7}	10^{-11}

Table 1: Four sets of parameters that could fit the same interference screw experimental data.

The common parameters used for all cases in Table 1 are listed below: $Ce_0=17300$ (mol/m^3); $n=0.5$; $\chi_2 = 1$; $m=4$; $\alpha=28$; $\beta=2$; $X_{c0} = 0$; $X_{cmax} = 0.2$; $C_{o10}=0$ (mol/m^3); $Mn_0 = 201176$ (g/mol).



(a)



● Experimental — Case A - - - Case B - · - · Case C - - - - Case D

(b)

Figure 22: Using mathematical model to fit (a) average molecular weight and (b) degree of crystallinity screw experimental data for all parameters listed in Table 1 Cases A, B, C, and D, respectively.

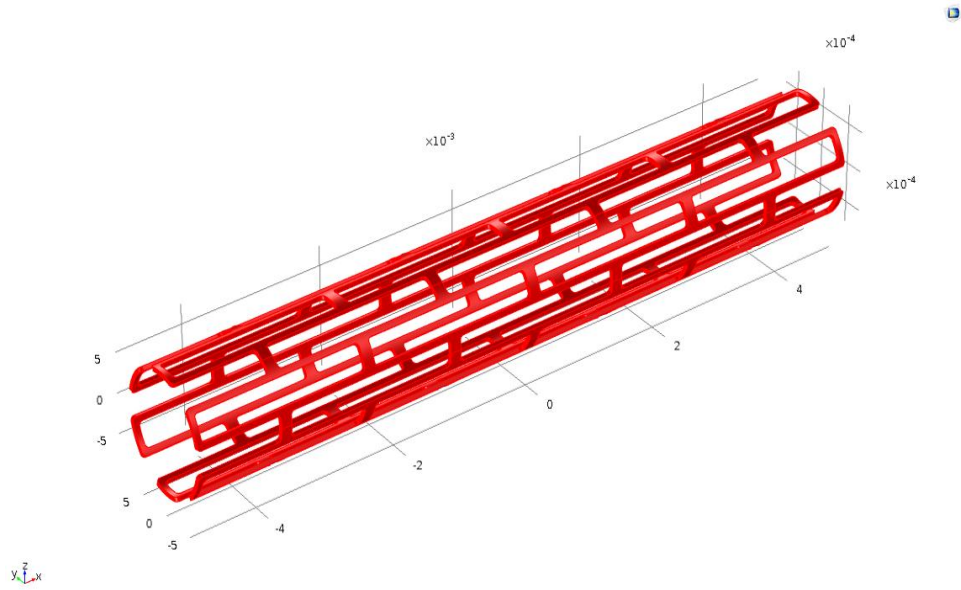
Table 1 Cases A, B, and C all used $\chi_1 = 0$ and $\chi_2 = 1$ (only short chains contribute as catalyst) but take different diffusion coefficients. The diffusion coefficient for Cases A and B takes 10^{-14} (m^2/s) and 10^{-22} (m^2/s), respectively, which are the upper and lower cases for the amorphous polymer diffusion coefficient (Lyu, 2007). A large diffusion coefficient was given to Case C as 10^{-10} (m^2/s), which is even bigger than the water diffusion coefficient: 10^{-13} (m^2/s). Theoretically, the diffusion coefficient of an amorphous polymer could not be bigger than the water diffusion coefficient. However, degradation sometimes causes the sample to fall to pieces and generates a great number of tiny crystalline residues (Li, 1995). This phenomenon could cause degradation rate change and massive mass loss, which has not yet been captured by the current mathematical model. Using a large diffusion coefficient could get a better understanding of this phenomenon, but further studies still need to be carried out. In fact, that is the next topic for the Leicester group. Cases A and D share the same diffusion coefficient, 10^{-14} (m^2/s), but for Case D long chains have been added to count as catalyst by setting $\chi_1 = 1$ and $\chi_2 = 1$. The same set of experimental data could be fitted by all four sets of parameters by setting different k_1, \bar{k}_2 values, as shown in the parametric study of Chapter 4.

6.3 Cross-reading with a coronary stent

For many countries, biomedical stents have been available wildly in heart patients to expand the narrowed blood vessel and remain the flowing of blood. It also hold and slowly releases drugs to heal the opened tissue. Because many stents are needed to deal with very complex situations and special arteries, and one heart patient could need municipal stents, optimising the design to suit different surgical situations and understanding the degradation behaviour of such devices is very import. This makes the biomedical stent a perfect example for the cross-reading method. Such a method would help with design optimisation and understanding of degradation behaviour.

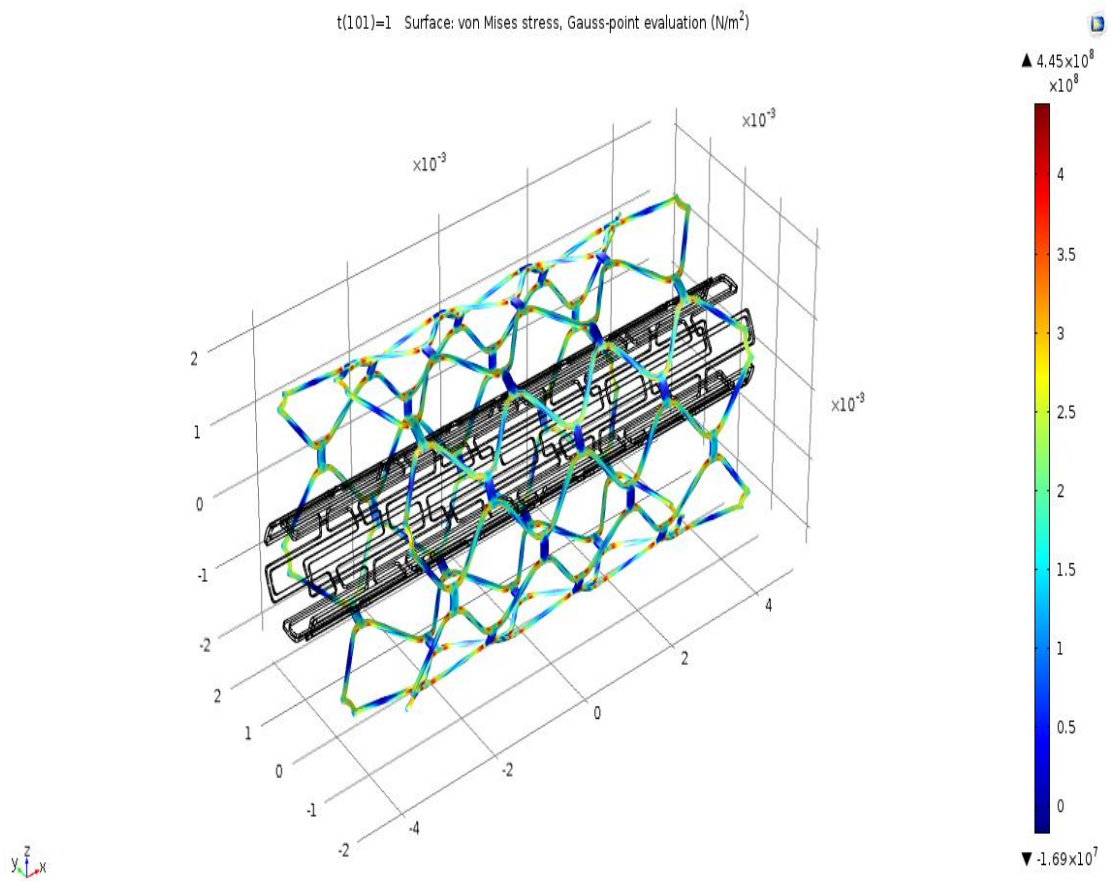
A biomedical stent model with a length of 8mm was implanted as a case study, as shown in Fig. 23. The model was achieved from the database of commercial software COMSOL Multiphysics (license number 7074366). The stent has an original diameter of 0.74mm, shown in Fig. 23(a). Once the stent reached the narrowed artery a balloon

was then used to expand it into position, as shown in Fig. 23(b). The balloon was removed after use, with the stent remaining expanded to act as a scaffold, keeping the blood vessel open. Biodegradable stents degrade over time, eventually disappearing fully when the narrowed artery heals and gains back its full function. Therefore, the expanded stent would be more appropriate to use in the degradation model. Fig. 23(c) shows the average molecular distribution of the whole stent at week 16 using parameter Case D in Table 1. Because of symmetry, only the part shown in Fig. 24 was used in the analysis, which is the highlighted part in Fig 23 (c). The mesh used for calculation is also shown in Fig. 24, which contains 2,210 elements and the degree of freedom is 25,220.

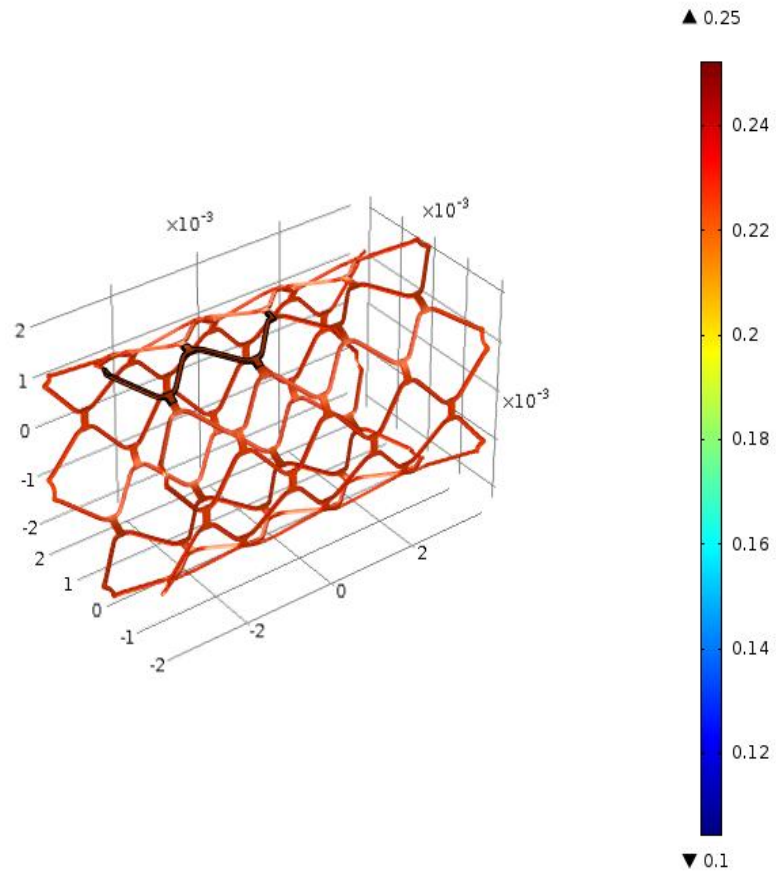


(a)

t(101)=1 Surface: von Mises stress, Gauss-point evaluation (N/m²)



(b)



(c)

Figure 23: Biomedical stent (a) before deformation, (b) after deformation, (c) Molecular weight distribution of the whole stent, at week 16 using parameter listed in Table 1 Case D (all length units in m) (COMSOL database was applied to obtain the geometry).

The same mathematical model that was used for the interference screw model was applied here. The stent model was also assumed to be surrounded by a watery environment, i.e. $C_{ol} = 0$ for all surfaces. The four sets of mathematical parameters listed in Table 1, which were successfully used to fit the interference screw experimental data, were applied to the expanded biomedical stent model. Convergence was checked by refining the mesh, which increased the elements to 4,420 and the degree of freedom to 45,396. The same results were achieved.

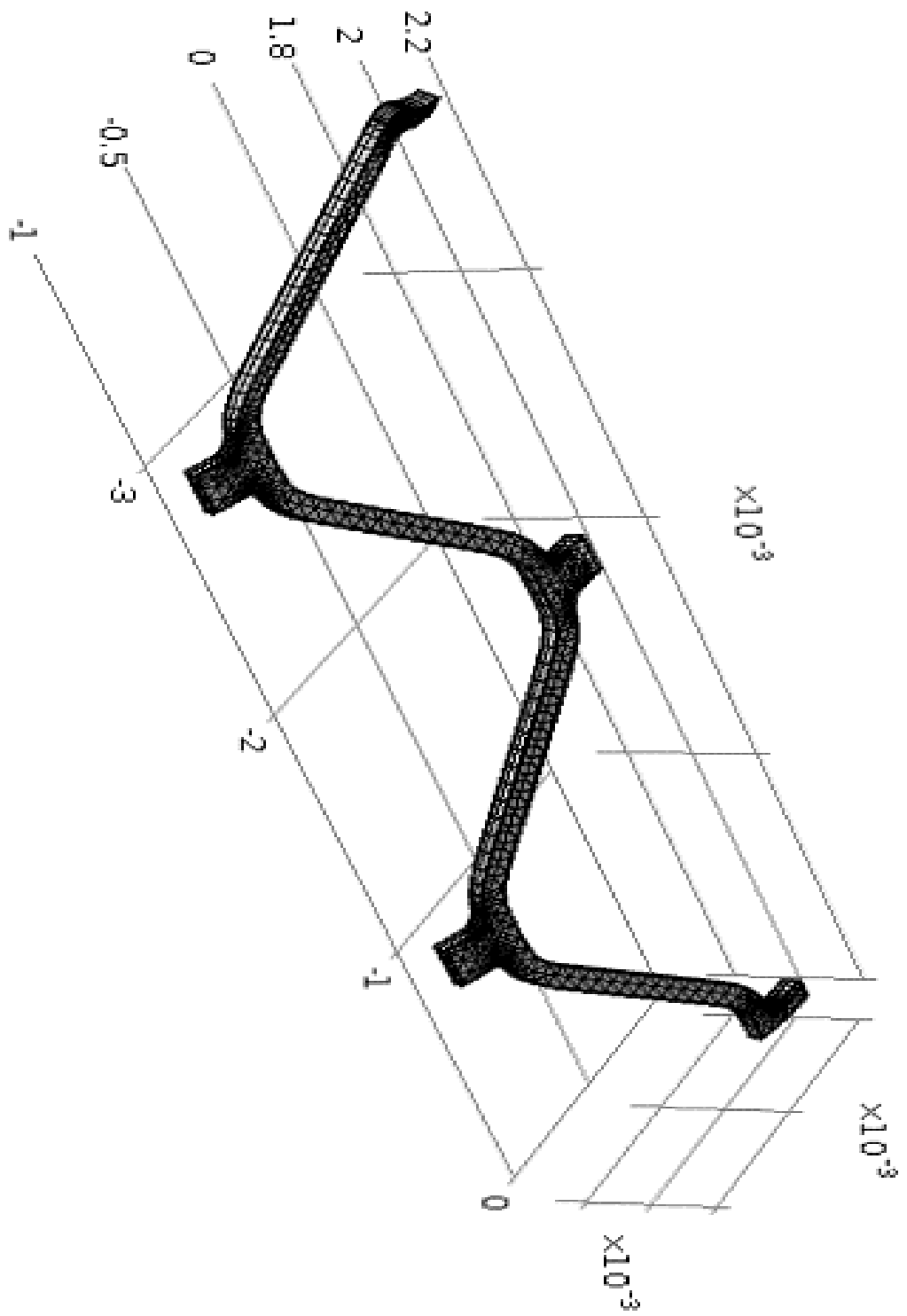
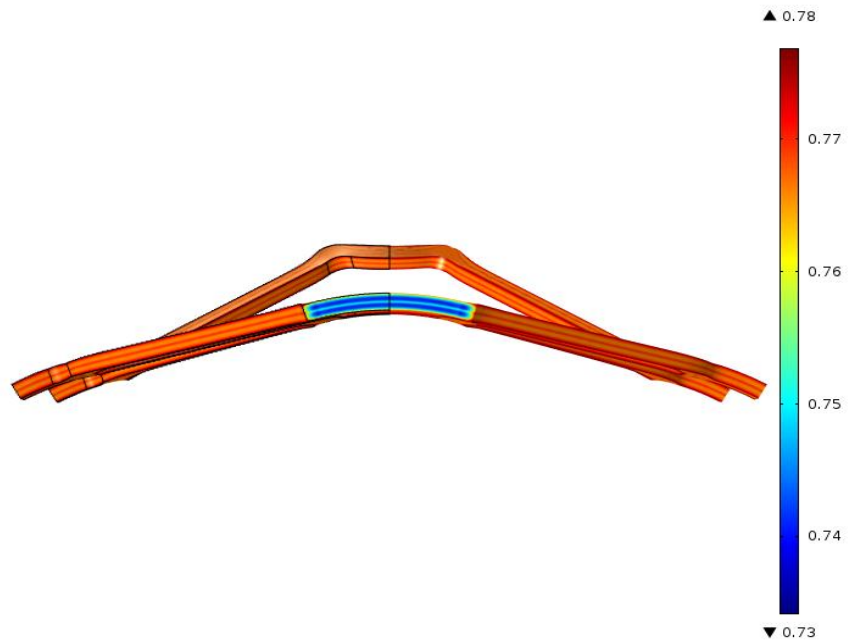
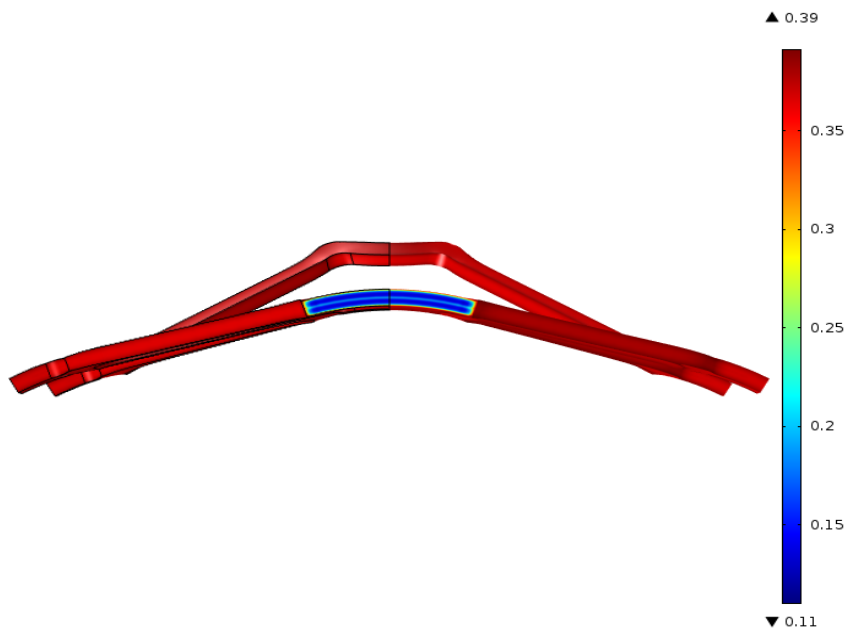


Figure 24: Partial mesh of the stent highlighted part in Fig. 23 (c) (all length units in m).

Fig. 25 and Fig. 26 show the longitudinal view of a 1/12 stent's, which is the mirror image of the mesh part shown in Fig. 24. Fig. 25 and Fig. 26 (a) average molecular weight and (b) degree of crystallinity distribution for different degradation times using parameters listed in Table 1 Case C and D, respectively.

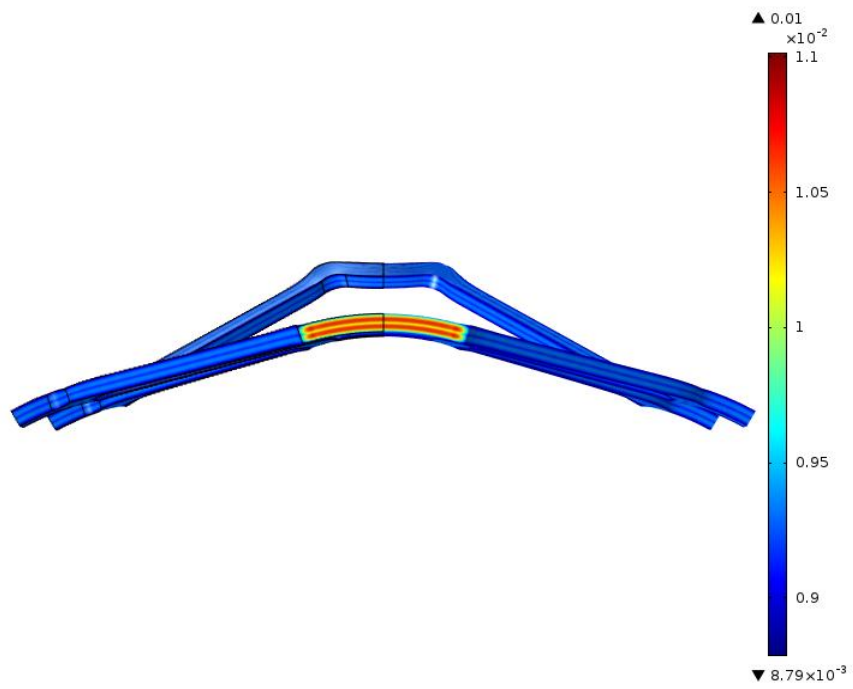


week 5

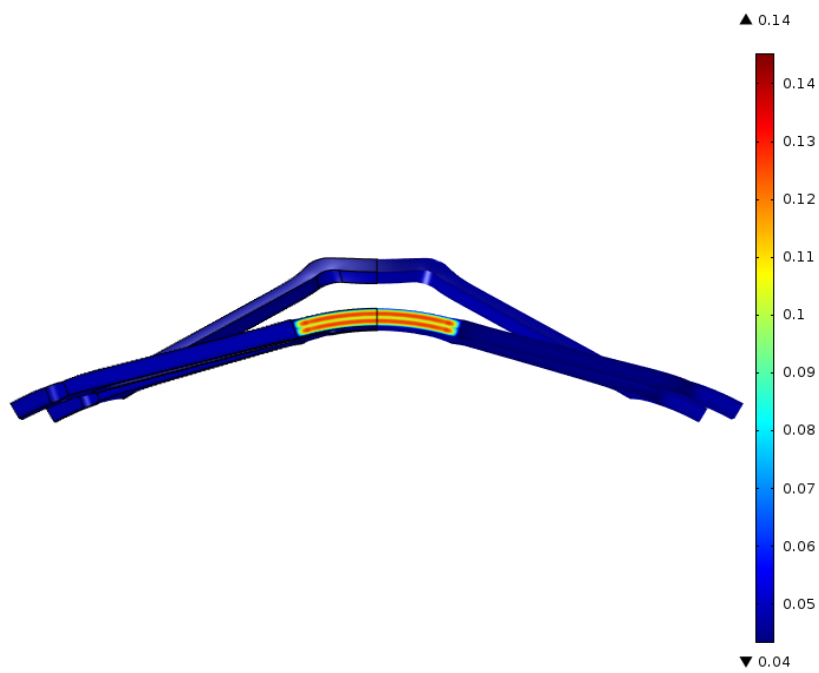


week 15

(a) Average molecular weight distribution for weeks 5 and 15.



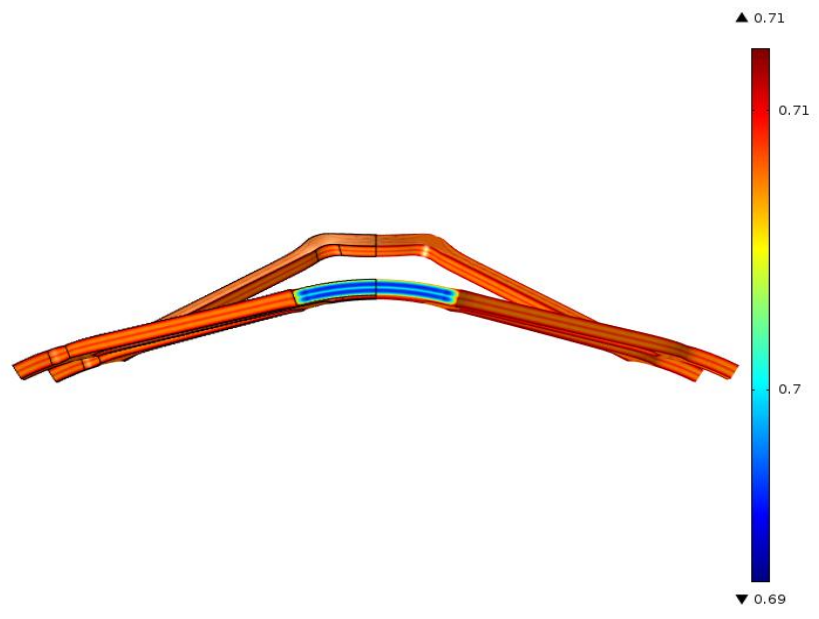
week 5



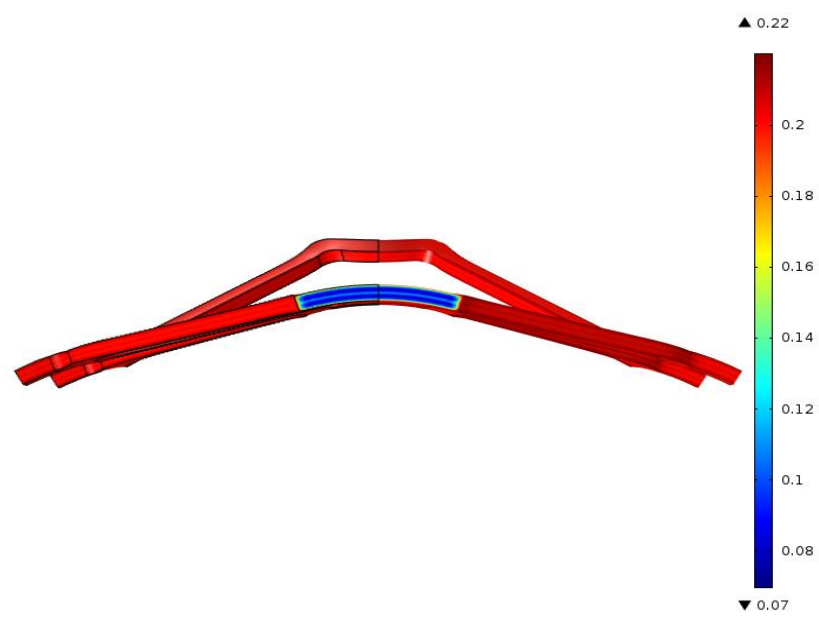
week 15

(b) Degree of crystallinity distribution for weeks 5 and 15.

Figure 25: Distributions of 1/12 of the stent viewed along longitudinal axis for (a) average molecular weight and (b) degree of crystallinity under different degradation times: weeks 5 and 15, which used the parameters listed in Table 1 Case D.



week 8

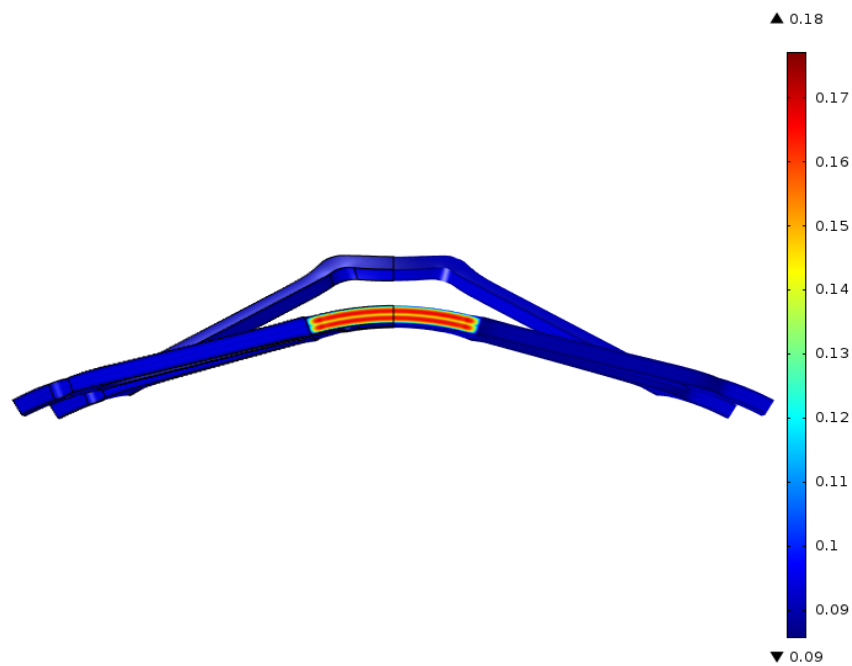


week 24

(a) Average molecular weight distribution for weeks 8 and 32.



week 8

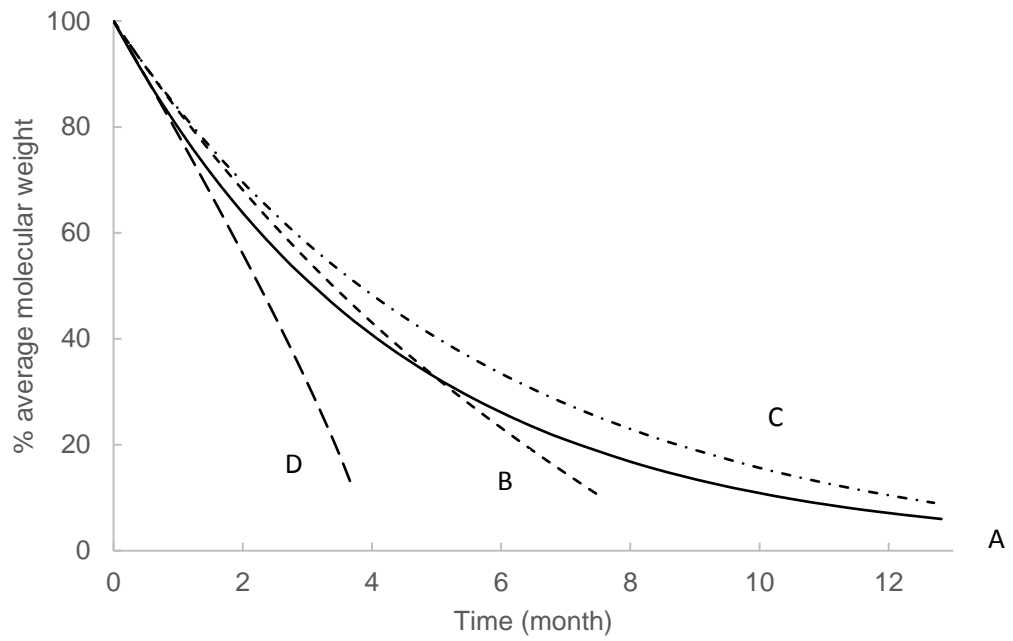


week 24

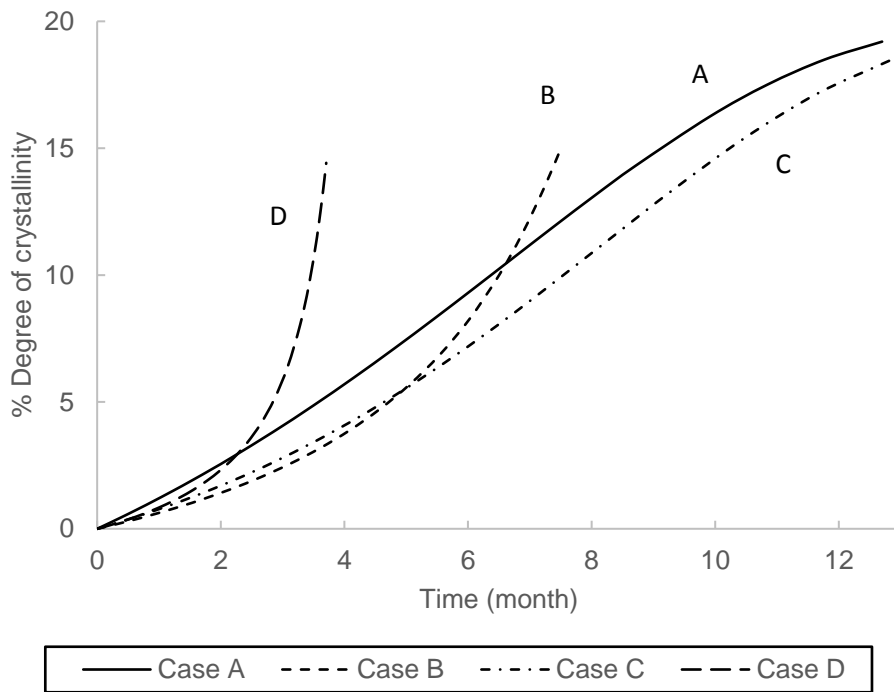
(b) Degree of crystallinity distribution for weeks 8 and 32.

Figure 26: Distributions of 1/12 of the stent viewed along longitudinal axis for (a) average molecular weight and (b) degree of crystallinity under different degradation times: weeks 8 and 32, which used the parameters listed in Table 1 Case C.

The calculated average molecular weight and degree of crystallinity data for all four sets of parameters in Table 1 is shown in Fig. 27. It could be observed that four sets of parameters now give different trends in both average molecular weight and degree of crystallinity. All four trends formed into a region, which have Case D and Case C for their upper and lower limits. For average molecular weight reduction shown in Fig 25(a), Case D has long chain and short chain both working as catalyst, which would lead to faster degradation; Case C has the largest diffusion coefficient, which would lead to a slower degradation. Similarly, for degree of crystallinity, Case D has the fastest crystalline growth and Case C has the slowest crystalline growth. The region can be seen as a prediction of the degradation behaviour for the biomedical stent. The exact average molecular weight and degree of crystallinity trend was assumed to be located in this region. A designer who would like to design this kind of biomedical stent could use this region as a guide, which would help them to have a preview of the stent degradation behaviour for the newly designed stent. As shown in Fig. 27, four different parameters could be assumed to have identical degradation behaviour in the first two months. A huge difference then starts to show up and divides the sets of parameters into an upper and a lower limit. Similar behaviour can also be obtained from Fig. 25 and Fig. 26, which shows the degradation distribution for the upper and lower limit.



(a)



(b)

Figure 27: Predicted biomedical stent degradation behaviour (a) average molecular weight (b) degree of crystallinity, for different sets of parameters listed in Table 1.

6.4 Effect of water diffusion

The mathematical model for degradation introduced previously in this thesis assumed that water molecules are abundant inside of the polymer for all times during degradation. That is based on Li's (2000) finding of water uptake in as short a time as several days. However, Li's finding was based on PLA films with an average thickness of 0.4mm, while many biodegradable medical devices have thicknesses or diameters of several millimetres. Water diffusion for medical devices with a thickness of several millimetres could be a delay factor for the degradation, as the thicker the device, the harder it is for water molecules to diffuse into the core of the device. In this section, the effect of water diffusion under different sample thicknesses will be studied. Secondly, the water diffusion effect will be added to the interference screw model, which was presented in the first half of this chapter, to be able to analysis the effect that water diffusion on the previous model fitting. Finally, storage condition was predicted under different atmospheric environments.

6.4.1 Degradation equations for semi-crystalline polymers adding in water diffusion

All previous models by the Leicester group have assumed that water diffusion is much faster than the degradation rate. This is, however, not always justifiable, in particular when modelling device degradation during storage. This section presents the mathematical equations for polymer degradation that include time-dependant water diffusion into the devices.

From the early model presented by Pitt (1981 and 1987), the concentration of the ester bond and concentration of water are two important factors which will affect the rate of hydrolysis reaction, which can be repented as C_e and C_w , respectively. The rate of chain scission equation can be presented as:

$$\frac{dR_s}{dt} = k_1 C_e C_w + k'_2 C_e C_w C_{H^+} \quad (6-1)$$

in which R_s is the total number of chain scissions per unit volume, k_1 and k'_2 are the reaction rate constant of non-catalytic hydrolysis and autocatalytic hydrolysis, respectively, and C_{H^+} is the concentration of catalyst H^+ .

In Chapter 4, the effect of concentration of water C_w was ignored, as we assume that water molecules are abundant everywhere in polymer. That is based on Li's (2000) finding on water uptake being as short as several days, whereas polymer degradation takes month or years (Grizzi, et al., 1995). Furthermore, the water diffusion coefficient is $10^{-13} \text{ m}^2/\text{s}$ (Liu, et al., 2011), the polymer diffusion coefficient can be as small as $10^{-22} \text{ m}^2/\text{s}$ (Lyu, et al., 2007), and theoretically water diffusion inside of polymer happens much faster than oligomers diffuse out into the surrounding environment. However, Li (2000) obtained the water uptake data by using PLA films, which have average thickness of 0.4mm. For such films, water uptake may happen very fast, but for many medical devices, such as interference screws, the diameter could be up to 10mm, which could change the ability of water absorption. In addition, the oligomer diffusion coefficient could be assumed to be bigger than water diffusion to cover the erosion, which happens at the surface of many polymer devices. Further study on counting erosion into the mathematical model will be the future task for the Leicester group. For now, it is necessary to consider the effect of water diffusion for some devices with thicker diameter or thickness.

Based on equations (6-1) and (5-11), the master equation for the rate of chain scission for semi-crystalline polymers could be modified to include water diffusion, shown as follows:

$$\frac{dR_s}{dt} = \frac{C_w}{C_{e0}} C_{e0} \psi(R_s) \left\{ k_1 + k_2 C_{e0}^n \left[\left(\chi_1 \varphi(R_s) + \frac{\chi_2}{m} \left(\frac{C_{ol}}{C_{e0}} \right) \right) \frac{1}{1 - X_c} \right]^n \right\} \quad (6-2)$$

in which

$$\psi(R_s) = 1 - \alpha \left(\frac{R_s}{C_{e0}} \right)^\beta - \frac{\omega}{C_{e0}} (X_c - X_{c0}) \quad (5-12)$$

$$\varphi(R_s) = \frac{C_{chain\ 0}}{C_{e0}} + \frac{R_s}{C_{e0}} - \frac{\alpha}{m} \left(\frac{R_s}{C_{e0}} \right)^\beta \quad (5-13)$$

Oligomer diffusion equation:

$$\frac{dC_{ol}}{dt} = \alpha \beta \left(\frac{R_s}{C_{e0}} \right)^{\beta-1} \frac{dR_s}{dt} + \sum_{i=1}^3 \frac{\partial}{\partial x_i} \left(D \frac{\partial C_{ol}}{\partial x_i} \right) \quad (5-28)$$

Water diffusion equation:

$$\frac{dC_w}{dt} = \sum_{i=1}^3 \frac{\partial}{\partial x_i} \left(D_w \frac{\partial C_w}{\partial x_i} \right) \quad (6-3)$$

in which D_w is the diffusion coefficient for water, which takes as $10^{-13} \text{ m}^2/\text{s}$ according to Liu (2011). All other symbols were defined previously.

A new term C_w/C_{e0} was involved in the rate of chain scission equation to monitor the abundance of water inside semi-crystalline polymers. If $\frac{C_w}{C_{e0}} = 1$ we assume water molecules are abundant. If $\frac{C_w}{C_{e0}} < 1$ rate of scission will be slowed down as there are not abundant water molecules inside the polymer to cause full degradation. Although C_w can take a value of $55600 \text{ mol}/\text{m}^3$, C_w/C_{e0} cannot be larger than 1, as we assume that water molecules will be already abundant when $C_w = C_{e0} = 17300 \text{ mol}/\text{m}^3$. The uptake of water molecules can be obtained by equation (6-3).

6.4.2 Effect of water diffusion for 2D square plate

Fig. 28 shows a 2D square plate models with mesh, which have side length 1mm. A 1mm plate was chosen to represent the film model as the PLA films used in Li's paper (2000) were all less than 1mm thickness. Also, a plate with a side length of 5mm is also considered in this section. A 5mm plate was chosen to represent the medical device with a relatively big average thickness or diameter, such as an interference screw or biomedical stent.

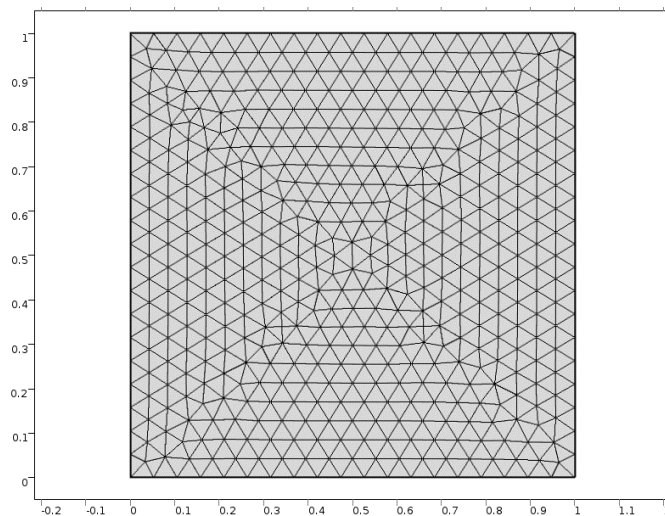
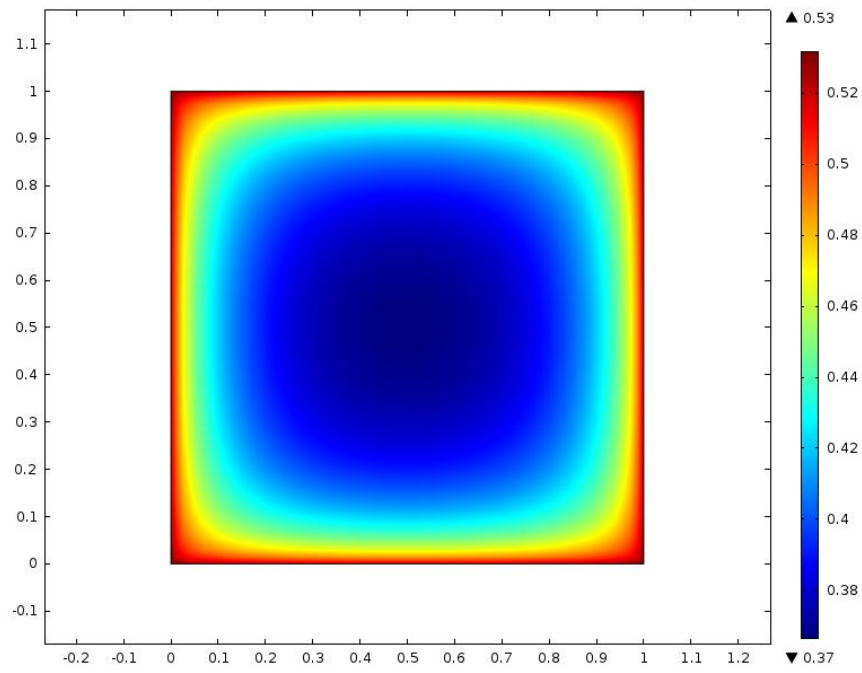
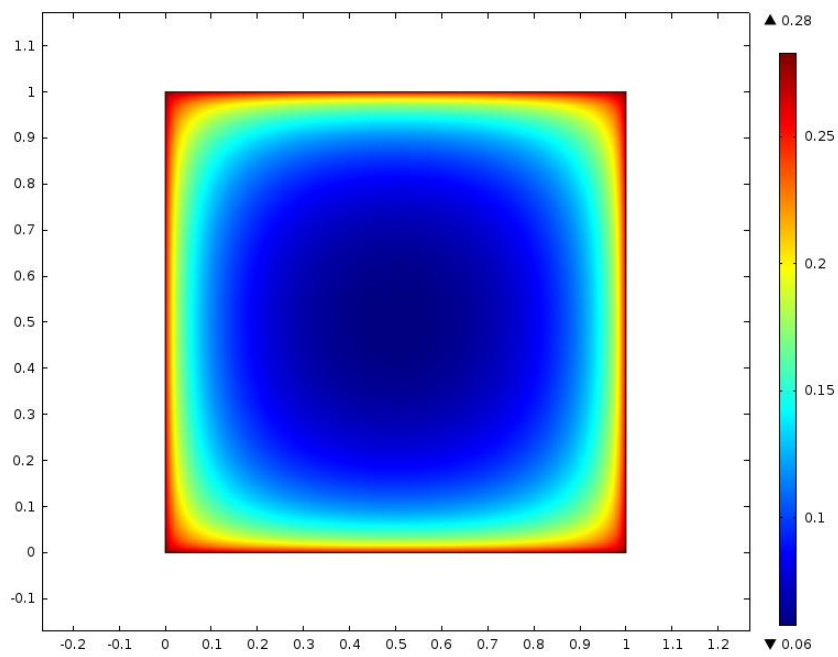


Figure 28: 2D square plate model with side lengths of 1mm.

Mathematical equations (5-11), (5-28), and (5-18), which do not count the effect of water diffusion, were used to calculate the normalised average molecular weight distribution for 2D plate models shown in Fig. 28. Mathematical equations (6-2), (5-28), (6-3), and (5-18), which count the water diffusion effect, were also used to calculate the normalised average molecular weight distribution for the 2D plate models. Both mathematical models, with and without counting the water diffusion, used the same model parameters listed in Table 1 Case A. Boundary conditions were set as no resistance of oligomer, $C_{ol} = 0$, at all boundaries for the 2D plate model, and 5,799 degrees of freedom were used in the calculation. Fig. 29 and Fig. 30 show the average molecular weight distribution and water uptaking distribution for 2D plate models under different degradation times. The threshold of water untaking for Fig. 29(c) and Fig. 30(c) is taken as $C_w = C_{e0} = 17300 \text{ mol/m}^3$, whereas the water is considered to be abundant, in which shows dark red in figs, scale is 1. Otherwise when water is not abundant the area shows dark blue in figs, scale is 0. Fig shows pure green when water is fully abundant across all 2D plant. From Fig. 29(c) it can be observed that for water molecules to fully diffuse into a 1mm thick plate only four to five days are needed. As a result, Fig. 30 (a) and (b), which represent the mathematical models not counting water diffusion and counting water diffusion, show no significant difference. From Fig. 30 (c), data shows water molecules take 17 weeks to fully diffuse into the 5mm thick plate model. As a result, Fig. 30 (a) not counting water diffusion and (b) counting water diffusion show significant differences. In Fig. 30(b), the core area has greater average molecular distribution, which is caused by water molecules not reaching the core area yet.

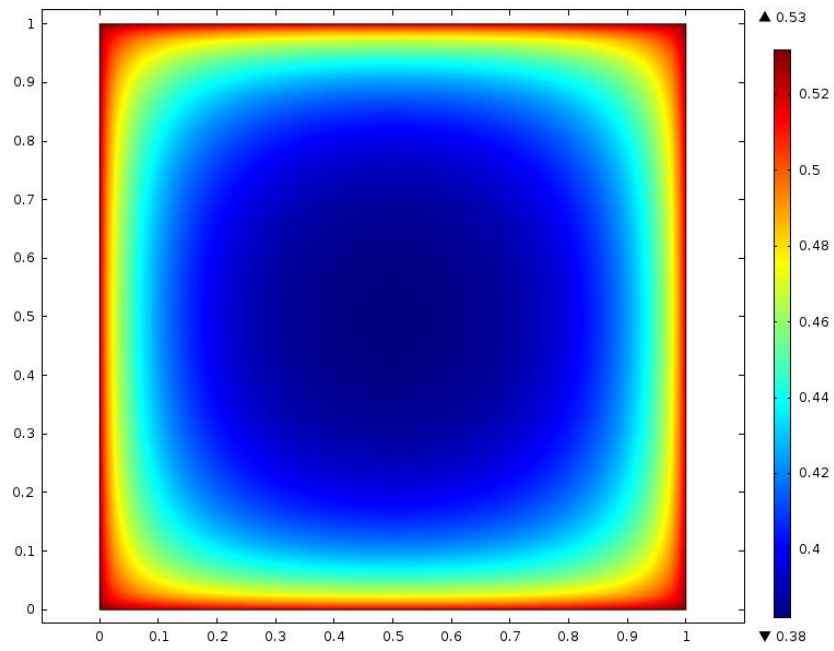


week 14

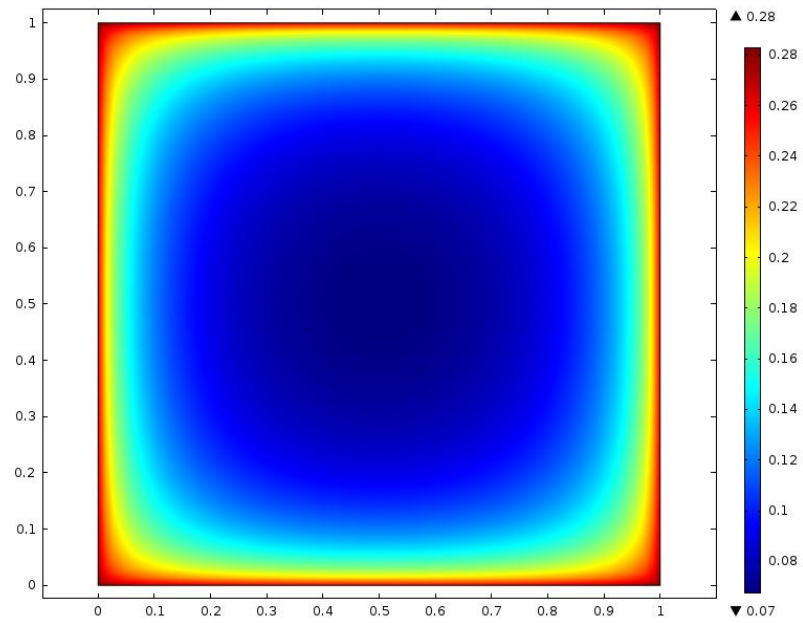


week 28

(a) Average molecular weight distribution not counting water diffusion at week 14 and week 28, respectively

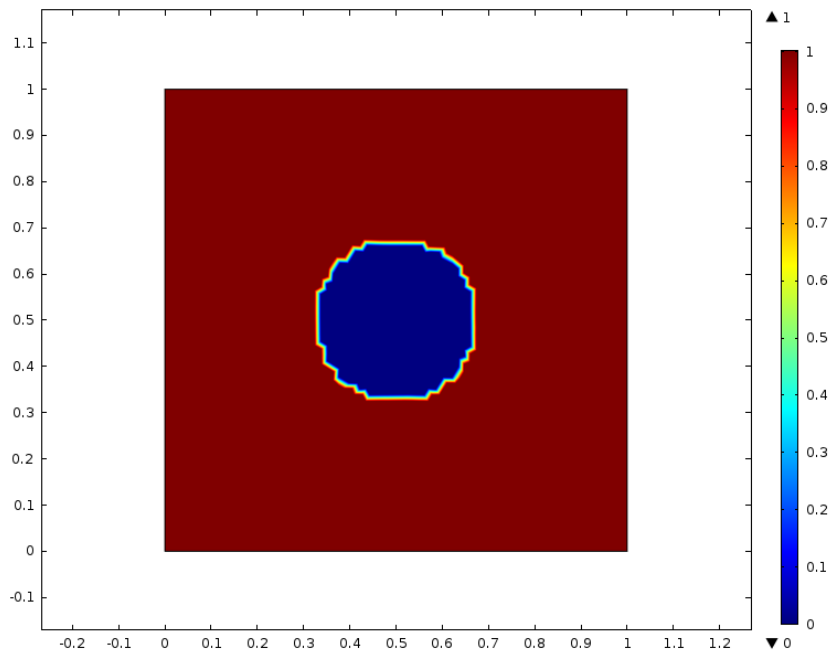


week 14

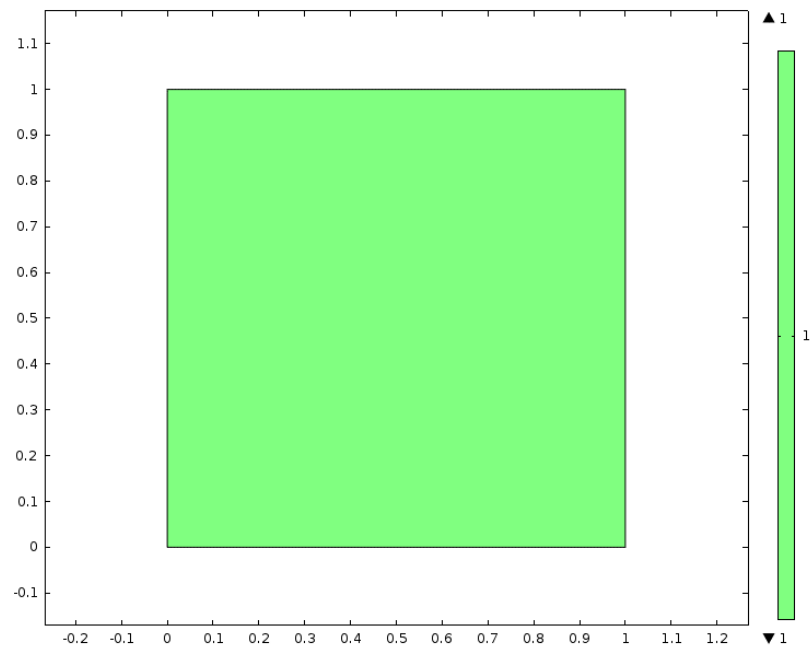


week 28

(b) Average molecular weight distribution counting water diffusion at week 14 and week 28, respectively



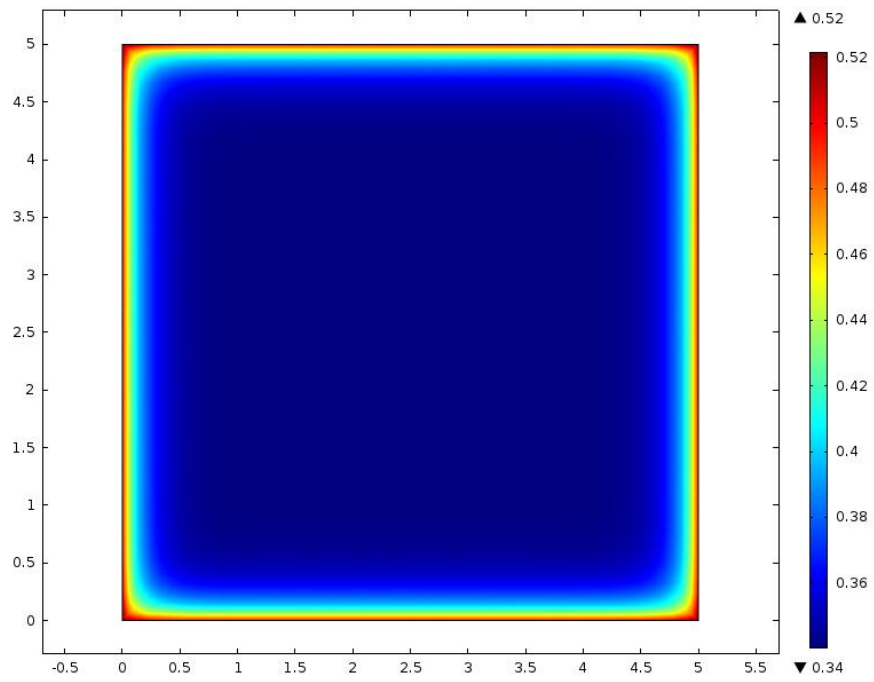
day 4



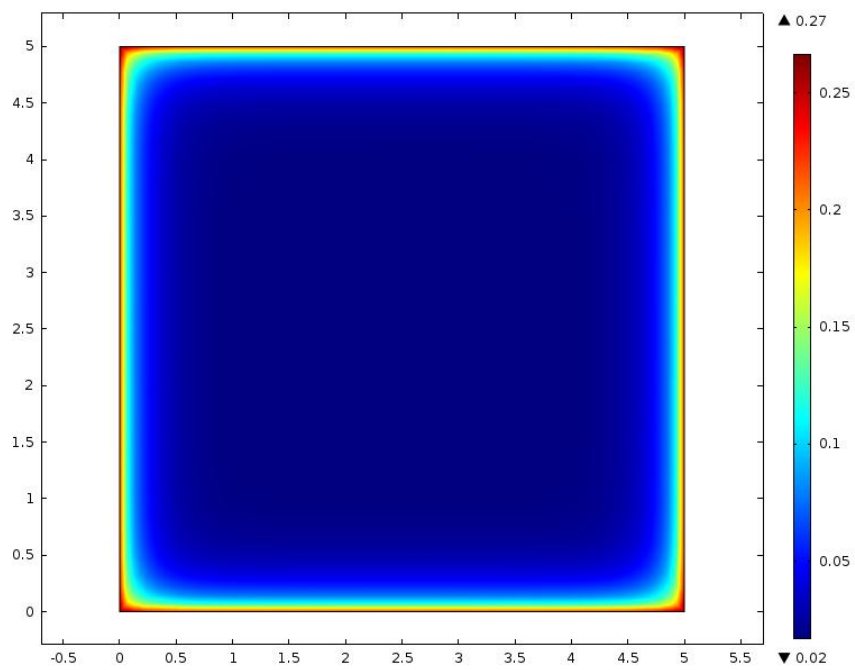
day 5

(c) Water uptake distribution counting water diffusion at week 14 and week 17, respectively

Figure 29: Average molecular weight and water uptake distribution for 2D plate with side length 1mm.

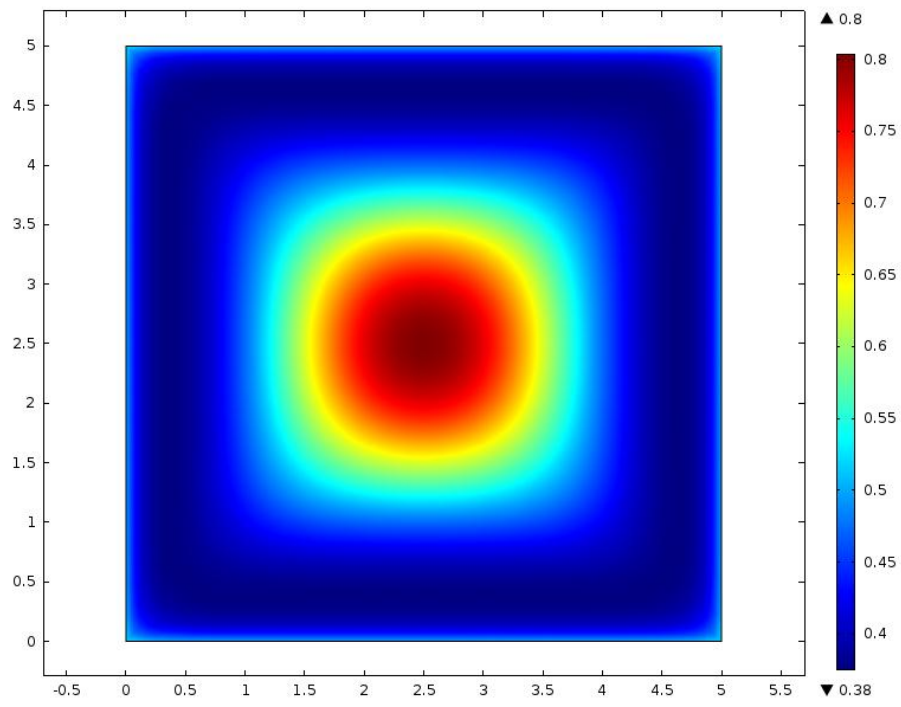


week 14

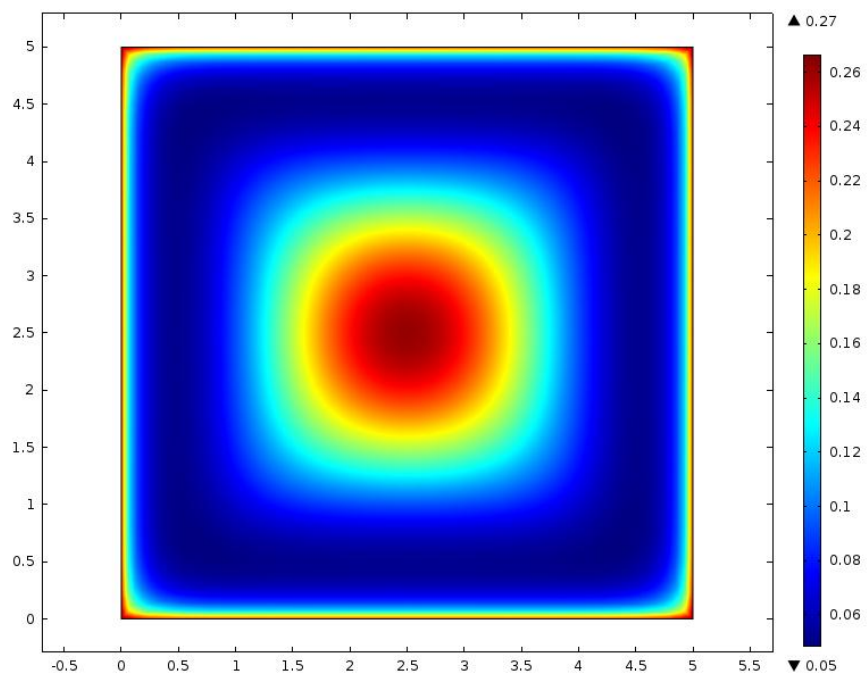


week 28

(a) Average molecular weight distribution not counting water diffusion at weeks 14 and week 28 respectively

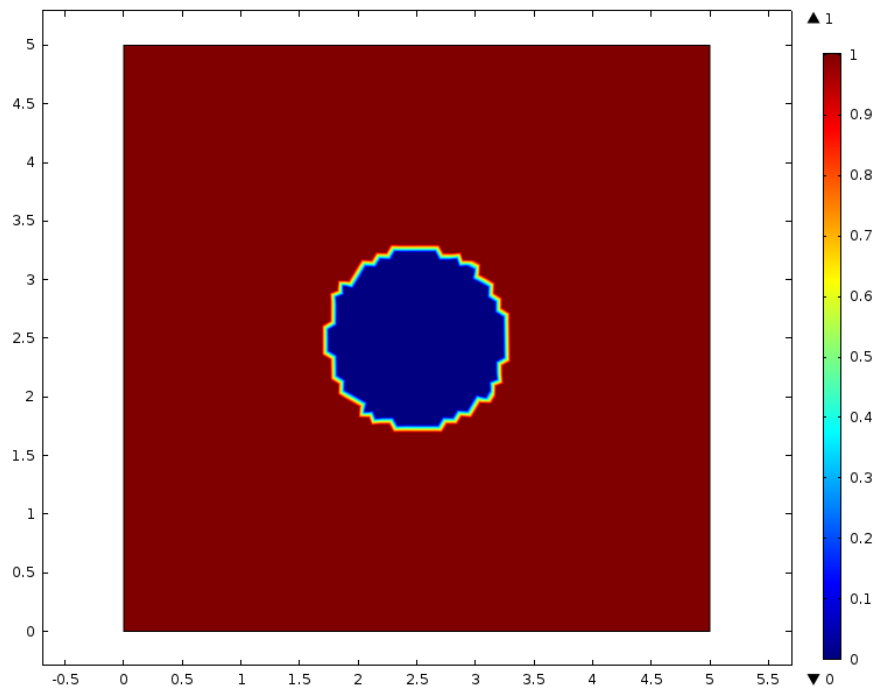


week 14

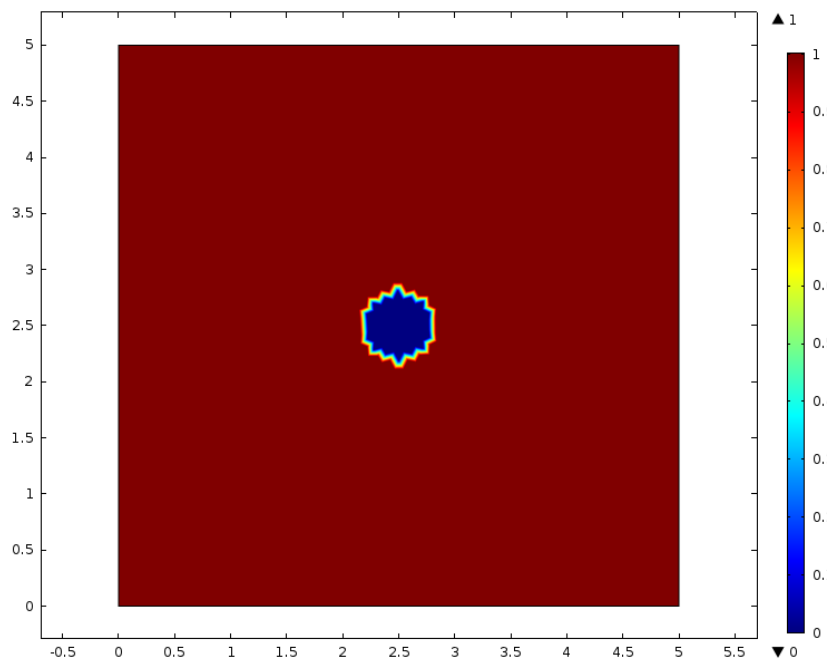


week 28

(b) Average molecular weight distribution counting water diffusion at weeks 14 and week 28 respectively



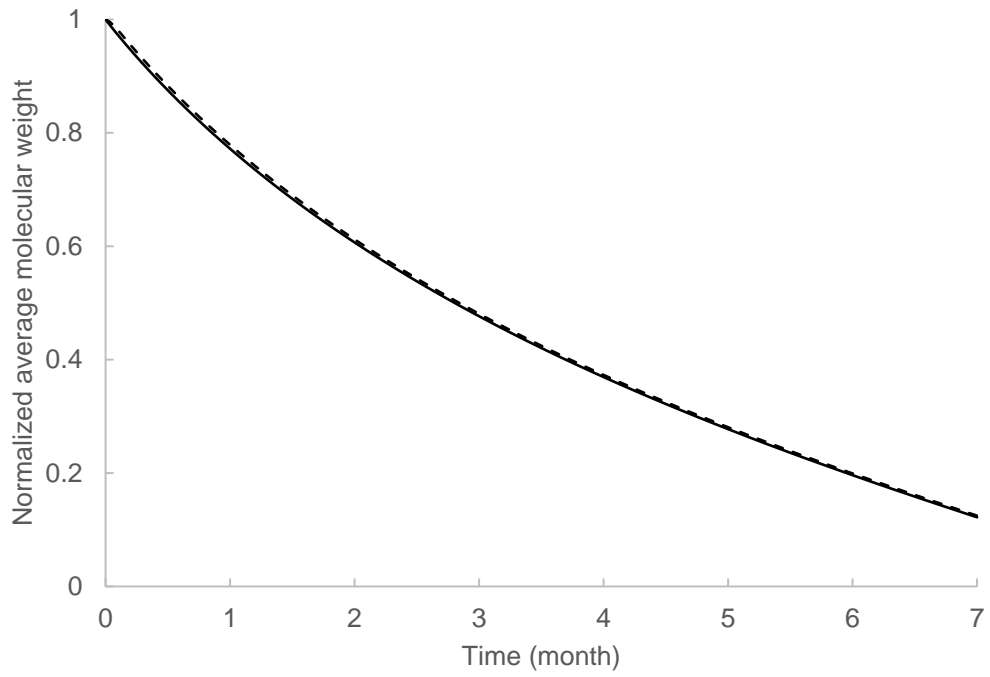
week 14



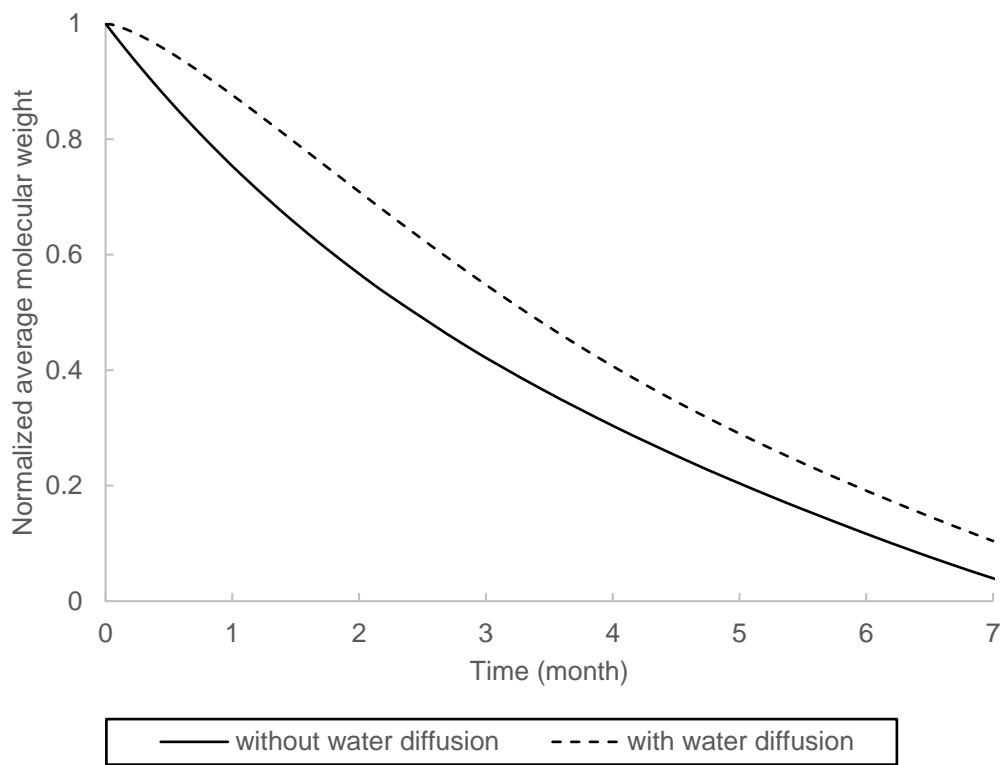
week 17

(c) Water uptake distribution counting water diffusion at weeks 14 and 17

Figure 30: Average molecular weight and water uptake distribution for 2D plate with side length 5mm.



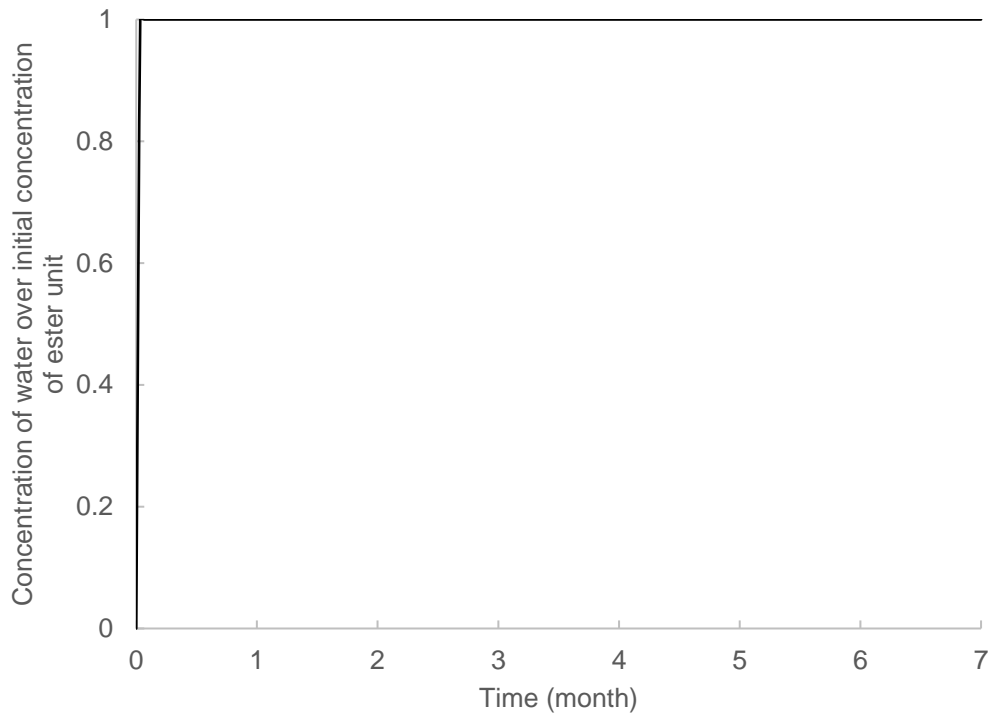
(a) 1mm 2D plate



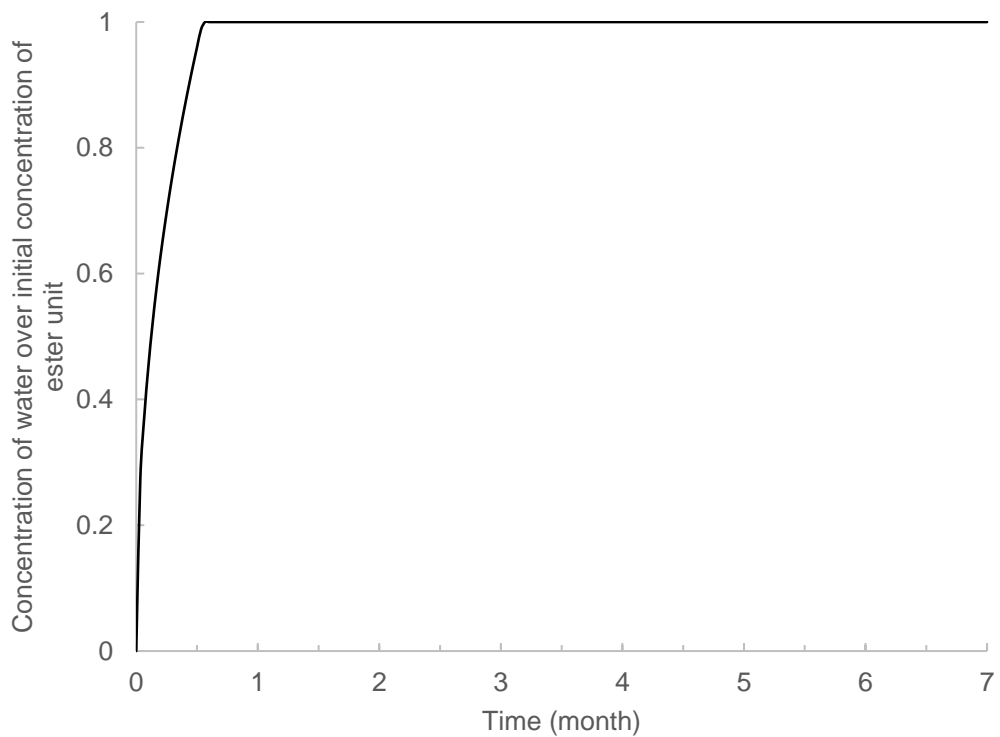
(b) 5mm 2D plate

Figure 31: Normalised average molecular weight reduction with time for the 2D plate with and without counting the effect of water diffusion with side length of (a) 1mm and (b) 5mm.

Fig. 31 compared the normalised average molecular weight reduction trend between the mathematical model without water diffusion term and with water diffusion term for the 2D square plate with side lengths (a) 1mm and (b) 5mm, respectively. Where shows that, for the 2D square plate model with a side length of 1mm, a mathematical model with or without counting water diffusion will not affect the average molecular weight reduction; that is due to the thickness of the plate being thin enough that time for the water molecules to diffuse inside the core of the plate is relatively short. Therefore, the whole degradation process was counted as water abundant. Fig 31(a) clearly shows that for water molecules to rise from 0 to 1 takes a short time, therefore it happens fast. Concentration of water over initial concentration of ester unit, C_w/C_{e0} , was used to demonstrate whether water molecules were abundant inside the polymer. Initially, $t = 0$, for the mathematical model counting water diffusion, the entailed geometry, it was assumed that no water molecules existed inside; $C_w = 55600 \text{ mol}/\text{m}^3$ was set as the boundary conditions for all boundaries. Normalised average molecular weight and water uptake was integrated through the entailed geometry and divided by the volume of the geometry. We assume that when C_w/C_{e0} reaches 1 water molecules are abundant. Growth of C_w/C_{e0} stops at 1; once it reaches 1 it will take constantly as 1, as shown in Fig. 32.



(a) 1mm 2D plate



(b) 5mm 2D plate

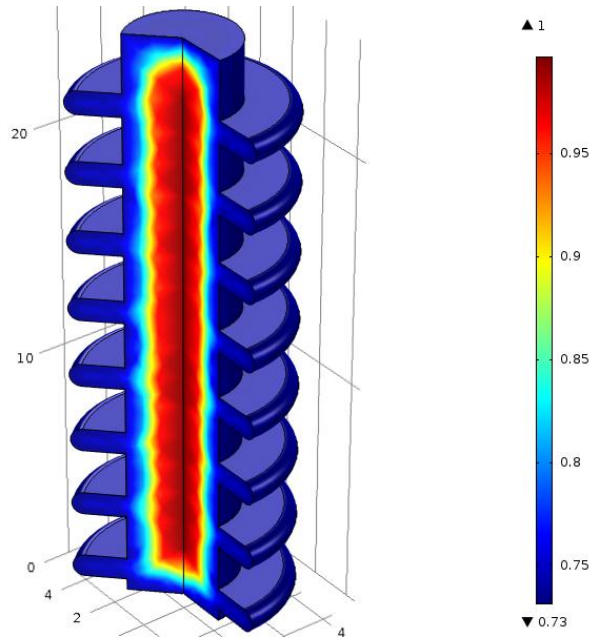
Figure 32: Water diffusion against time for 2D plate with side length of (a) 1mm and (b) 5mm.

Fig. 32 shows a different average molecular weight reduction between the mathematical models with and without counting water diffusion. The reason for that can be found in Fig. 32(b), which shows that water takes about one month for the plate to be abundant in water molecules, thus causing the initial delay of the average molecular weight reduction shown in Fig. 31(b). Therefore, different thicknesses have different water absorbability. For thinner medical devices, such as biodegradable films, which have a thickness less than 1mm, the water diffusion should not have any effect on the degradation rate. However, for the thicker devices, such as interference screws which have a thickness or diameter of several millimetres, water diffusion would delay the degradation at the beginning, thus slowing down the total degradation rate.

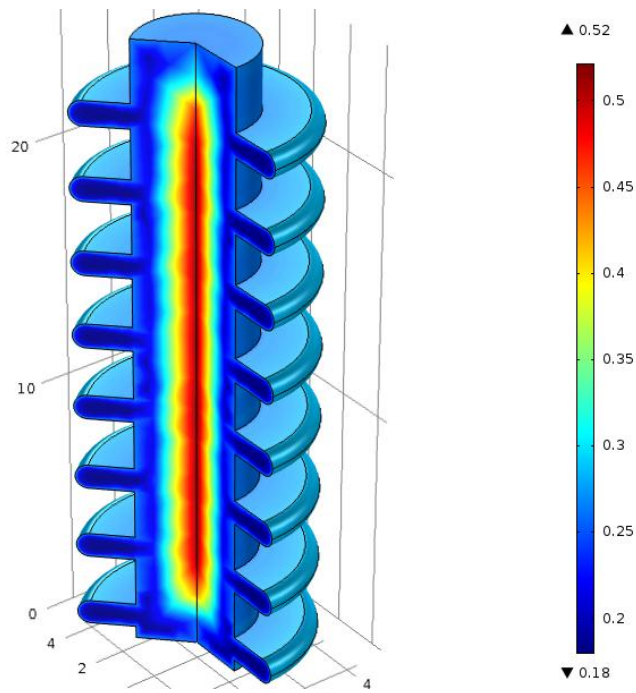
Refining mesh with 1,856 elements and 11,463 degrees of freedom were used to check convergence. The same results were obtained, so the model can be assumed as convergent.

6.4.3 A finite element model for interference screw with water diffusion counted

The interference model that been used in the first half of this chapter was used as a case study for the effect of water diffusion. The mathematical model counting the water diffusion, equations (6-2, 6-3, 5-28 and 5-18), was applied to the screw model. Parameters listed in Table 1 Case A were used. Boundary conditions were set the same as before, i.e. no oligomer residue in all surfaces of the screw. Mesh with 1,146 elements and 7,605 degrees of freedom was used for the calculation. Fig. 33 below shows the (a) average molecular weight distribution, (b) degree of crystallinity distribution, and (c) water uptake distribution for the interference screw model that counts the effect of water diffusion. Convergence was checked with a refined mesh of 1,938 elements and 12,585 degrees of freedom, and the same result was able to be achieved.

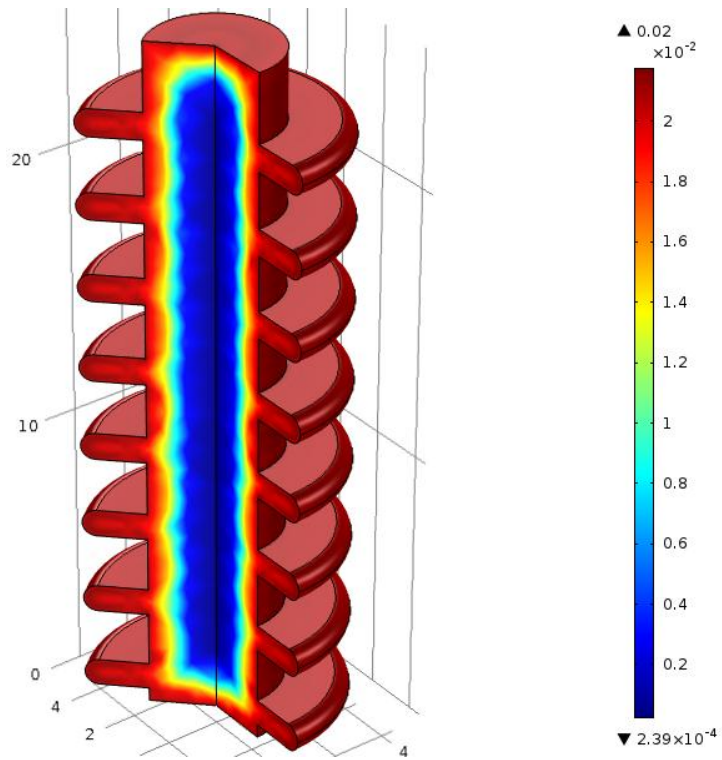


week 7

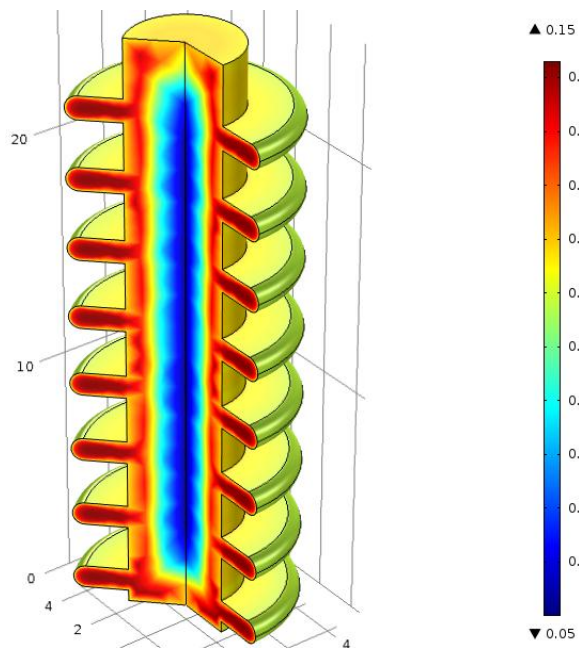


week 28

(a) Average molecular weight distribution counting water diffusion at weeks 7 and 28

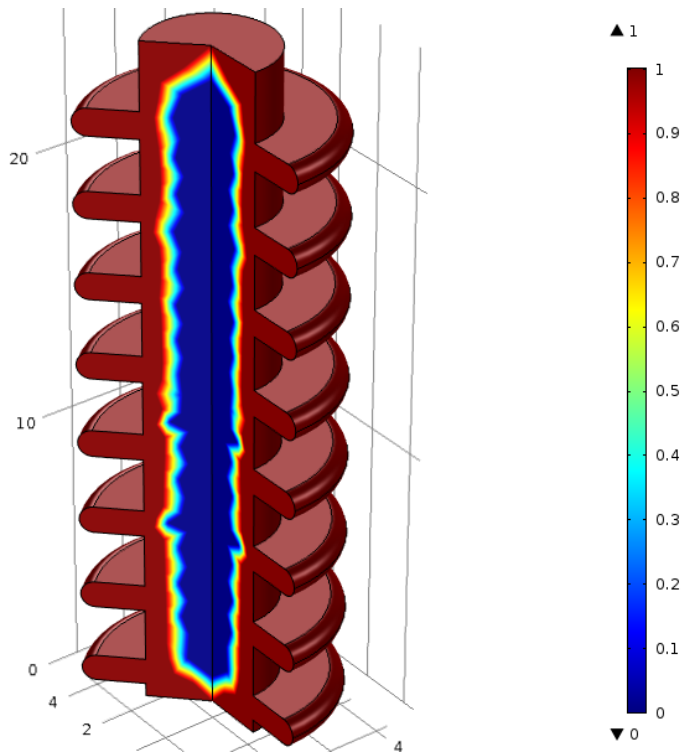


week 7

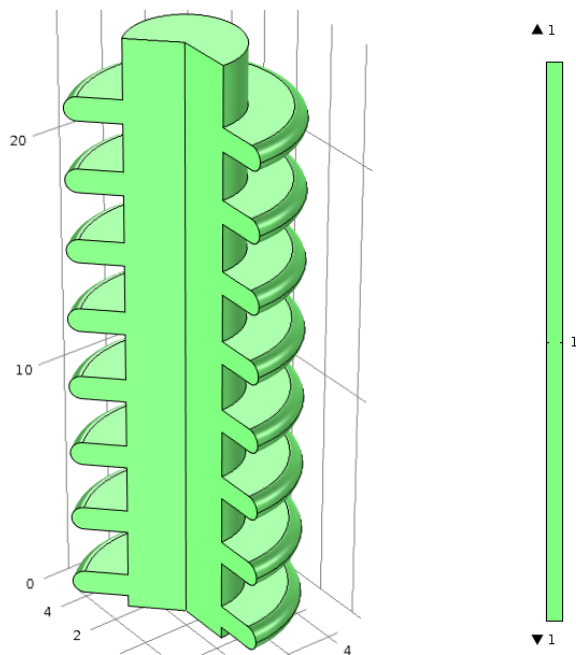


week 28

(b) Degree of crystalline distribution counting water diffusion at weeks 7 and 28



week 7

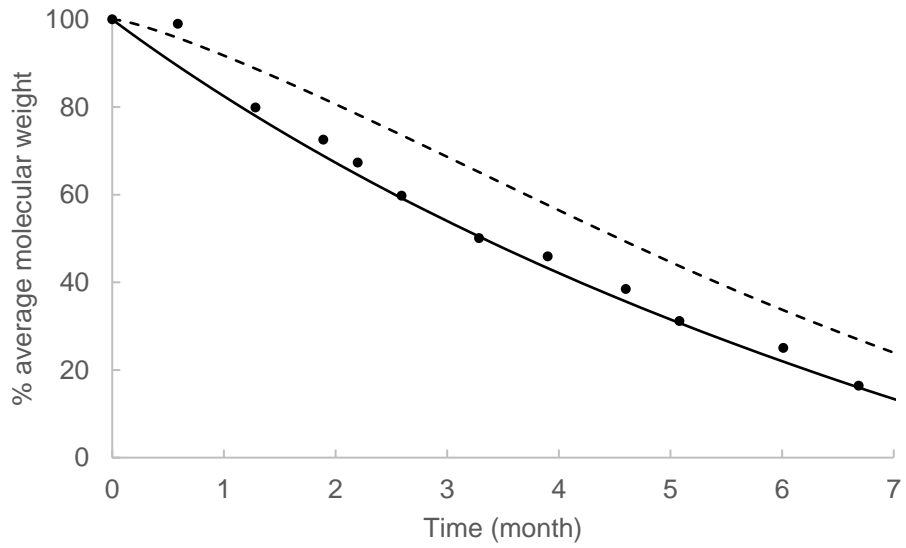


week 28

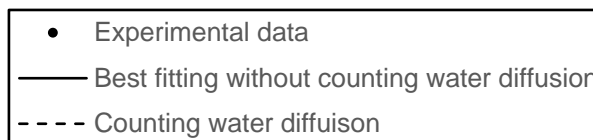
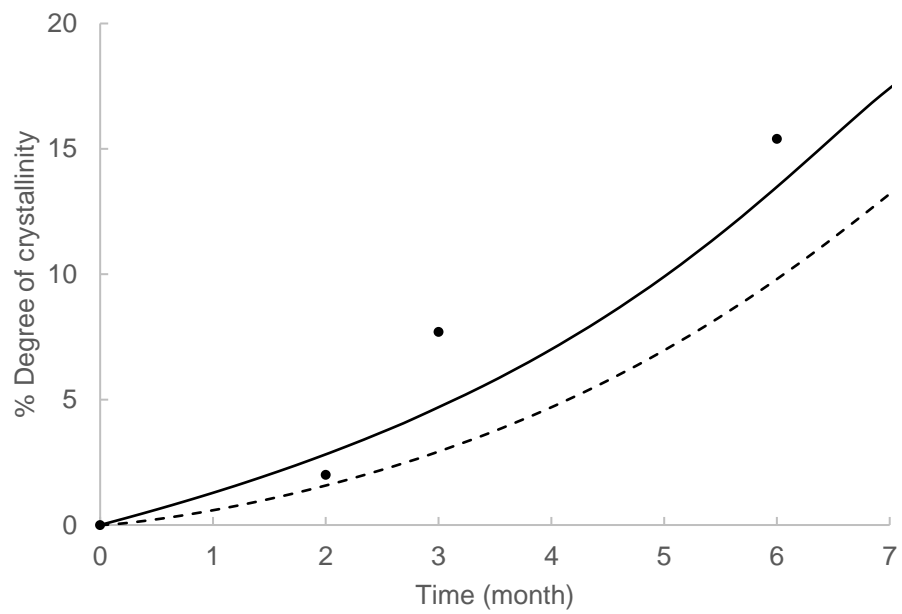
(c) Water uptake distribution counting water diffusion at weeks 7 and 28

Figure 33: (a) average molecular weight (b) degree of crystalline and (c) water uptake distribution for the interference screw model counting the effect of water diffusion at weeks 7 and 28.

Comparing the average molecular weight distribution for the mathematical model without counting the effect of water diffusion, Fig. 19, and the ones with the effect of water diffusion being counted, Fig. 33(a), it can be observed that the degradation behaviours are different. With the average molecular weight distribution shown in Fig. 31 we assumed that water is abundant all the time and everywhere in the screw, so the core area degrades faster than the surface area, which was led by an autocatalysis hydrolytic reaction happening straight after degradation. Whereas, in Fig. 33(a) and (c) it can be observed that water needs time to diffuse into the core of the screw, leading to the surface degrading faster than the core initially, because the core area still does not have enough water molecules to kick off the degradation at the early stage. As degradation passes the half way mark and the screw is almost abundant with water molecules, autocatalytic hydrolytic reaction starts to show its influence, as shown in the dark blue area in Fig. 33(a) week 28. The core area still degrades slower than the surrounding areas; however, the core area can be observed in the later degradation. This actually shows a better agreement with the *in vivo* experimental finding presented by Schwach (1998).



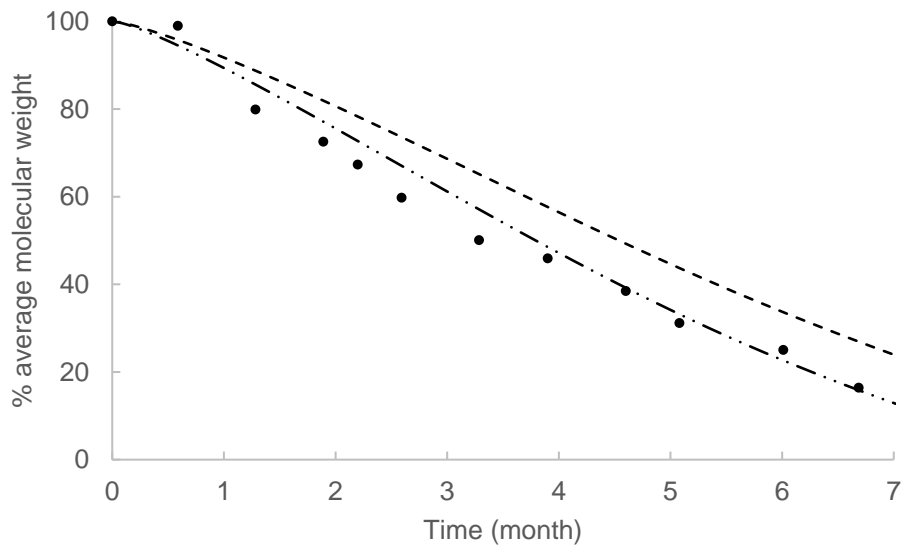
(a)



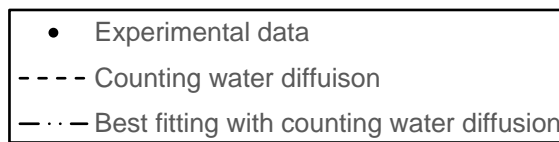
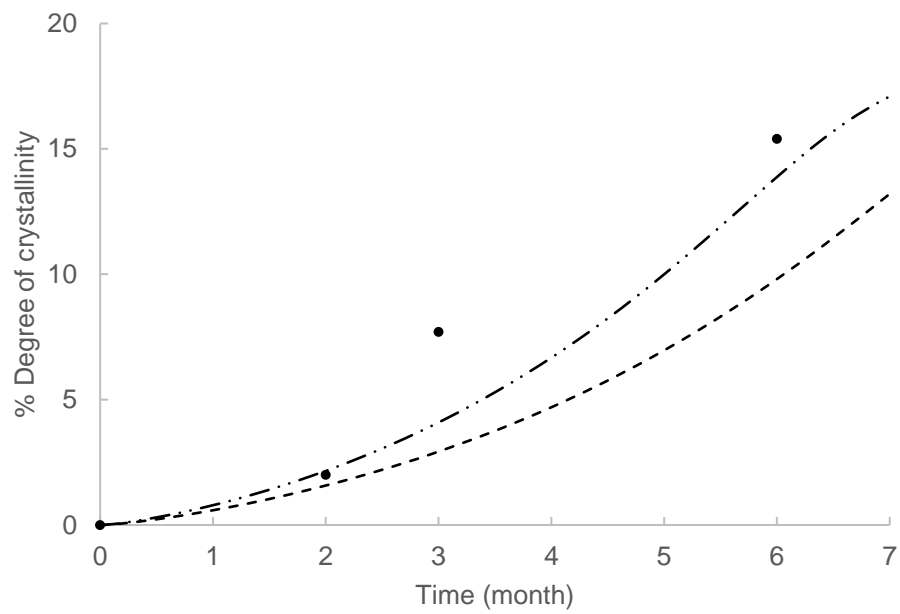
(b)

Figure 34: Counting water diffusion in the interference screw model and comparing the result for (a) average molecular weight and (b) degree of crystallinity.

Fig. 34 shows the (a) average molecular weight and (b) degree of crystallinity trend against degradation time for the mathematical model with and without counting the effect of water diffusion. Data was obtained by integrating average molecular weight and degree of crystallinity through the entire geometry and divided by the whole volume. The experimental data and best-fitting line for without counting water diffusion was presented before. The same set of parameters was used (listed in Table 1 Case A) for the mathematical model with water diffusion counted; however, a different trend can be observed. Therefore, water diffusion does have an effect on this interference model.



(a)



(b)

Figure 35: Best fitting of the mathematical model counting water diffusion for (a) average molecule weight and (b) degree of crystallinity.

For the mathematical model with water diffusion counted, best fitting can be achieved by set $k_1 = 0.008$ ($1/d$), with other parameters remaining the same as listed in Table 1 Case A. It can be observed from Fig. 35(a) that the initial delay of degradation can be better fitted by incorporating the water diffusion effect into the mathematical model.

Biodegradable medical devices are widely in use, but little is known about their storage condition. Atmosphere contains water molecules, and biodegradable devices' contact with the atmosphere could cause loss of average molecular weight and mechanical stiffness. The mathematical model adding the effect of water diffusion could be used as a tool to predict the storage condition.

Water is present in variable amounts in the atmosphere, from 0% to 4%. If we use the interference screw as an example and consider that the screw was stored in such an atmosphere, then its degradation behaviour is given in Fig. 36. It can be observed that models can be used to predict the storage behaviour. For the same screw to reduce to 80% of its original average molecular weight, this could happen in less in a year if the screw had been placed in the atmosphere with 4% of water and in five years if the screw was placed in the atmosphere contain only 0.5% of water.

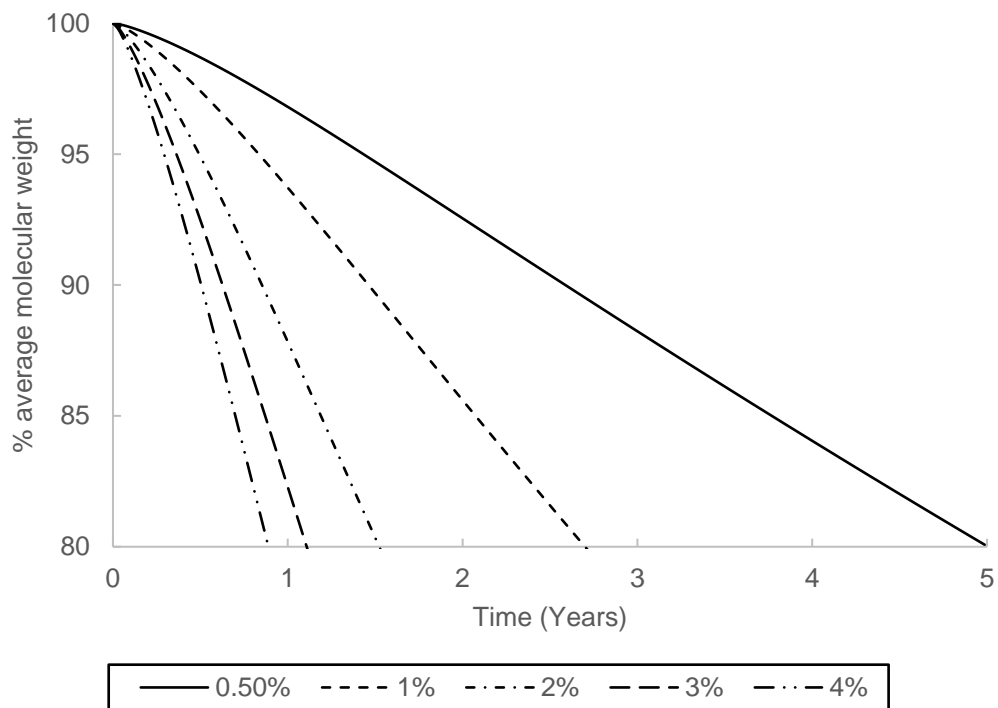


Figure 36: Average molecule weight reduction for storage assuming the atmosphere contains 0.5% to 4% of water.

6.5 Conclusion

It was proved in this chapter that mathematical models can not only provide a fitting to the existing experimental data, but also many sets of mathematical parameters could be found to successfully fit the same set of experimental data. By applying these sets of parameters into a newly designed model or optimising the size of the current model, a range of degradation rates, degrees of crystallinity, and other material properties could be calculated. The new model was expected to have degradation behaviours and material properties inside the predicted range. Instead of using the trial-and-error method for designing, this computer modelling method could be used to save a huge amount of time and resources. The only condition for this method is that the designer has to use a material that has been experimentally tested and has degradation data available to use. This should not be an issue considering that biomedical device design would most likely be using clinically familiar material and most of these materials would be experimentally tested before used in human trials.

Water diffusion was proved to be effective to the degradation rate for thicker biodegradable medical devices. Water molecules take longer to fully diffuse inside of such devices, causing initial delays for the degradation. Further heterogeneous degradation behaviour can be observed, which is more likely to be the real case by counting the *in vivo* experimental results. Furthermore, the mathematical model with the water diffusion term can be used to predict the storage condition for biodegradable devices. Using the interference screw, which has been presented in this chapter, as an example, the average molecular weight reduced to 80% of the original value in one to five years, dependent on the water vapour level of the atmosphere. Still, it provides an indication of storage time if one wanted to store such a screw in atmospheric conditions.

Chapter 7: A simplified Effective Cavity Theory

An effective cavity theory was developed previously by the Leicester group. However, the previous theory is over-complicated for practical applications. This chapter presents a simplified version of the Effective Cavity Theory and its validation using existing experimental data.

7.1 Introduction

The Effective Cavity Theory was first introduced by Gleadall (2015) and Samami (2016) to analysis the effect of polymer chain scission on Young's modulus change. Young's modulus is such an important factor for biodegradable medical implants as they are all required to provide a temporary mechanical function and then gradually hand over the control to the human biological system. Therefore, it is very important to understand and fully capture the regulation of it for design purposes. There is many experimental data measuring Young's moduli change with degradation, but few mathematical models that provide the simulation. Before Gleadall, et al. (2015) there was only one other computational model that links the Young's modulus change to the average molecular weight variation during degradation in biodegradable polymers. Which is the entropy spring model developed by Wang, et al. (2010). This model focuses on amorphous polymers which are above their glass transition temperature. Successful experimental data fitting was presented by the model for Young's modulus degradation. However, in reality, biodegradable polymers are more like to be used below their glass transition temperature. Ding, et al. (2011) presented a numerical analysis using molecular dynamics (MD) simulations, which could capture the Young's modulus change due to chain scission for biodegradable polymers which are used above and below their glass transition temperature. The interaction force between polymer chains was found reduced after a chain breaks when the polymer was below the glass transition temperature. Simple polyethylene chains were considered in the MD simulation. Due to computational limitations, analysing complex biodegradable polymers such as poly(lactide) is not available. After Andrew's study on Effective Cavity Theory, Samami, et al. (2016) presented a constitutive law for degrading biodegradable polymers on their mechanical property change due to degradation.

However, the model was over-complicated and a huge amount of background knowledge was required, which was considered not designer-friendly. Therefore, Gleadall's method was still the best 'designer-friendly' mathematical analysis to study the effect of chain scissions on Young's modulus during degradation. However, Gleadall's model added in many parameters that would affect the volume of each effective cavity, which is one of the most crucial factors in the Effective Cavity Theory. Therefore, this chapter aims to simplify the Effective Cavity Theory and reduce the input factor to one while achieving the same result as previous model. The simplified Effective Cavity Theory was used to fit several sets of experimental data and was also compared the result with the previous work. Also, this chapter combines the simplified theory with the degradation mathematical model presented previously and forms them into a simple model that could simulate degradation of molecular weight and crystallinity as well as Young's modulus.

7.2 Previous Effective Cavity Theory

In the Effective Cavity Theory, polymer chain scission was assumed to be able to produce a volume of area which contains reduced stiffness of polymer. Crystals that have higher mechanical properties and lower water absorbable than amorphous polymers can be treated as inclusions. Therefore, modelling degradation of semi-crystalline polymer can be treat as modelling a continuum solid which have reduced stiffness void cause by chain scission and crystal as solid inclusions. It has been assumed in the Effective Cavity Theory that the size of each cavity and the inclusion remain the same, as scission increases the total effective volume increases as well.

7.2.1 Numerical model by Gleadall, et al. (2015)

Gleadall used the AFEM method to simulate chain scission, whereas one polymer repeat unit was removed from the structure to represent one scission. The shapes of the effective cavities were achieved by analysing the atomic force transfer reduction. With one scission, a volume could be created in which average atom force transferred been reduced at least 10%. After 10 individual scissions, the shape of a flat-tipped cone

was suggested to be treated as volume of the reduced stiffness polymer. Therefore, Gleadall, et al. (2015) suggested that a shape of flat-tipped cones oriented tip-to-tip may exist around chain scissions as effective cavities, which is shown in Fig. 37.

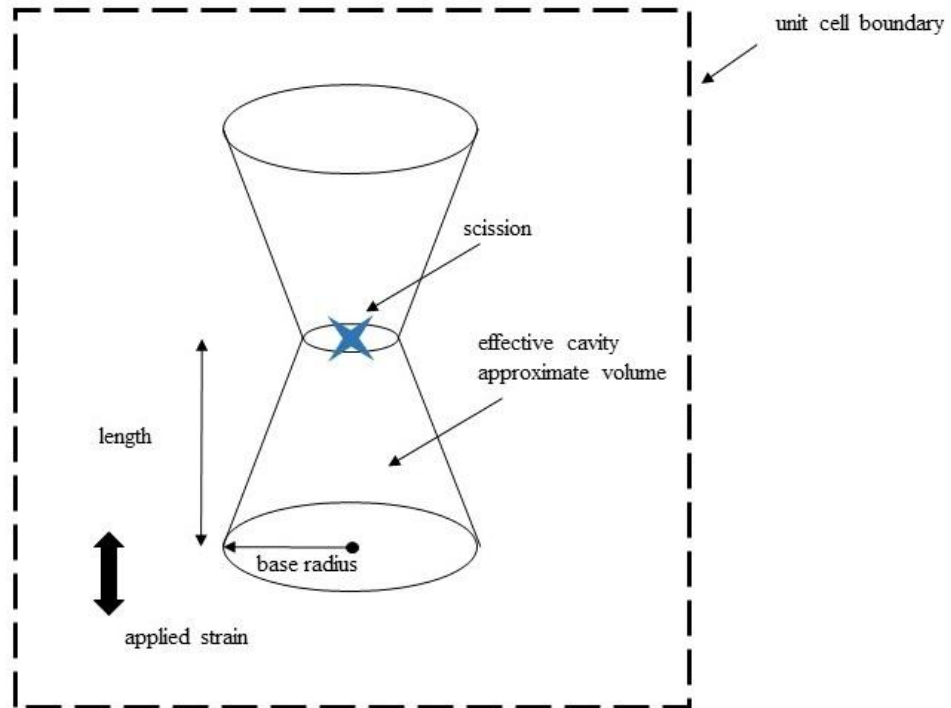


Figure 37: Apply individual scissions to the amorphous polymer. Shape of the effective cavity suggested by Gleadall, et al. (2015) in the previous Effective Cavity Theory.

Like the chain scission to the volume change of the effective cavities, Gleadall, et al. (2015) take a cubic matrix and applied one quarter of a flat-tipped void to it. Whereas the cubic matrix represents the amorphous polymer and the void represents scissions. A finite element model has been set in COMSOL (license number 7074366) as shown in Fig. 38. The volume shown in Fig. 38 was used to represent 1/8 of a unit amorphous polymer cell, therefore, left, front, and bottom faces were set as symmetry.

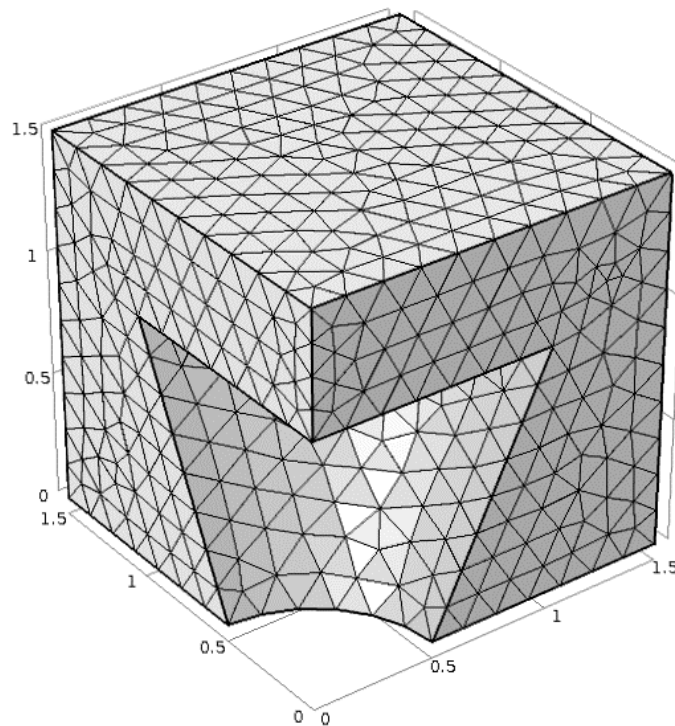


Figure 38: Use FEA model to analysis the effect of the effective cavity to Young's modulus in cubic matrix by Gleadall, et al. (2015) (length unit in nm).

A range of cone height, cone large radius, and cone small radius was required to study the change that the shape of the cone caused to the Young's modulus reduction, which contains too many parameters. Changing the shape of the effective cavity and reducing the parameter that controls the shape to only one is necessary in order to simplify the whole Effective Cavity Theory, which will be presented later in this chapter.

The exact shapes of the crystals are not yet well understood. However, crystallisation was assumed to be formed by polymer chains lined up or folded back and forth to plates. Based on this Gleadall, et al. (2015) assumed that these plates can be simplified into cube shapes, as shown in Fig. 39. The highlighted part is referenced as crystalline, which has been given a bigger Young's modulus (nearly twice) as the amorphous polymers, which is area without highlighting in Fig. 39. A similar method is in use of developing the analysis as was used in the effective cavity model: the set-up was kept unchanged other than the shape of the void has been replaced by cube solid inclusion, which was used to indicate crystallites. The left, front, and bottom faces are again set

symmetrically, and Fig. 39 shows that 1/8 of a whole cube contains amorphous and crystalline.

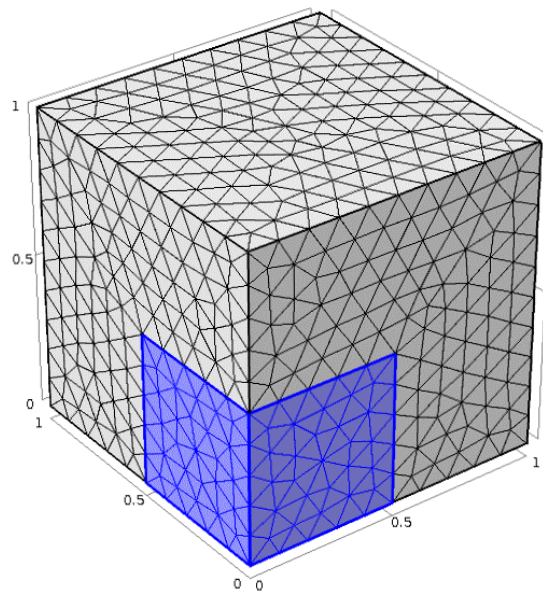


Figure 39: Use FEA model to analysis the effect of changing in crystallinity to Young's modulus (Gleadall, et al., 2015) (length unit in nm).

To form into the Effective Cavity Theory model, Gleadall combined the chain scission model and the crystallinity model, as shown in Fig. 40. Whereas the effective cavities are incorporating with crystal particles and the matrix of amorphous polymers. However, Gleadall's work did not include crystallite and effective cavities interactions. Which would hugely complicate the model and the model had already shown a good agreement with experimental data.

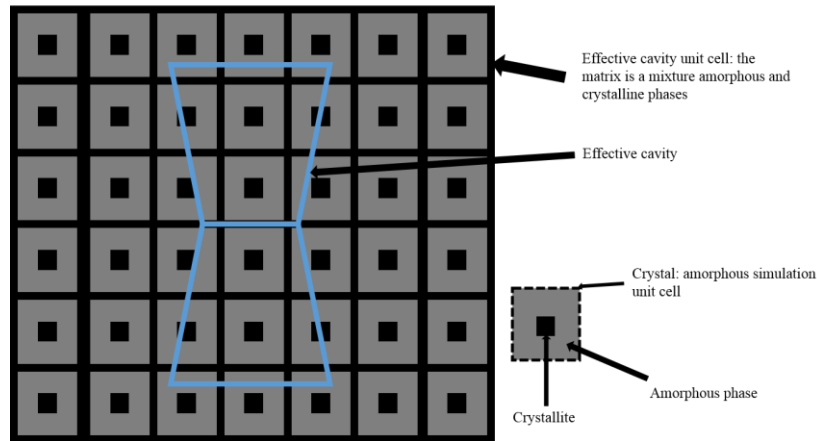


Figure 40: Semi-crystalline polymer matrix which contains effective cavity and crystal particle (Gleadall, et al., 2015).

7.2.2 Analytical model by Samami (2016)

Different to Gleadall's work, Samami assumed that both effective cavities are caused by scission and that the crystals are formed into simple spherical shapes. As with Gleadall's work, each chain scission has been treated as a void and each crystal as a solid inclusion, whereas the cavity region has no stiffness at all and the crystal region has high mechanical properties than amorphous area of the polymer.

By assuming both cavity and inclusion as inhomogeneity, Fig. 42 can be used to represent the semi-crystalline polymer.

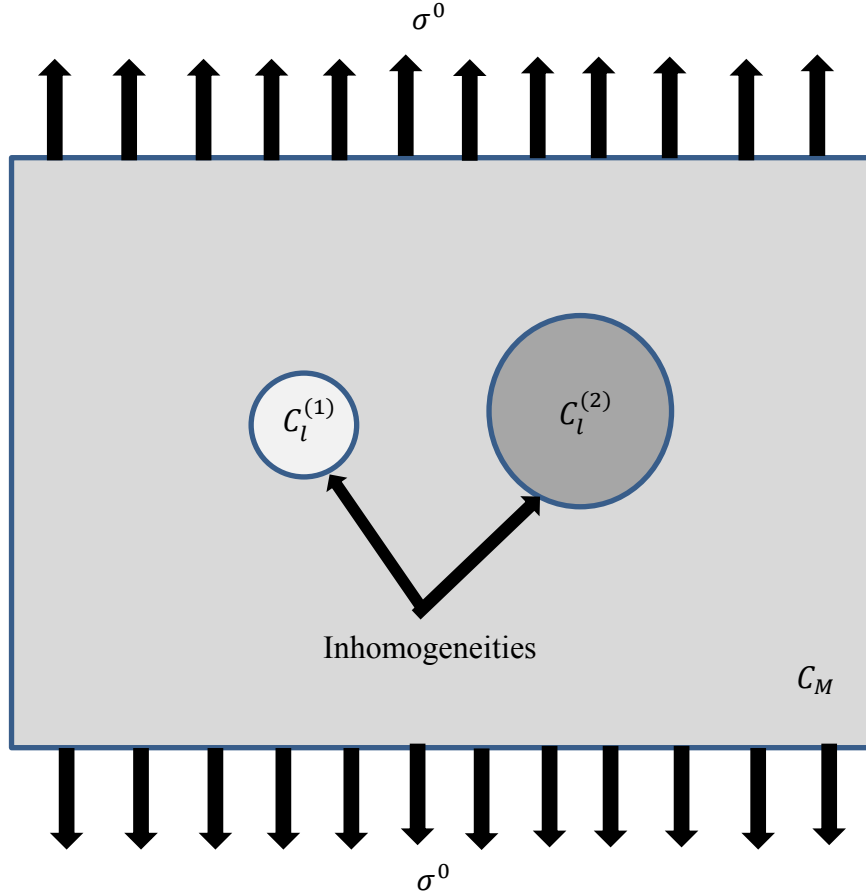


Figure 42: Semi-crystalline polymer which contains two inhomogeneities particles: effective cavity and crystal (Samami, et al., 2016).

In this, σ^0 is the uniformly remote stress of the solid polymer. The solid polymer contains an inhomogeneity $\Omega^{(1)}$ with elastic stiffness $C_I^{(1)}$ (which is zero) and an inhomogeneity $\Omega^{(2)}$ whose elastic stiffness is $C_I^{(2)}$, and $C_M^{(2)}$ is the elastic stiffness of the amorphous polymer surround. Again, the interaction between the boundaries is not considered here.

Samami, et al. (2016) presented the constitutive law of effective stiffness of degrading biodegradable polymer as

$$C = C_M - C_M f_I^{(1)} (\bar{\varepsilon}_I^{(1)} / \varepsilon^0) + (C_I^{(2)} - C_M) f_I^{(2)} (\bar{\varepsilon}_I^{(2)} / \varepsilon^0) \quad (7-1)$$

Put into the form of tensor notation, equation (7-1) can be changed into

$$C_{ijkl} = C_{Mijkl} - C_{Mijkl} f_I^{(1)} (\bar{\varepsilon}_{Ikl}^{(1)} / \varepsilon_{kl}^0) + (C_{Iijkl}^{(2)} - C_{Mijkl}) f_I^{(2)} (\bar{\varepsilon}_{Ikl}^{(2)} / \varepsilon_{kl}^0) \quad (7-2)$$

For the bulk and shear moduli when Effect Cavity Theory is subjected to remote hydrostatic pressure ε_{kk}^0 and share strain ε_{12}^0 , this is given by

$$K = K_M - K_M f_I^{(1)} (\bar{\varepsilon}_{kk}^{(1)} / \varepsilon_{kk}^0) + (K_I^{(2)} - K_M) f_I^{(2)} (\bar{\varepsilon}_{kk}^{(2)} / \varepsilon_{kk}^0) \quad (7-3)$$

$$\mu = \mu_M - \mu_M f_I^{(1)} (\bar{\varepsilon}_{12}^{(1)} / \varepsilon_{12}^0) + (\mu_I^{(2)} - \mu_M) f_I^{(2)} (\bar{\varepsilon}_{12}^{(2)} / \varepsilon_{12}^0) \quad (7-4)$$

Whereas Young's modulus and poisson's ratio can be shown as

$$E = 9K\mu / (3K + \mu) \quad (7-5)$$

$$\nu = 3K - 2\mu / 2(3K + \mu) \quad (7-6)$$

To link the Young's modulus change to the rate of chain scission we have

$$f_I^{(1)} = \sum \frac{4}{3} \pi r^3 R_s \quad (7-7)$$

The symbols that are used in the equation are listed in Samami's paper (Samami, et al., 2016).

It has been proved that the model presented by Samami, et al. (2016) could be used to fit experimental data. However, as seen above, the model is over-complicated, even when just used a simple spherical shape to represent the cavity and crystal. A huge amount of background knowledge is required, which is hard to follow for any non-engineering end users or biodegradable medical device designers. Therefore, a simplified model is required to achieve the same purpose.

7.3 Simplified Effective Cavity Theory

The simplified Effective Cavity Theory is basically a combination of the numerical model (Gleadall, et al., 2015) and the analytical model (Samami, et al., 2016). The numerical model has been used as a fundamental structure but the shape of the effective cavity has been changed to spherical in order to reduce the parameter that controls the effective cavity volume fraction to only one, the radius of the spherical cavity. As the number of chain scissions increase along with degradation, total volume of the effective cavities will increase as well. The FE model of effective cavities links the volume fraction of effective cavities to the change of Young's modulus. The shape of the crystal remains cubic, and has been assumed as an inclusion in the cubic polymer of amorphous phase. The effective volume of crystallinity increases with degradation and the Young's modulus goes up with it, due to crystallite has higher mechanical properties compare to amorphous phase. The simplified Effective Cavity Theory can

be achieved by combining the FE analysis of Young's modulus change for effective cavity and crystallinity. Simplified method is very easy to achieve and is proved to be valid by fitting the same experimental data used in Gleadall's paper (Gleadall, et al., 2015) and Samami, et al., (2016).

7.3.1 Analysis the Young's modulus change due to chain scission using the simplified model

As a change, the spherical shape of the effective cavity was used, as shown in Fig. 43, and the commercial FE software COMSOL Multiphysics (license number 7074366) was used. The cube shown in Fig. 43 reflects one eighth of a unit, which represent a small part of the sample polymer. The spherical void shape in the centre of the cube relates to one eighth of the unit's effective cavity, which assumed no stress. Therefore, the boundary conditions for the cube shown in Fig. 43 would be set as follows: the left, front, and bottom faces are symmetrical; free condition has been set to the back and right faces which kept plan and allows the effect of Poisson's ratio; the bottom face is fixed in z direction. On the top face of the cube, a displacement of 2% was given. As the simulation shown in the figure, the radius of the spherical effective cavity takes 1nm and keeps the same. The overall side length of the cube takes 3nm, which can be adjustable to achieve the different effective cavity volume fraction; for example, the side length of the overall cube could be reduced to represent an increased number of chain scissions (or a later stage degradation), which would be related to a larger effective cavity volume fraction.

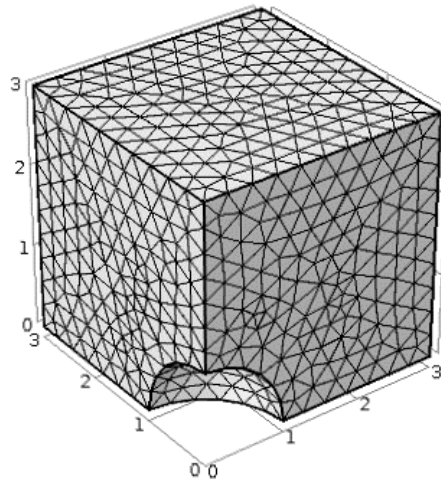


Figure 43: The FEA model with mesh for a spherical effective cavity in a cubic matrix which stand for amorphous polymer (length unit in nm).

An initial Young's modulus value applied in cubic polymer has been set as 37.1 GPa and Poisson's ratio is 0.255 (Gleadall, et al., 2015). Twenty cubic side lengths have been used, which varies from the same size of the radius of the unit spherical effective cavity to 20 times its radius (which keeps constant as 1nm). Refining meshes not giving a significant impact to the result. Average stress existed in the top surface of the FE model in the direction of applied strain, which is 2%, was found. Average stress divided by 2% strain gives the Young's modulus, which has then been normalised by the original value that was applied to the cube (37.1 GPa). The effective cavity volume fraction is achieved by the volume of the overall cube divided by the unit volume for spherical effective cavity. The plot for normalised Young's modulus against the effective cavity volume fraction of all 20 sets of data has been shown in Fig. 44. Whereas, a best fitted exponential line was given.

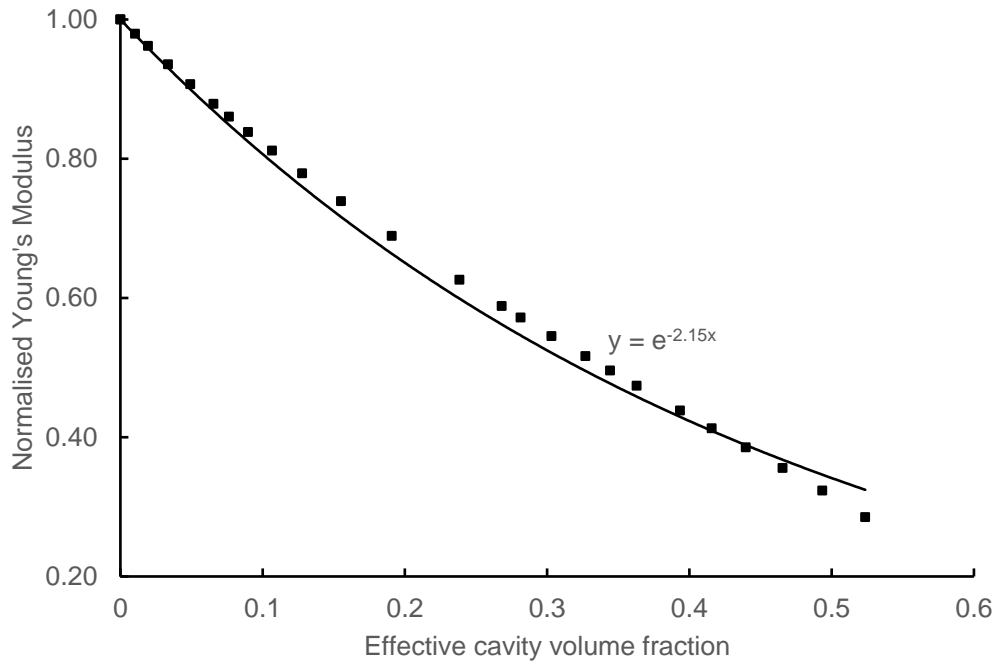


Figure 44: Effect of the volume fraction of spherical effective cavity on normalised Young's modulus during degradation with a best fit of exponential line.

Expression of the best fitting line is

$$\bar{E} = e^{-2.15X_{ec}} \quad (7-8)$$

Whereas \bar{E} is the normalised Young's modulus and X_{ec} represent effective cavity volume fraction in the polymer matrix. We assume that in reality the spherical effective cavity caused by scission is constant for each type of polymer. Therefore, the volume fraction X_{ec} should only be affected by number of chain scissions, as X_{ec} is achieved by unit spherical effective cavity multiplied by the number of scissions.

7.3.2 Effect of crystallinity on Young's modulus using the simplified model

The effect shape of the crystal is assumed to be the same as in Gleadall's work (2015). Because crystals are assumed to be picked and folded together this is more likely to be a cubic shape. Therefore, Gleadall's work for effect of crystallinity on Young's

modulus can be applied here, as represented in Fig. 45. A similar approach is applied. Boundary conditions are still set as follows: free condition has been set to the back and right faces which kept plan and allows the effect of Poisson's ratio; the bottom face is fixed in z direction. On the top face of the cube, a displacement of 2% was given, which also demonstrates that Fig. 45 shows one eighth of a unit part of the polymer which expands infinitely in every direction. Only difference here will be initial Young's modulus for amorphous polymer (cube in Fig. 45 other than the highlighted area) and the crystalline phase (highlighted cube in Fig. 45). The actual value of the initial Young's modulus was set as 37.1 (GPa) for the amorphous phase and 77.4 (GPa) for the crystalline phase. However, these actual numbers are not important for the result; what important is the rate between the crystalline and amorphous Young's modulus. In this case, the ratio is 2:1, which is reasonable. The Poisson's ratio for the amorphous matrix is taken as 0.255 and for the crystal particle as 0.239.

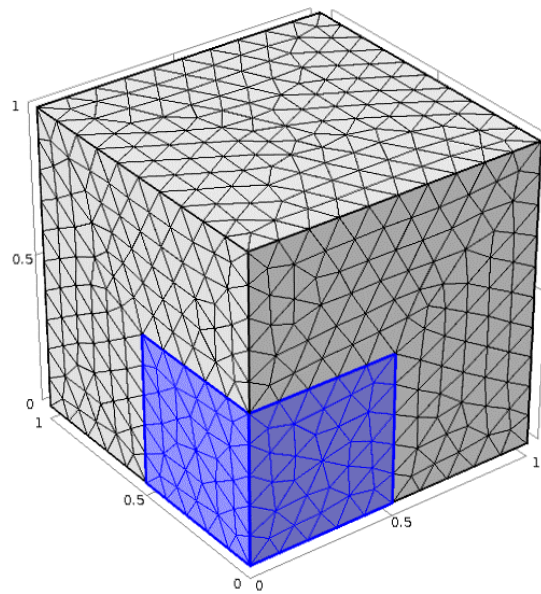


Figure 45: Use FEA model to analysis changing in crystallinity to Young's modulus in cubic matrix by Gleadall, et al. (2015) (length unit in nm).

FE method again been used to analysis the effect of crystallinity to Young's modulus. Same as the effect cavity method, the size of the crystallite inclusion kept the same whereas the total volume of the cube increases to simulate the volume fraction change of crystallite. When the length of the amorphous cell reduces, the volume fraction of

the crystal particle increases. Ten different simulations were carried out to achieve the normalised Young's modulus against the crystal partial volume fraction graph, gives in Fig. 46. Whereas, a best fitted exponential line was given.

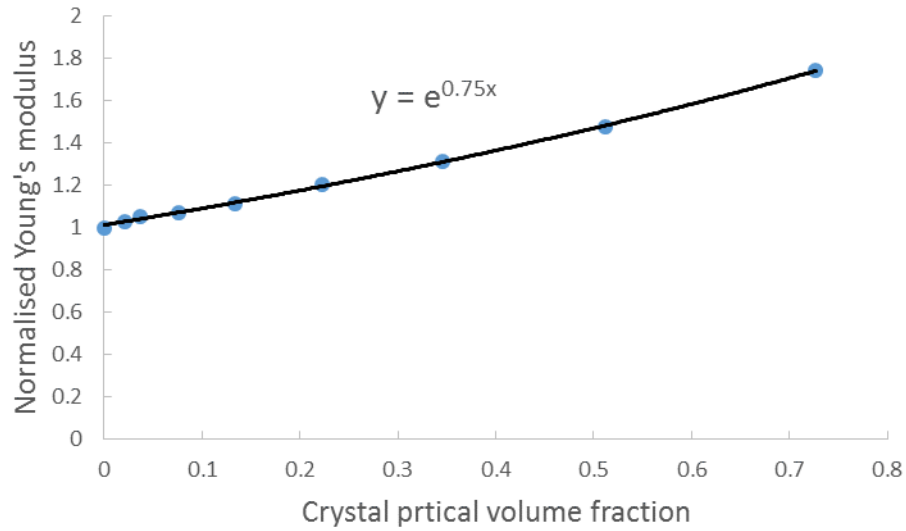


Figure 46: Effect of the volume fraction of crystal particle on normalised Young's modulus during degradation with a best fit of exponential line (Gleadall, et al., 2015).

The expression of the best-fitted exponential line is referred to as:

$$\bar{E} = e^{0.75X_c} \quad (7-9)$$

In which \bar{E} is the normalised Young's modulus and X_c is the volume fraction of crystal.

7.3.3 Analysing Young's modulus change for semi-crystalline polymer during degradation using the simplified model

By combining the model of chain scission and model of crystallinity, the simplified model of the Effective Cavity Theory can be achieved.

From the relationship of equation (7-9), the Young's modulus of the overall semi-crystalline polymer without count effective cavity, E_c , can be achieved by

$$E_c = E_\infty e^{0.75X_c} \quad (7-10)$$

whereas the pure amorphous polymer Young's modulus without count the effect of crystallinity and effective cavity, E_∞ (GPa), could be work out from initial polymer conditions which has been given in the experimental result. E_c represent the Young's modulus of polymer in which effective cavity take in place. Whereas, in simplified Effective Cavity Theory, equation (7-8) is applied to calculated the average Yong's modulus of the semi-crystalline polymer, E_p (GPa), according to

$$E_p = E_c e^{-2.15X_{ec}} \quad (7-11)$$

Taking the initial condition of $t=0$, $R_s=0$, $X_{ec0}=0$, E_∞ can be calculated as

$$E_\infty = E_{p0} / e^{-2.15X_{ec0}} * e^{0.754X_{c0}} \quad (7-12)$$

in which E_{p0} stand for initial Young's modulus of the overall polymer and X_{c0} is the initial degree of crystallinity; these two values can normally be found in the experimental data. With the assumption of X_{ec0} is the effective cavity volume fraction at the beginning of the degradation, which should be 0. Pure amorphous polymer Young's modulus without counting the effect of crystallinity and effective cavities, E_∞ , can be work out as a constant initially. Combining equation (7-12) and (7-11) into equation (7-11), an overall polymer Young's modulus change with degradation can be achieved by

$$E_p = E_\infty e^{0.745X_c} e^{-2.15X_{ec}} \quad (7-13)$$

Whereas

$$X_{ec} = V_{ec} * R_s \quad (7-14)$$

in which V_{ec} is the unit volume of the spherical effective cavity, which is

$$V_{ec} = \frac{4}{3} \pi r^3 \quad (7-15)$$

in which r is the radius of the unit spherical effective cavity, which is also the only input needed for equation (7-13) to achieve the overall average Young's modulus trend during degradation for the whole semi-crystalline polymer. This assumes that R_s and X_c are achievable for the degradation model or from experimental data.

7.4 Using experimental data to check the reliability of the Simplified model

The same five sets of experimental data that were used by Gleadall, et al. (2015) are represented in Table 2. The reason for choosing these sets of experimental studies is because they use poly(lactide), which not possible to study by using Ding's (2011) MD model. Additionally, the experimental studies contain crystallinity change trend during degradation, molecular weight reduction trend and Young's modulus measurements were also given. With the full set of measurements, the mathematical model can be better validated. The density, ρ_p , of all five cases is taken as 1250 kg/m³.

Data Set (reference)	A (Weir, et al., 2004)	B (Tsuji, et al., 2000)	C (Duek, et al., 1999)	D (Duek, et al., 1999)	E (Lam, et al., 1994)
Initial M_n (g/mol)	159,000	584,000	153,000	152,000	42,000
Initial X_c	0.448	0.540	0.480	0	0.570
Initial Young's modulus (GPa)	0.668	0.100	6.86	5.58	1.43
Sample type	0.8 mm plate	0.050 mm film	2 mm Rod	3mm Rod	0.033 mm film
Polymer type	PLLA	PLLA	PLLA	PLLA	PLLA
Degradation medium	37°C PBS pH7.4	37°C PBS pH7.4	38°C PBS pH7.4	38°C PBS pH7.4	37°C PBS pH7.4
E_∞ (GPa)	0.4765	0.06655	4.7769	5.58	0.930
N_{chain0} (mol/m ³)	7.86	2.14	8.17	8.22	29.76

Table 2: Experimental set-ups, initial measurements, and calculations for the five individual sets of experimental data that were used in the simplified Effective Cavity Theory.

The initial conditions of the five sets of experimental data are listed in Table 2, in which pure amorphous polymer Young's modulus without counting the effect of crystallinity and effective cavities, E_{∞} , can be worked out initially for each set of experimental data using equation (7-12).

$$E_{\infty} = E_{p0}/e^{-2.15X_{ec0}} * e^{0.754X_{c0}} \quad (7-12)$$

The initial number of chains per unit volume, N_{chain0} (mol/m³), can also be calculated initially as

$$N_{chain0} = \rho_p/M_{n0} \quad (7-16)$$

The initial number of chains, N_{chain0} , will be used in the normalised average molecular weight calculation, \bar{M}_n , equation (5-18) in Chapter 5, to achieve the number of chain scissions per unit volume, R_s .

$$\bar{M}_n = \frac{M_n}{M_{n0}} = \frac{1 + \bar{\omega} X_{c0} - \alpha \bar{R}_s^{\beta}}{(1 + \bar{\omega} X_{c0}) \left[1 + \frac{C_{e0}}{N_{chain0}} \left(\bar{R}_s - \frac{\alpha}{m} \bar{R}_s^{\beta} \right) \right]} \quad (5-18)$$

The average molecular weight M_n is measured experimentally, as well as initial average molecular weight M_{n0} and X_{c0} . The initial concentration of ester unit of long chains in the amorphous phase $C_{e0} = 17300$ (mol/m³). The normalised crystalline phase ester unit number per unit volume $\bar{\omega} = \frac{\omega}{C_{e0}} = 1$ as we assume that the crystalline phase ester unit number per unit volume is the same as the number of ester units of amorphous phase long chains per unit volume $\omega = C_{e0} = 17300$ (mol/m³). $\alpha = 28$, $\beta = 2$, $m = 4$ is given to the equation. Additionally, normalised chain scissions numbers per unit volume $\bar{R}_s = R_s/C_{e0}$; therefore, the chain scissions numbers R_s can be calculated from equation (5-18).

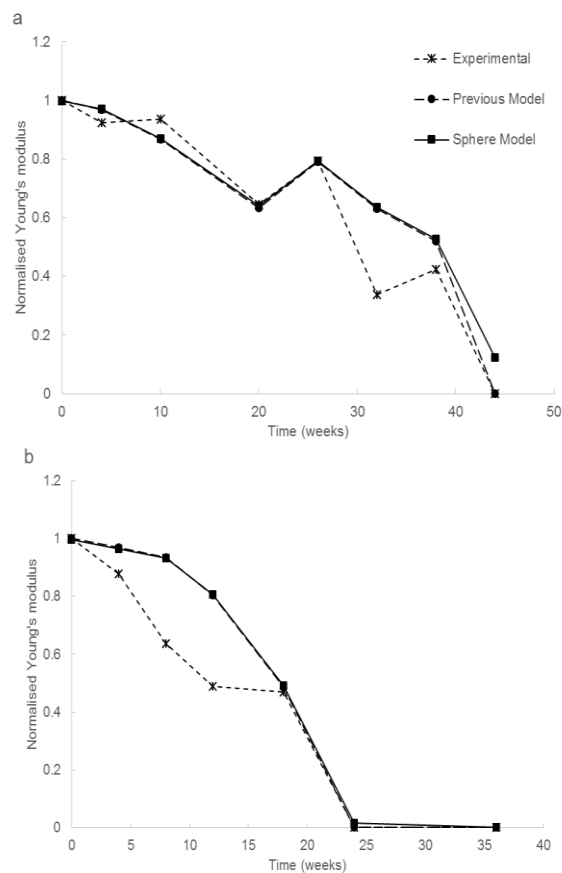
Combining equation (7-14) and (7-15) into equation (7-13) gives

$$E_p = E_{\infty} e^{0.745X_c} e^{-2.15 * \frac{4}{3} \pi r^3 * R_s} \quad (7-17)$$

This leaves only one variable to be adjustable to fit the experimental data, the unit radius of the spherical effective cavity. Equation (7-17) can then be considered as the simplified Effective Cavity Theory equation. The simplified Effective Cavity Theory has been used to fit both the experimental data and the previous Effective Cavity Theory model data.

The experimental data for polymer degrading of average molecular weight and crystallinity for five sets of experimental data listed in Table 2 are all presented in literature, therefore could be straight applied in the model. Crystallinity has not been measured in week 12 for Table 2 C and D, so an averaged value between the crystallinity at weeks 8 and 16 was used for the crystallinity at week 12.

Fig. 49 shows the simplified Effective Cavity Theory used to fit both experimental data and the previous Effective Cavity Theory result. The only variable needed in the simplified model, unit radius of the spherical effective cavity, is been set as 2.0nm. This single radius value is able to achieve all five fittings in Fig. 49. The unit radius of the spherical effective cavity can be set as individual values for different experimental data as each sample could give a different behaviour of degradation for individual experimental set-up; a better fitting can be achieved by doing so. However, a single value of the radius has been used here in order to limit the number of parameters needed in the model.



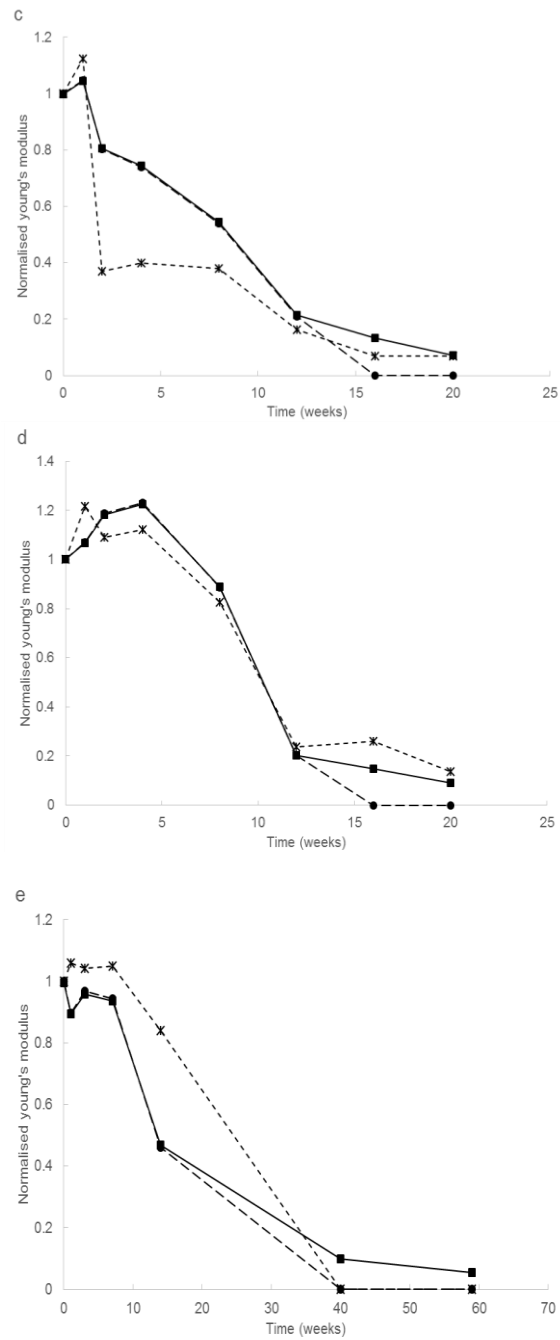


Figure 49: Five degradation experimental data listed in Table 2 were used to check the reliability of the simplified Effective Cavity Theory, previous model fitting was also included: (a) Weir, et al. (2004), (b) Tsuji, et al. (2000), (c) and (d) Duek, et al. (1999), and (d) Lam, et al. (1994).

It can be observed from Fig. 49 that a good agreement can be achieved between the simplified Effective Cavity Theory and the experimental data, especially fitting between the simplified Effective Cavity Theory and the previous model, can be

achieved. This proves that a spherical shape of effective cavity can be used to simplify the Effective Cavity Theory by replacing the flat-tipped cone shape, which contains many parameters that would affect the effective cavity volume fraction. The theory has shown in Fig. 49(c) and (d) that it can successfully capture the increase of Young's modulus because of crystallinity at early stage of degradation. Additionally, it shows that the theory could respond to the slight instability in reduce of Young's modulus, which is shown as the previous five points of Fig. 49(a). As discussed before, the theory does take account of the overlapping between each effective cavity. Therefore, Young's modulus reduction below around 50% of its original value should be treated with caution. Nevertheless, we can observe from Fig. 49 that the trend for Young's modulus below 50% of its original value can still be well captured.

7.5 A full equation list of the mathematical model for polymer degradation adding in a simulation of mechanical properties

The simplified Effective Cavity Theory can be combined together to degradation caputation model introduced in Chapter 5 to form a full mathematical model that could capture the simulation of average molecular weight reduction trend, increase of degree of crystallinity during degradation, and effect of chain on Young's modulus of the same degradation. Equations for the full mathematical model are presented below.

The governing equation for rate of chain scission for semi-crystalline polymers is

$$\frac{dR_s}{dt} = C_{e0} \psi(R_s) \left\{ k_1 + k_2 C_{e0}^n \left[\left(\chi_1 \varphi(R_s) + \frac{\chi_2}{m} \left(\frac{C_{ol}}{C_{e0}} \right) \right) \frac{1}{1 - X_c} \right]^n \right\} \quad (5-11)$$

in which

$$\psi(R_s) = 1 - \alpha \left(\frac{R_s}{C_{e0}} \right)^\beta - \frac{\omega}{C_{e0}} (X_c - X_{c0}) \quad (5-12)$$

$$\varphi(R_s) = \frac{C_{chain\ 0}}{C_{e0}} + \frac{R_s}{C_{e0}} - \frac{\alpha}{m} \left(\frac{R_s}{C_{e0}} \right)^\beta \quad (5-13)$$

The short chain diffusion equation is

$$\frac{dC_{ol}}{dt} = \alpha\beta \left(\frac{R_s}{C_{e0}} \right)^{\beta-1} \frac{dR_s}{dt} + \sum_{i=1}^3 \frac{\partial}{\partial x_i} \left(D \frac{\partial C_{ol}}{\partial x_i} \right) \quad (5-28)$$

$$D = D_{matrix} + (1.3V_{pore}^2 - 0.3V_{pore}^3)(D_{pore} - D_{matrix}) \quad (5-29)$$

in which

$$V_{pore} = (1 - X_{c0}) \left[\alpha \left(\frac{R_s}{C_{e0}} \right)^{\beta} - \frac{C_{ol} - C_{ol0}}{C_{e0}} \right] \quad (5-30)$$

$$D_{matrix} = (1.3V_{am}^2 - 0.3V_{am}^3)D_{polymer} \quad (5-31)$$

Whereas

$$V_{am} = \frac{1 - V_{pore} - X_c}{1 - V_{pore}} \quad (5-32)$$

Degree of crystallinity equations are

$$X_c = \begin{cases} X_{cmax} - (X_{cmax} - X_{c0})e^{-k_c \left(\frac{R_s}{C_{e0}} \right)}, & \lambda = 1 \\ X_{cmax} - \left[(\lambda - 1)k_c \left(\frac{R_s}{C_{e0}} \right) + (X_{cmax} - X_{c0})^{1-\lambda} \right]^{\frac{1}{1-\lambda}}, & \lambda \neq 1 \end{cases} \quad (5-5, 5-6)$$

The average molecular weight at any location can be calculated using equation

$$\frac{\bar{M}_n}{M_{n0}} = \frac{M_n}{M_{n0}} = \frac{1 + \bar{\omega} X_{c0} - \alpha \bar{R}_s^{\beta}}{(1 + \bar{\omega} X_{c0}) \left[1 + \frac{C_{e0}}{N_{chain0}} \left(\bar{R}_s - \frac{\alpha}{m} \bar{R}_s^{\beta} \right) \right]} \quad (5-18)$$

In addition, the simplified Effect Cavity equation is

$$E_p = E_{\infty} e^{0.745X_c} e^{-2.15 \frac{4}{3} \pi r^3 * R_s} \quad (7-17)$$

All samples are predefined.

This full mathematical model has been used in the next chapter to simulate the change of average molecular weight, degree of crystallinity, and Young's modulus for a single degradation.

7.6 Conclusion

A simplified Effective Cavity Theory has been introduced and proved to be valid by fitting with five sets of experimental data as well as the previous Effective Cavity Theory. Furthermore, a full mathematical model for degradation has been formed, which could be used to capture the trend of average molecular, degree of crystallinity, and Young's modulus for a single degradation.

Chapter 8: Detection of degradation using vibration analysis

In a previous work, Samami and Pan (2016) proposed to use mode shape analysis in order to detect degradation in polymeric devices. They used a solid element in their finite element model. In this chapter, it is demonstrated that the much simpler beam elements can be used to detect degradation, which makes the mode analysis very simple for any end user.

8.1 Introduction

A numerical study is used in the chapter to detect degradation in a degrading medical plate. The plate is considered to follow the normal behaviours of amorphous copolymers of PLA and PGA. Because of the auto-catalytic reaction (size effect), non-uniform degradation occurs in almost all the degradations of biodegradable medical devices. The Effective Cavity Theory introduced in the previous chapter is used to relate the non-uniform degradation to the Young's modulus change for plate across thickness in different degradation stages. The method used for damage detection introduced by Pandey (1991) is used in this chapter to detect degradation. Difference of the centre and edge Young's modulus difference as well as absolute curvature difference, which has been used in the degradation detection, has been presented. In the second part of this chapter, a cube is introduced with the assumption that it has the material property of PLLA, which is found in Weir's paper (Weir, et al., 2004). A small central part of the cube has been taken out as a cantilever beam. Degradation detection has been applied to the beam to study the local mechanical property change due to the degradation. Finally, a different polymer diffusion coefficient was used to analysis effect it has to degradation detection.

8.2 Vibration analysis and damage detection

Vibration analysis has been widely in use in structural and mechanical systems to detect, locate, and characterise damage. The basic idea behind the analysis is that the physical properties change due to the damage will lead to a detectable change in model behaviour. This is due to the model behaviour is a function of the mechanical properties for material. Many experimental analyses have been taken in place to investigate effect for a crack or local damage on the dynamic behaviours. The sensitivity of the damage detection model and finding the location of the damage are the two main issues in deciding whether the model is effective. Many methods have been introduced to detect local damage by using vibration analysis. For example, Salawu (1997) and Doebling (1996) have proved that damage detection can be achieved by analysing resonant frequencies change. However, the frequency change produced from the damage is normally too small to relate back, and would be impossible to use to locate the damage. Therefore, Yuen (1985) presents that mode shape, especially the derivatives of mode shape could be used as better sensor to detect the location of damage. Pandey (1991) proved that second order mode shape derivative, mode curvature, is highly sensitive to local damage and could also be used to localise it. Local damage causes reduction of local flexibility, and curvatures of the mode shape for a beam are linked with local mechanical properties. Big local damage causes an increased change in mode curvature, and the amount of change in curvature could give an indication of the size of the damage. Fan and Qiao (2011) developed an algorithm that could effectively detect local damage and also locate the damage. For a damaged and intact structure, curvature absolute difference could be worked out and be used for the damage detection and location detection. It has been shown that highest absolute curvature difference along a beam indicates the damage location.

An absolute curvature difference feature was used in this chapter to detect degradation. Assuming that a finite element discretisation has been used, an eigenvalue equation can be solved to find the displacement mode shape of a structure (Samami, 2016).

$$[K][U^{(n)}] = \omega_n^2[M][U^{(n)}] \quad (8.1)$$

Whereas, $[K]$, $[M]$ and $[U^{(n)}]$ stand for the mechanical properties stiffness matrix, mass matrix, and eigenvector (the displacement mode shapes). ω_n^2 is the structure natural frequency of the n th circle. In this chapter, the mode shape displacement will

be obtained from the beam element of finite element analysis. Curvature mode shapes could be calculated from the central difference approximation, given below (Pandey, et al., 1991):

$$u_i'' = (u_{i+1} - 2u_i + u_{i-1})/h^2 \quad (8.2)$$

In which h represent elements length.

The absolute curvature difference between the degrading structure and the intact structure can be calculated as follows:

$$\Delta U'' = |U_{intact}''(n) - U_{degrading}''(n)| \quad (8.3)$$

8.3 Detection of degradation for a plate model using beam element study

8.3.1 The plate model has been used

A simple rectangular plate shown in Fig. 50(a) was presented by Samami (2016). He used this plate to study the degradation detection using the finite element method. The left side of the model was fixed during vibration analysis, which was used to detect degradation. The beam was treated as a cantilever beam and all the surface of the plate can be assumed to have diffuse of short oligomer chains, which means no short chains remain at the surface of the plate. Before degradation start, the polymer assumes to have no monomers existing. Samami first applied degradation model, which is shown in Chapter 4 of this thesis, into the commercial FE software COMSOL Multiphysics which will calculated the distribution of molecular weight. Then, he used an analytical constitutive law, which was created by himself and Pan (Samami and Pan, 2015), Young's modulus distribution can then be achieved from the obtained molecular weight distribution. The initial constants used are Young's modulus $E_0 = 10GPa$ and Poisson's ratio $\nu=0.35$. Fig. 50(b) gives Young's modulus distribution for the 2D plate during degradation along centre x direction. Both two dimensional and three-dimensional analyses were presented. It was shown that degradation can be detected and located by applying the absolute curvature difference analysis. However, a very high-level accuracy measurement is required to measure the mode shape displacement

in order to support his method. Furthermore, in both his two dimensional and three dimensional finite analyses, layers had been created to input the distribution of Young's modulus for different behaviours of degrading location. Specifically, nine layers were made and each layer was given by an averaged Young's modulus rather than accurate Young's modulus distribution. Other parts for plate were given a constant Young's modulus value, and the thickness of the nine layers kept the same at different stages of degradation. As we can observe from Fig. 50(b), Young's modulus drops start forming on the end and remain constant at the core, with the drop rate increasing with degradation time. Therefore, using layers and applying average Young's modulus will not be following the distribution accurately. Additionally, applying different layers of Young's modulus to the 2D and 3D models is time consuming. A simpler and more designer-friendly model would be better. In the next section, a 1D beam element was presented to solve the above problems.

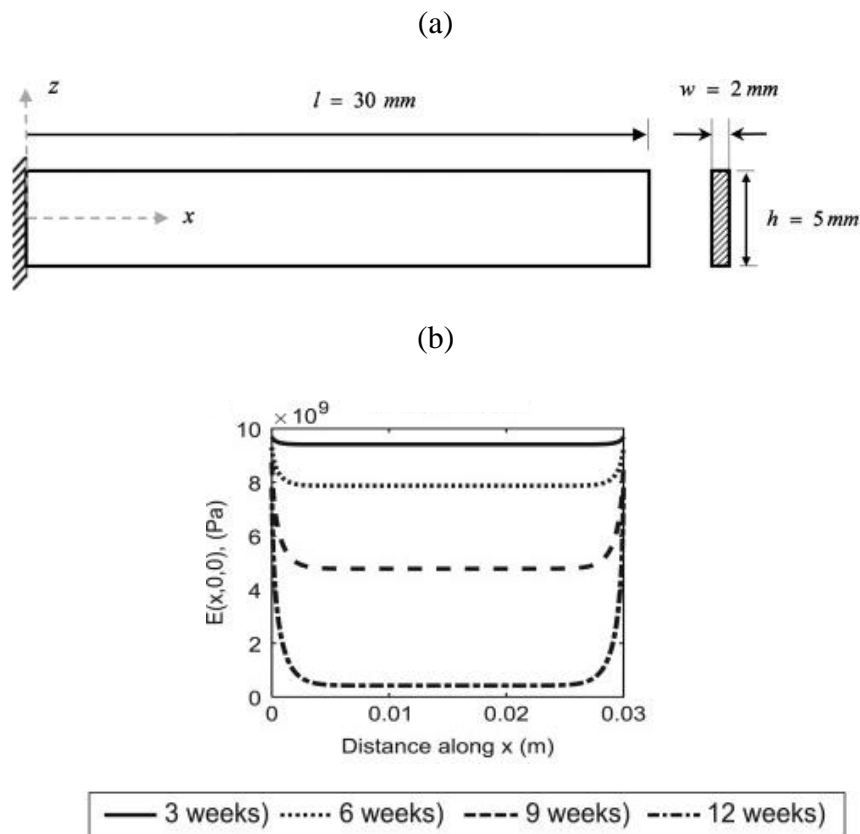


**Figure 50: (a) 2D plate used in Samami's paper for degradation detection model
(b) Young's modulus distribution for the 2D plate during degradation along
centre x direction (Samami and Pan, 2015)**

8.3.2 1D beam element model for degradation detection

Treat the plate as a 1D beam, as shown in Fig. 50. Other conditions remain the same as in Samami's model. The Young's modulus distribution shown in Fig. 50(b) can be inputted into the 1D beam element model following their exact axial coordinates. The reason for using the Young's modulus distribution directly rather than calculating a new set of degradation data is because this model was used to show a comparison to Samami's model. In this, degradation condition should be kept the same; thus, Young's modulus distribution will be the same as well. Degradations and molecule weight will be calculated in the following model. The left beam end is fixed also the other end is free to move.

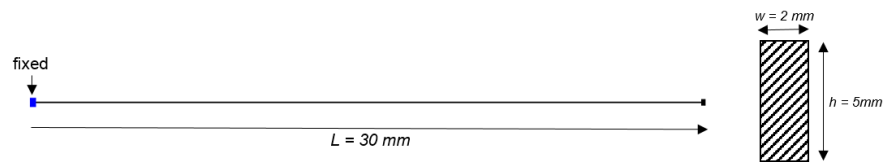
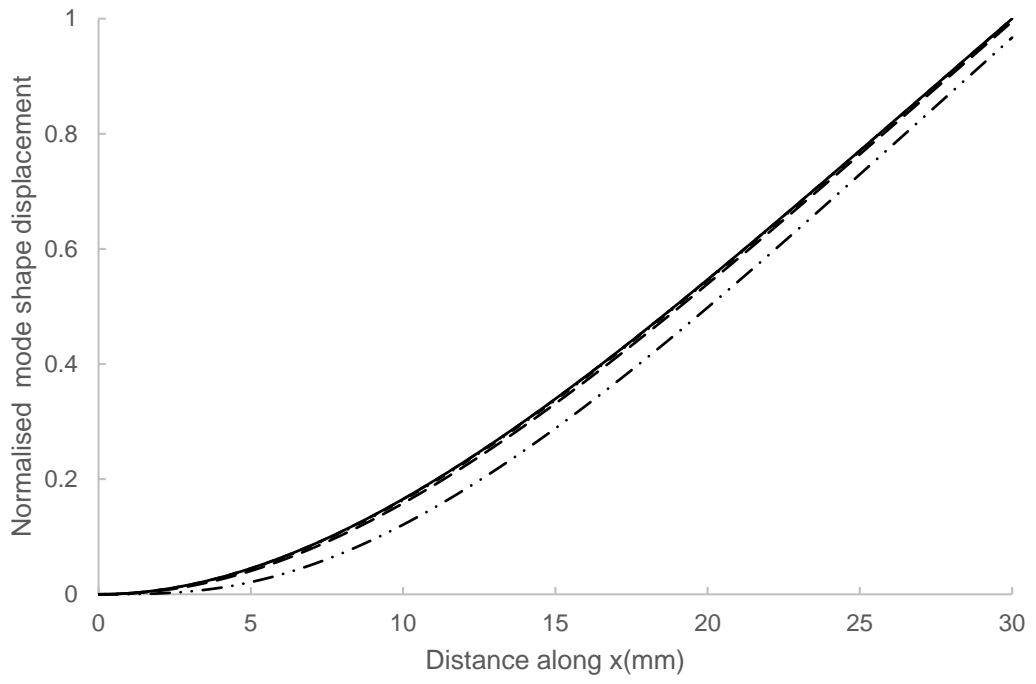


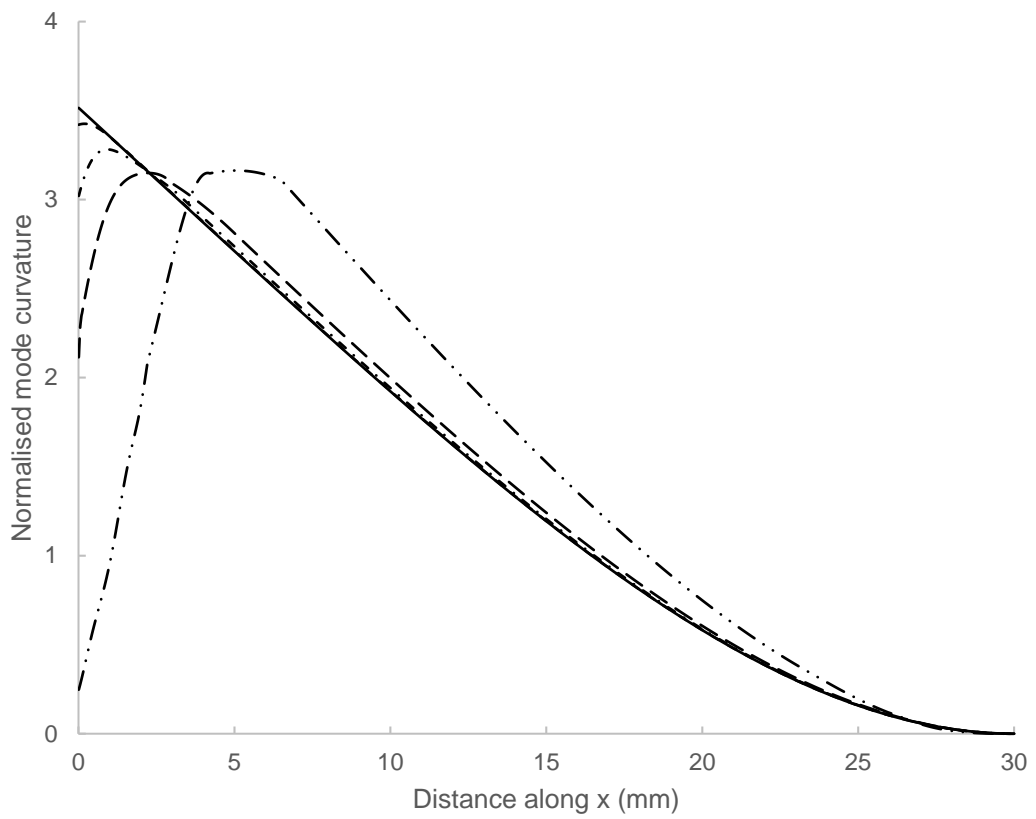
Figure 51: 1D beam modal of the degrading plate.

For the 1D beam element model, COMSOL allows the Young's modulus distribution to be related exactly to its axial coordinates. After that, vibration analysis can be recalculated. The first displacement mode shape, mode curvature, and absolute curvature difference between the degrading and intact plates are shown in Fig. 52(a), (b) and (c).

(a)



(b)



— week 0 - - - week 3 - · - · - week 6 - - - week 9 - · - · - week 12

(c)

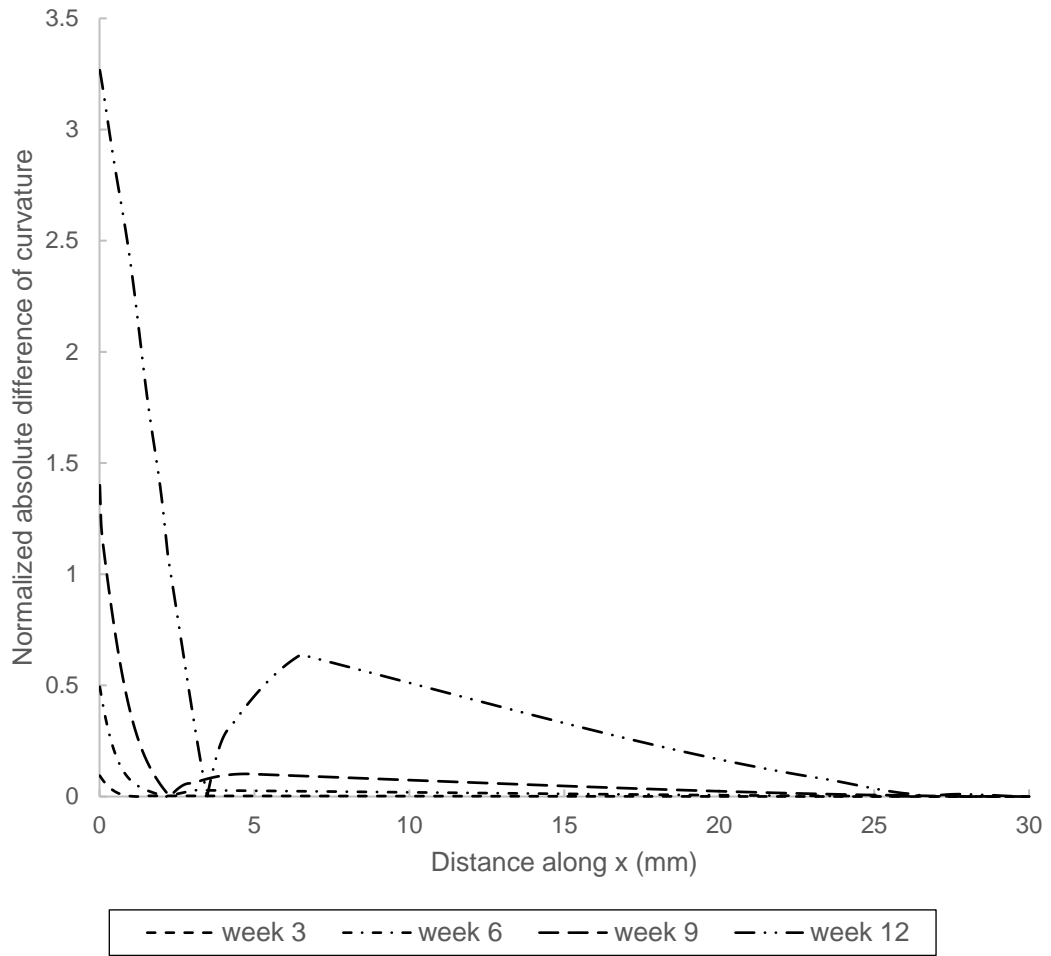
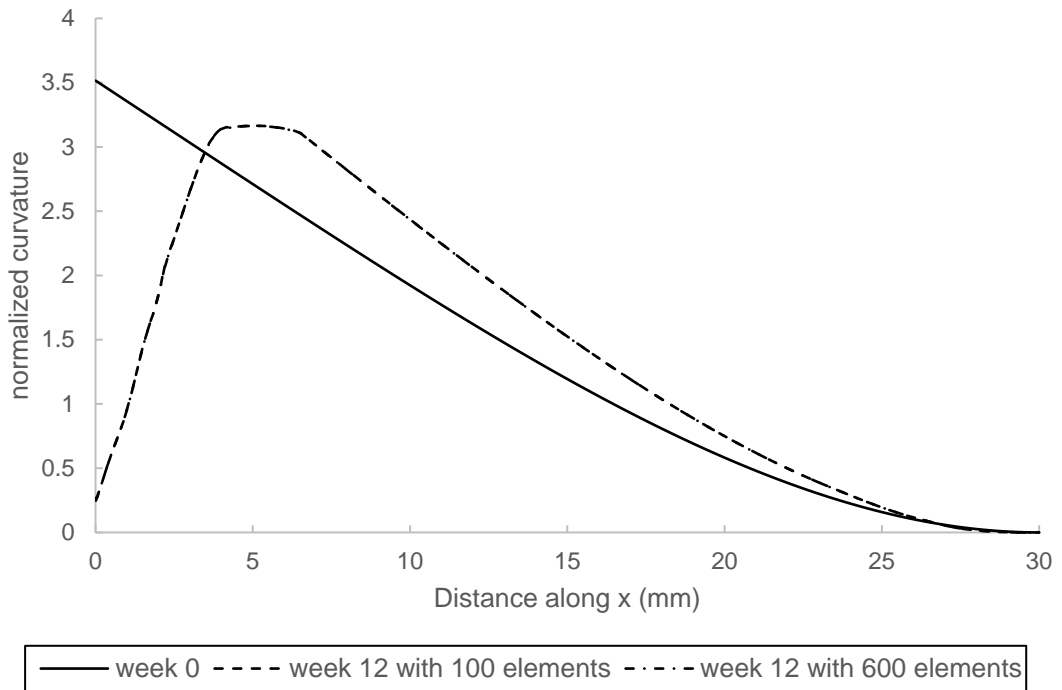


Figure 52: First mode shape achieved from beam element study using commercial software COMSOL (a) normalised mode shape displacement, (b) normalised curvature, (c) normalised absolute difference between the intact beam mode shape curvature (week 0) and degraded beam mode shape curvature, along beam shown in Fig. 51 at various degradation times.

It was shown in Fig. 52(a) that displacement mode shape has not changed much during degradation, whereas in Fig. 52(c), a clear difference can be observed at the surface of the plate. Furthermore, the difference increases during degradation. From the degradation mechanisms, a conclusion can be made as the surface degrades slower. Therefore, the surface has more stiffness and absolute curvature difference should be bigger, which was shown in Fig. 52(c). Conclusively, the vibration analysis could be used to detect and localise the degradation of the medical device. The big difference of the absolute curvature difference between intact plate and degrading plates indicated the location of less degradation. The amplitude of the difference gives an indication of the degradation stage. A bigger amplitude difference indicates longer degradation.

(a)



(b)

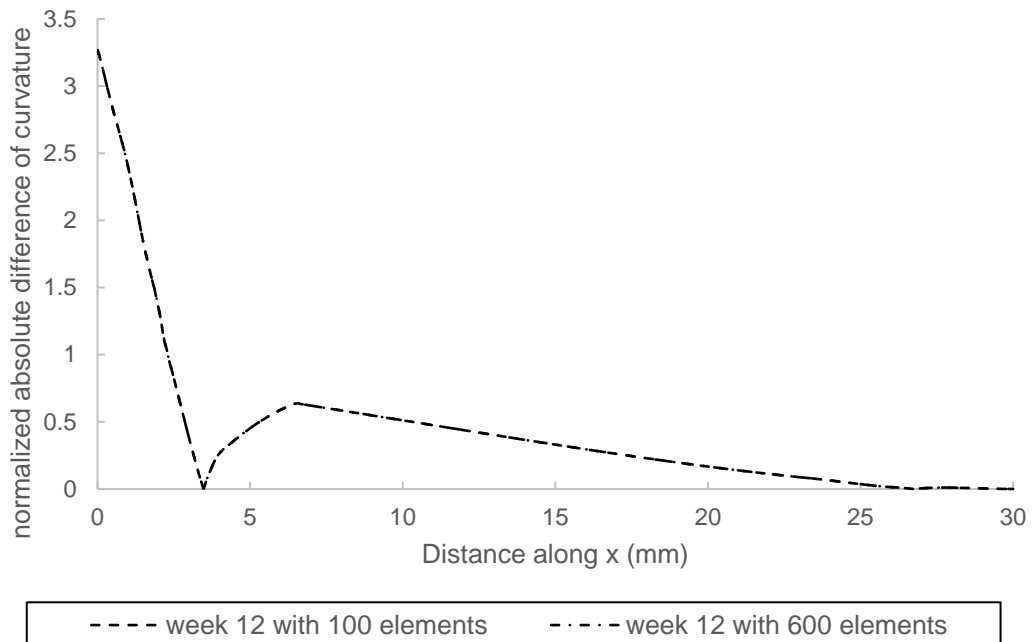


Figure 53: Check convergence of the model using (a) normalised curvature at week 0 and week 12 (b) normalised absolute difference of curvature at week 12, with 100 and 600 elements respectively.

Fig. 53 shows a convergence check for the above model. The result of mode curvature and absolute curvature difference at week 12 was compared for beams that contain 100 elements and 600 elements. Exact fitting can be observed, indicating the convergence of the model.

As we noticed from Fig. 53(b), there is a drop between end Young's modulus from centre Young's modulus. Amplitude of the drop includes with degradation. If we normalise the drop by dividing the initial Young's modulus, $E_0 = 10GPa$, percentage for drop compared to the initial Young's modulus could be achieved. Fig. 54 shows the maximum absolute curvature difference against the Young's modulus percentage drop for weeks 3, 6, 9, and 12, respectively. It can be shown that the relationship between the maximum absolute curvature difference and the surface/centre Young's modulus difference almost follows a straight line. At week 12, the Young's modulus difference between surface and centre for plate can be as high as 75% of the intact plate Young's modulus.

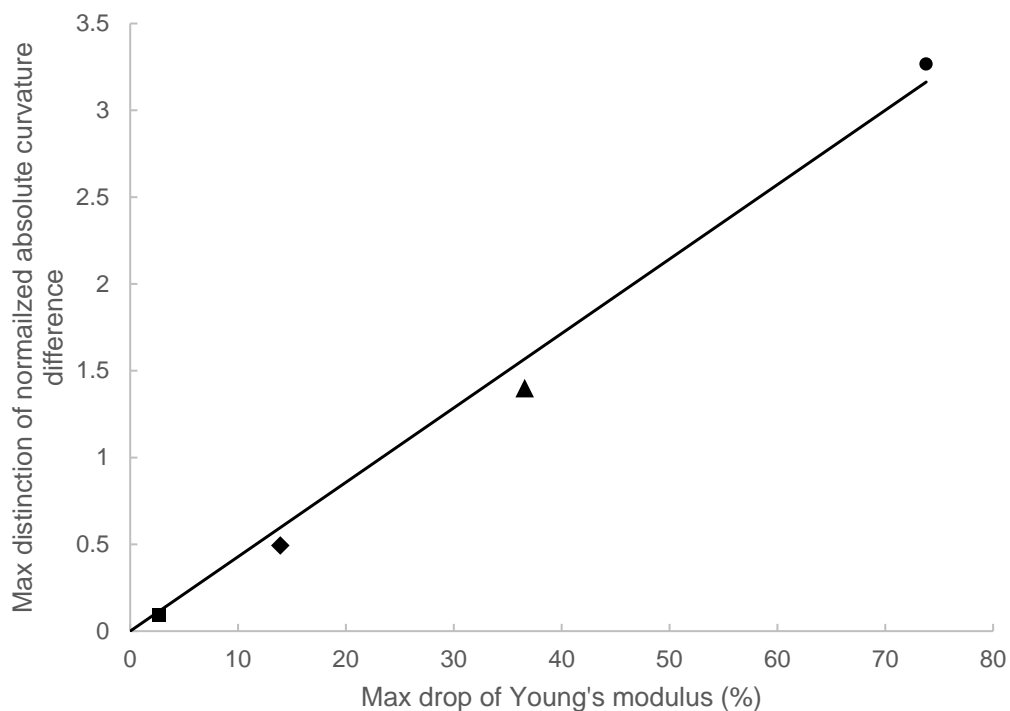


Figure 54: Maximum distinction of normalised absolute curvature difference against maximum percentage drop of Young's modulus from the surface to the centre of the plate on different degradation stages at weeks 3, 6, 9, and 12.

To sum up, by applying vibration analysis: degradation is detectable and the location of degradation can be found; the stage of degradation could be indicated from the maximum absolute curvature difference; and, finally, surface and centre Young's modulus difference is proportional to maximum absolute curvature difference.

8.4 Local degradation detection – using a 3D cube as a unit of biodegradable implant device

For most of the medical implants, finding the local degradation is crucial for predicting the mechanical behaviours during degradation. Fig. 55(a) shows a cube with $l = 0.1\text{m}$. The cube was used as a unit of any medical implants. A centre part was taken apart from the cube, shown in Fig. 55(b). The degradation detection method was applied to this part. As before, the centre part has been assumed to be a 1D beam, as shown in Fig. 55(c). The material's property takes the same as the above plate model, intact cube Young's module $E_0 = 10\text{GPa}$, and Poisson's ratio $\nu=0.35$.

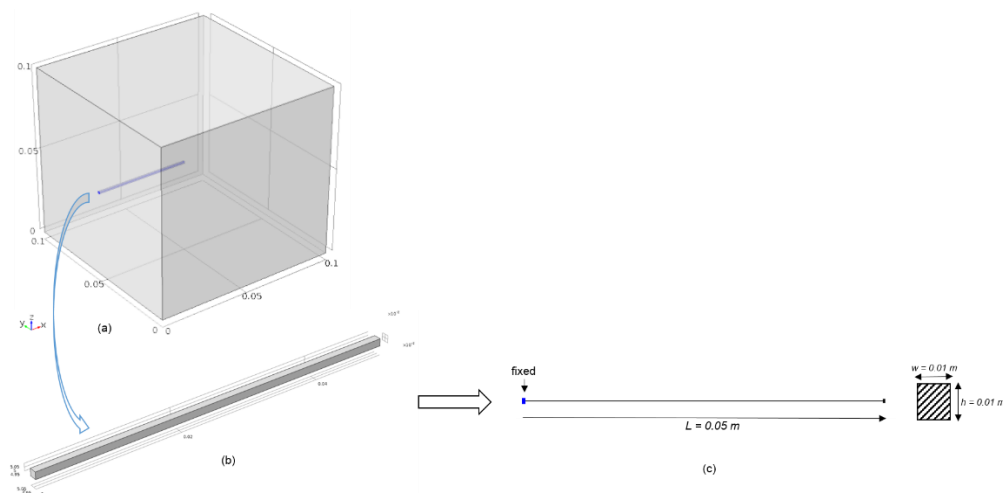


Figure 55: (a) a 3D cube model (b) a centre part of the cube model (c) convert the centre part of the cube into a 1D beam model.

Firstly, degradation has been taken into account. Assume that short polymer chains (oligomers) can diffuse out from every surface of the cube. The master equation presented in Chapter 4 was used to run the degradation model. Fig. 56 shows a normalised average molecule weight reduction trend over time for the whole cube. Fig.

57 shows the degradation distribution at week 20. A list of parameters that were used in the degradation model is shown in Table 3.

$C_{e0} \text{ (mol/m}^3\text{)}$	$Mn0 \text{ (g/mol)}$	m	X_{c0}	α	$D_{polymer} \text{ (m}^2\text{/s)}$
17300	159000	4	0.448	28	10^{-14}
$k_1 \text{ (1/day)}$	$\bar{k}_2 = k_2/C_{e0}^n \text{ (1/day)}$	n	$X_{c \text{ max}}$	β	$D_{pore} \text{ (m}^2\text{/s)}$
0.01	0.001	0.5	0.59	2	10^{-11}
$C_{oi0} \text{ (mol/m}^3\text{)}$	$C_{chain0} \text{ (mol/m}^3\text{)}$	x_1	x_2	λ	$M_{mit} \text{ (g/mol)}$
0	7.834	0	1	1	72

Table 3: Parameters for the molecular weight distribution calculation for the cube model.

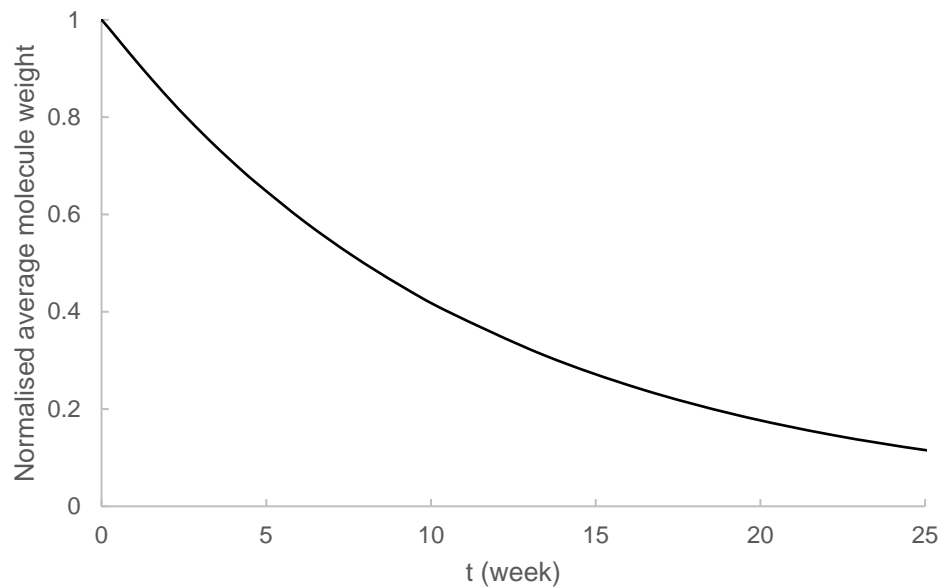


Figure 56: Normalised average molecule weight reduction over time for the whole cube model.

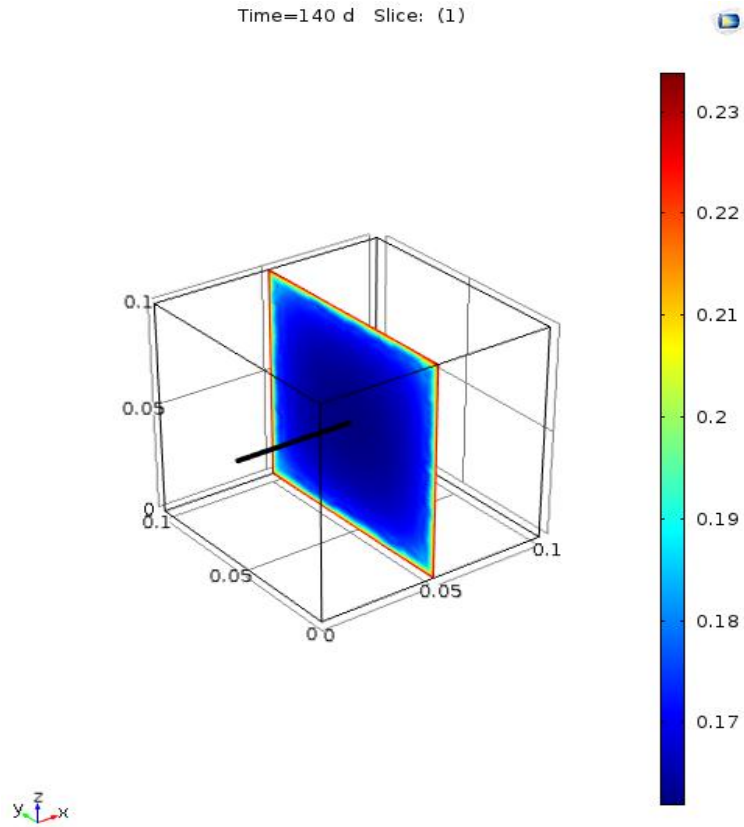
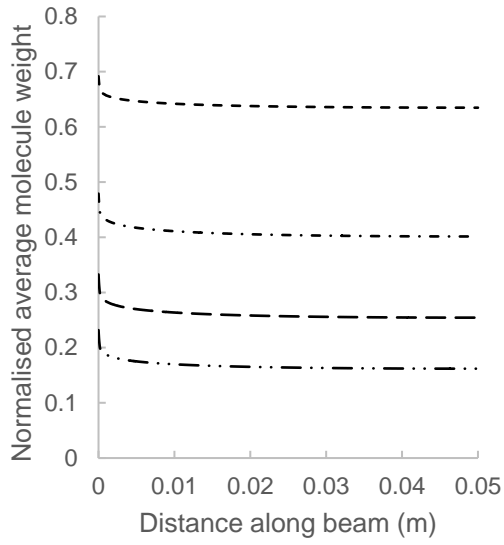
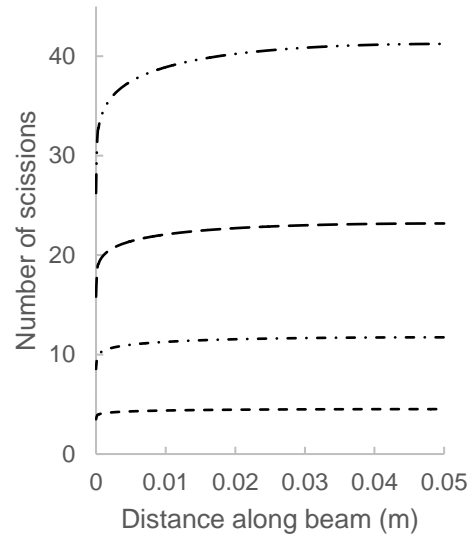


Figure 57: Distribution of normalised average molecular weight over the cross-section of the cube at week 20.

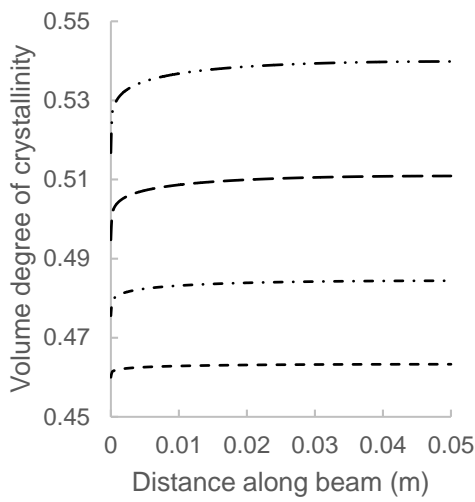
The degradation data along the beam shown in Fig. 55(c) was listed in Fig. 56 for degradation after 5, 10, 15, and 20 weeks, respectively. The figures in Fig. 58(a) average molecule weight along the beam, (b) number of scissions along the beam, and (c) degree of crystallinity along the beam were pulled out from the degradation model. Fig. 58(d) Young's modulus distribution across beam was calculated using the above data and the Effective Cavity Theory, which was shown previously. Molar volume for each effective cavity was taken as $V_{ec} = 0.021 \left(\frac{m^3}{mol}\right)$, therefore the radius of each spherical cavity is $r = 2.0267nm$. Young's modulus is calculated as $E = E_0(10GPa) * e^{0.745*X_c} * e^{-2.15*(0.021*R_s)}$, whereas, X_c is the volume degree of crystallinity and R_s is the number of scissions. By applying different sets of Young's modulus data into the beam, vibration analysis data can be achieved, as shown in Fig. 59



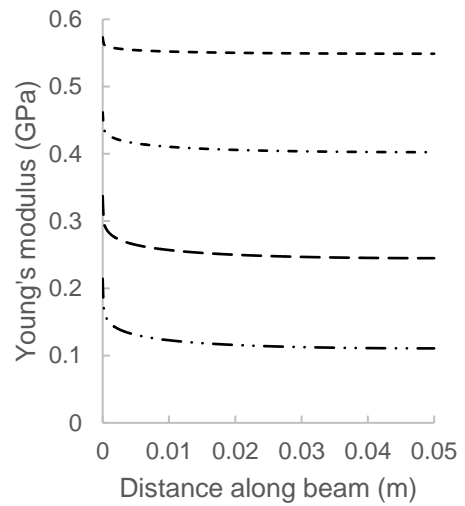
(a)



(b)



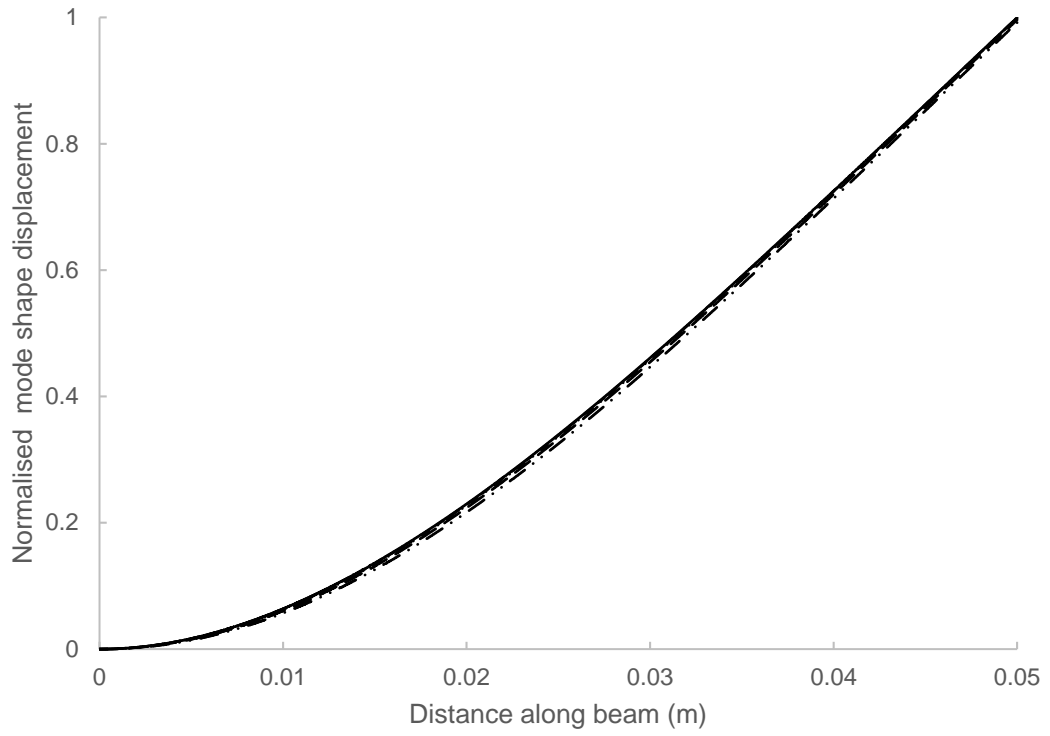
(c)



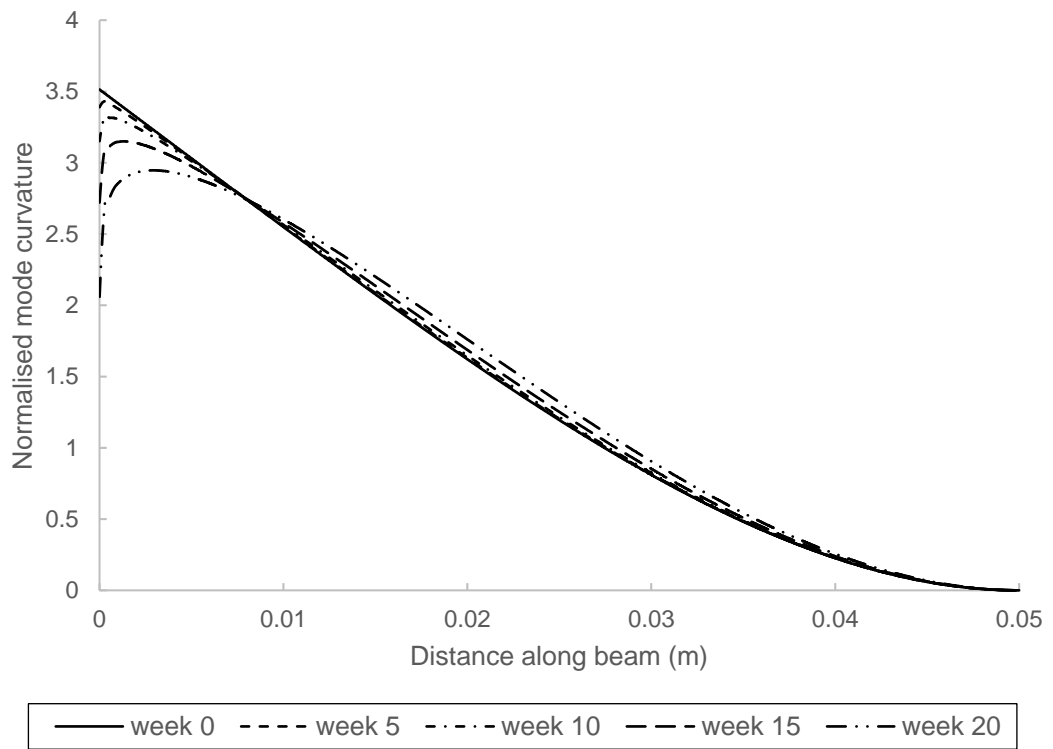
(d)



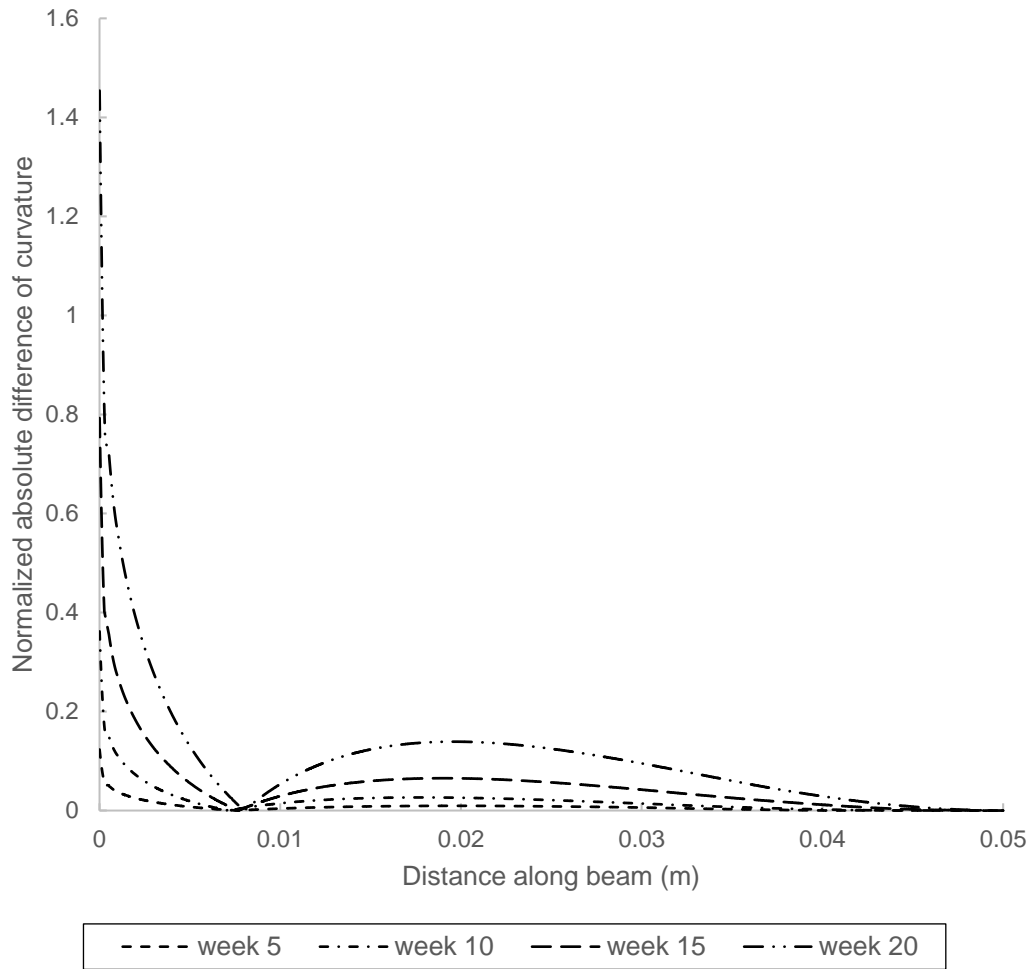
Figure 58: Distributions of (a) normalised average molecule weight, (b) number of scissions, (c) volume degree of crystallinity, (d) Young's modulus, along the beam shown in Fig. 55 at different degradation times.



(a)



(b)



(c)

Figure 59: First mode shape of (a) normalised mode shape displacement, (b) normalised curvature, (c) normalised absolute difference between the intact beam mode shape curvature (week 0) and degraded beam mode shape curvature, along beam showed in Fig. 55 at various degradation times.

Fig. 59 shows the first bending mode of (a) displacement mode shape, (b) mode curvature, and (c) absolute curvature difference. A similar degradation detection conclusion can be made from the above data.

The amorphous polymer short chain diffuse rate is a very important factor to study the non-uniform degradation and non-uniform Young's modulus distribution, and is therefore critical in degradation detection. Lyu and Untereker (2007) present that the

range of the short chain diffuse rate in pure amorphous polymer before degradation will be between $10^{-14} \text{ m}^2/\text{s}$ and $10^{-22} \text{ m}^2/\text{s}$. Data presented in Fig. 59 achieved this by taking account of the upper limit of this range, $D_{polymer} = 10^{-14} \text{ m}^2/\text{s}$. By replacing this value as $10^{-22} \text{ m}^2/\text{s}$ and doing a recalculation, the normalised absolute curvature difference at various degradation times can be shown in Fig. 60.

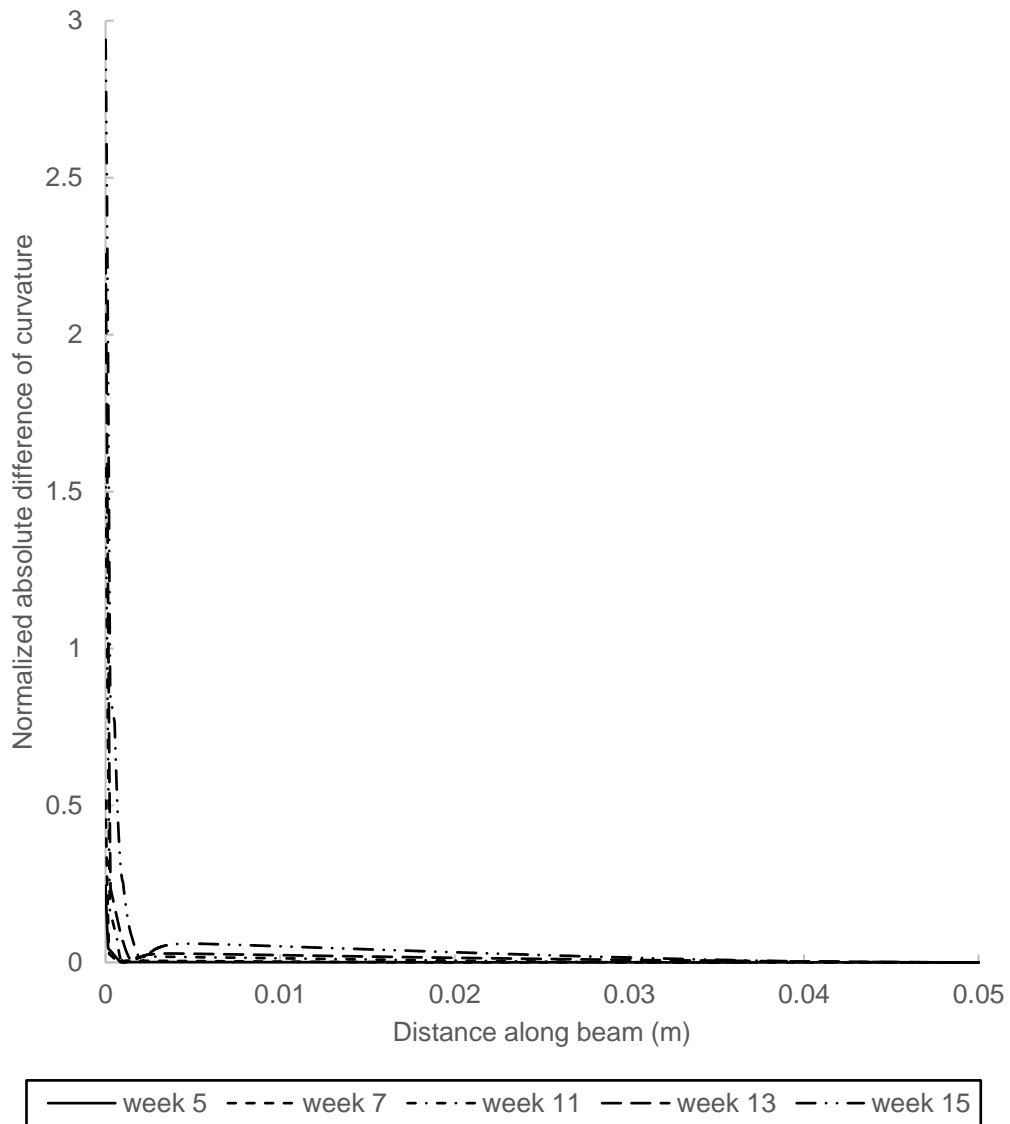


Figure 60: First mode shape of normalized absolute difference between the intact beam mode shape curvature (week 0) and degraded beam mode shape curvature at varies degradation times and when diffusion coefficient is $10^{(-22)}$.

Again, a maximum absolute curvature difference can be observed at the surface of the cube for every degradation time. The amplitude of the maximum difference increases with degradation. Furthermore, as the diffusion coefficient decreased to $10^{-22} \text{ m}^2/\text{s}$ the absolute curvature difference at the centre of the cube is limited. A thin layer with a thickness of about 0.002m starting from the surface of the cube can be clearly observed. Even though in Fig. 59(c) a surface layer could also be seen with a thickness of about 0.009m, the variation of absolute curvature difference toward the centre is still considerable. That is caused by the Young's modulus distribution along the beam following a slow reduction trend (see Fig. 58(d)). Back to Fig. 60, the limitation of the absolute curvature difference change indicated Young's modulus from cube centre is about constant. To sum up, when the diffusion coefficient decreases, the thickness of the surface thin layer decreases, and the variation of the absolute curvature difference at the centre of the cube decreases. However, the amplitude of the maximum absolute curvature difference, which is at the surface of the cube, increases. This phenomenon can be related to the autocatalytic hydrolysis mechanism.

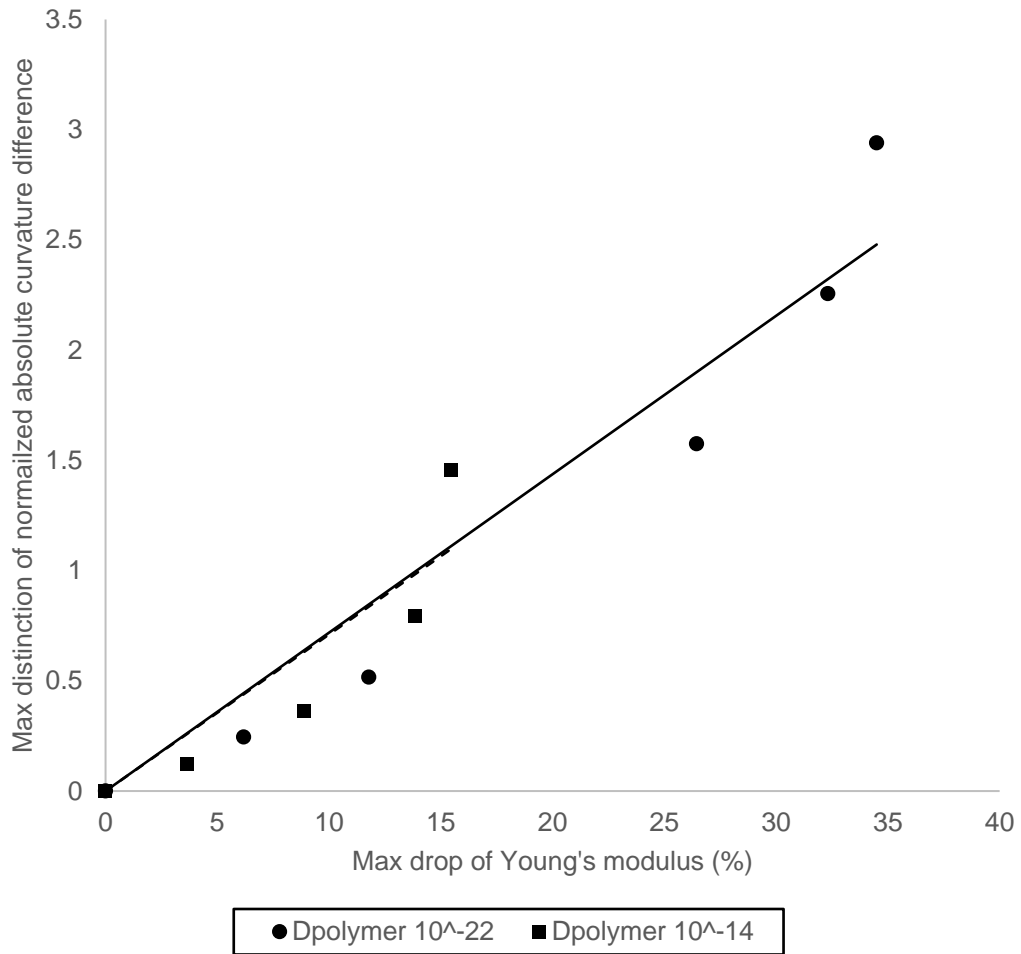


Figure 61: Max distinction of normalized absolute curvature difference against max percentage drop of Young's modulus from the surface to centre of the plate at different degradation times for diffusion coefficient taking as $10^{-14} \text{ m}^2/\text{s}$ and $10^{-22} \text{ m}^2/\text{s}$ respectively, dashed line and solid line are the best fitting straight lines for each set of data.

Fig. 61 shows the maximum distinction of normalised absolute curvature difference against maximum percentage drop of Young's modulus from the surface to the centre of the plate at different degradation times for diffusion coefficients taken as $10^{-14} \text{ m}^2/\text{s}$ and $10^{-22} \text{ m}^2/\text{s}$, respectively; dashed line and solid line are the best fitting straight lines for each set of data. It shows that, with a big diffusion coefficient, maximum surface and centre Young's modulus difference is relatively low. For example, when the diffusion coefficient is taken as $10^{-14} \text{ m}^2/\text{s}$, the maximum Young's modulus difference between the surface and the centre is just 15% of the initial Young's modulus when degradation ends. Whereas, when diffusion coefficient

is taken as $10^{-22} \text{ m}^2/\text{s}$, at the end of degradation the maximum Young's modulus difference between the surface and the centre is up to 35% of the initial Young's modulus. Following this trend, it can be assumed that an upper limit of diffusion coefficient is existing in which the surface and centre Young's modulus are the same. Therefore, if the thickness is kept the same, any increase of diffusion coefficient will decrease the level of non-uniform Young's modulus and decrease the level of non-uniform degradation, which is related to the level of autocatalytic hydrolysis reaction. Furthermore, it can be observed that the best straight fitting line for both sets of data in Fig. 61 has the same slope. Therefore, absolute curvature difference can also provide an indication of the level of autocatalytic hydrolysis reaction. For example, if by the end of the degradation the maximum normalised absolute curvature difference is small, less than 1, as seen in Fig. 61. The Young's modulus difference between the surface and the centre is low and indicates less autocatalytic hydrolysis reaction being carried out during the degradation, which then may be related to a big diffusion coefficient or a thin wall sample.

8.5 Conclusions

In this chapter, vibration analysis was used to detect degradation. It was proved that, from the absolute curvature difference, data detection and location degradation is possible. A large absolute curvature difference indicates less degradation. The beam element finite element method was suggested as a simplified method of solving the vibration analysis basis on its nature of easy use and could link the full Young's modulus distribution to its axial coordinate. In addition, the beam element method would save a lot of calculation time and computer memory. As a result, the beam element method can not only detect and locate degradation but can also indicate the stage of degradation by using the max amplitude of the absolute curvature difference. Using a cube as a unit of any biodegradable medical implants, local degradation detection was studied. A centre part of the cube was taken out and treated as a cantilever beam. Local degradation could be detected and located. The effect of different amorphous polymer diffusion coefficients was studied. A small diffusion coefficient will cause the device surface to form a thin wall. This thin wall contains high mechanical stiffness, whereas beyond this thin wall mechanical stiffness drops

hugely and keeps a constant low value until the centre of the device. When the diffusion coefficient decreases, the Young's modulus drop between the surface and the centre increases and the maximum amplitude of the absolute curvature difference increases. On the other hand, when the diffusion coefficient is big enough, there will be no Young's modulus drop between the surface of the device and the centre of the device. That is because very little autocatalytic hydrolysis reaction happens in the device, as oligomers diffuse out so quickly. Therefore, the absolute curvature difference through the device should be nearly constant.

Chapter 9: Major conclusion and future work

9.1 Conclusion

This thesis shows a newly development to the degradation mathematical model. Based on this new development, a full mathematical model that could capture the simulation of average molecular weight, degree of crystallinity, and Young's modulus for the same degradation was presented. Studies have been carried out to simplify the Young's modulus simulation during degradation and the method of degradation detection. Parametric study was used to help the user to better understand the mathematical model. Experimental suggestions have been made, which were proposed to help improve the degradation modelling. A break-down conclusion is listed below.

Chapter 4 compared the governing equations before and after adding the new development for the degradation of amorphous polymers. In the newly developed model, the carboxylic end groups on the short and long polymer chains are separated. Furthermore, seven analytical solutions were presented to show that the newly developed model can be reduced to the previous model in the literature. A parametric study was presented to understand the effect of the different parameters to degradation model. Suggested values were given to some of the parameters with the aim at letting end users with no modelling background knowledge have an easy start in using this degradation mathematical model. Suggested values are all given empirically and under the finding that the same set of degradation data can be achieved by many sets of parameters, i.e. non-uniqueness of the parameters. It has also been presented in this chapter that if oligomer production data can be experimentally measured, then there is a big change wherein α and β value can be found for a specific biodegradable polymer. An experimental suggestion has been made, which is if degradation for several thicknesses of the samples made of the same polymer under the same condition can be simultaneously experimentally measured then there is a big change in that a unique set of parameters can be found for that specific polymer.

Chapter 5 presented a list of governing equations for semi-crystalline polymers, including the crystallisation equation, oligomer diffusion equation, and their corresponding rate of chain scission equation. This chapter also presented a new development to the previous degradation model by abandoning the assumption of fast water diffusion. These equations are non-dimensionalised and used to solve and reproduce the degradation maps that were initially proposed by Wang, et al. (2008). The recalculation proved the validation of Wang's work, even though an over-simplified degradation model was used for the previous degradation map. Further studies of the degradation map also include the effect of other parameters, which widen the degradation map range to contain different shape samples.

Chapter 6 presented a possible designing method for biodegradable medical devices, which used the mathematical model presented in Chapter 5 to project degradation rate from one device to another, made of the same polymer and under the same manufacturing process. First of all, a set of experimental data for a medical device needed to be achieved. By using the mathematical model, the experimental data could be fitted probably by multiple sets of parameters. All these sets of parameters would then be inputted into the newly designed device, which has a different shape and different size but is assumed to have the same material and to be made under same manufacturing process. A range of degradation predictions can be calculated by the sets of parameters. It can be assumed that the actual degradation behaviour is located in the range that has been calculated. This will provide an indication for the designers before the actual experiment needs to be carried out. Additionally, in this chapter, it has been found that the effect of water diffusion should be added in for the medical devices that are thicker than a few millimetres, such as interference screw and some coronary stents. Water diffusing into the core area of such a device is not 'instant', and does delay the degradation rate. In fact, degradation with water diffusion could capture some of the experimental data of these devices better, as it could well capture the delay at the beginning of degradation. A storage condition has been assumed by using the water diffusion equations. This could provide an indication of how the storage condition could affect the use of biodegradable medical devices.

Chapter 7 simplified the previous Effective Cavity Theory and reduced the input needed to capture the Young's modulus change to only one, the radius of a unit's spherical effective cavity. The Effective Cavity Theory assumes that each scission produces a cavity that carries no mechanical strains and that each newly formed crystal acts as an inclusion surrounded by amorphous polymers. A numerical study has been used to provide a relationship between the rate of chain scission and the reduce of Young's modulus. For simplified method, the cavity is assumed to have the shape of a sphere and the newly formed crystal inclusion is in the shape of a cube. Combining the simplified Effective Cavity Theory with the degradation mechanical model that has been presented in Chapter 5, we can achieve a full model of the degradation of molecular weight, degree of crystallinity, and Young's modulus.

Chapter 8 simplified the degradation detection, presenting it by using a sample 1D beam element calculation, whereas the previous work developed by Samami and Pan (2016) used a solid element in their finite element model. Detection of degradation was proved possible by using mode shape analysis, which is a well-known method for damage detection in the engineering field. The maximum absolute difference between the degrading beam and the intact beam indicates degradation and its lactation. The amplitude of the absolute value could indicate the stage of the degradation. Change of the polymer diffusion coefficient could also influence the amplitude of the maximum absolute difference. However, the slope of the maximum absolute difference against the surface and centre Young's modulus change remains the same.

9.2 Further work

The degradation mathematical model has made of a lot of progress in recent years; it could now simulate the degradation to obtain molecular weight, mass loss, crystallinity, mechanical properties, and water diffusion. However, it is still in the early stages of design, because many important factors that influence the degradation have not yet been added, such as the degradation environment. Such a factor is too complicated and, therefore, continuous development and understanding of the degradation behaviour is required. The final goal, obviously, is to accurately capture the degradation behaviour

of any biodegradable medical device, and use the information to design such a device for different requirements. If we close our eyes and look to the future, mathematical modelling should be like this: the main users of such mathematical modelling tool would be surgeons, who will design the biodegradation medical device for each different individual to best suit the difference between the human discrepancies. Designing the tool would involve contact with a 3D printer, which would immediately print off the device that is needed. By using the 3D printer, the design could be in any shape to suit the requirement. This is, however, a preview for decades to come. The reality for current research work should be a step-by-step growth. Start from creating a more user-friendly mathematical model by not including so many parameters. In order to reduce and give fixed value to some parameters, an experimental method has been suggested in this chapter. So, in the future, when there are enough supporting experimental data, hopefully some parameters can be reduced.

One factor that is not easy for the current mathematical model to capture is weight loss. It is often found that high weight loss in the experimental data could not be simulated by the current model. There are two possibilities. 1) There are a lot of initial oligomers existing; with a high rate of polymer diffusion coefficient these pre-stored oligomers diffuse out of the device very quickly, causing a high weight loss at the very beginning of degradation, which has been observed from many experimental data. 2) Erosion of the surface, which causes the surface of the device to break into parts and fall piece by piece into the surrounding environment, especially the nano-crystals, which are packed and hard for water to diffuse into – they are assumed very likely to fall into the surrounding environment as a piece. This explains the certain weight loss increase in the middle or toward the end of some degradation, which has also been observed from experimental data.

The first point can be resolved by measuring the oligomer residents before any degradation experiments. The second point could not be captured by the current degradation mathematical model; new developments need to be carried out to study such a phenomenon. This is actually the next task of the Leicester group. Fortunately, there are many experimental data that could be used to verify the new development.

In this thesis, the non-uniqueness of parameters has been presented. This is caused by the lack of certain experimental data and also not fully understanding the effect of each parameter. The suggested value has been given to some of these parameters in order to help the end user have a quick start in using the mathematical model. However, the actual value could not be fixed. Therefore, further parameter study is necessary.

One aspect that was not available in computation modelling but draws a huge attention from the future research is how biodegradation polymer effect and interact with the living human tissue. The research on this is limited; one theory is that because a big number of oligomers diffusing out of the device into the surrounding environment will create an acidic environment, the surrounding tissue could have inflammation, which. There is a need to avoid any kind of surgery in this situation. Understanding this would have a big effect on the usage of such biodegradable polymers.

References

- Antheunis H, van der Meer J-C, de Geus M, Kingma W, Koning CE (2009). Improved Mathematical model for the Hydrolytic Degradation of Aliphatic Polyesters. *Macromolecules*, 42:2462-71.
- Avrami M (1939). Kinetics of phase change. I. General theory. *Journal of Chemical Physics*, 7(12):1103-1112.
- Avrami M (1940). Kinetics of phase change. II. Transformation-time relation for random distribution of nuclei. *Journal of Chemical Physics*, 8(2):212-224.
- Avrami, M (1941). Kinetics of phase change. III. Granulation, phase change, and microstructure'. *Journal of Chemical Physics*, 9(2):177-184.
- Batycky RP, Hanes J, Langer R, Edwards DA (1997). A theoretical model of erosion and macromolecular drug release from biodegrading microspheres. *Journal of Pharmaceutical Sciences*, 86:1464-77.
- Buchanan F, (2008) Degradation rate of bioresorbable materials: Prediction and evaluation. Woodhead Publishing Ltd, Chapter 1.
- Butany J, Carmichael K, Leong S, Collins M (2005). Coronary artery stents: identification and evaluation. *J. Clin. Pathol.*, 58:795-804.
- COMSOL, Plastic Deformation During the Expansion of a Biomedical Stent.
- Ding L, Davidchack R, Pan J (2011). A molecular dynamics study of Young's modulus change of semi-crystalline polymers during degradation by chain scissions. *Journal of the Mechanical Behaviour of Biomedical Materials*, 5:224-30.
- Doebing SW, Farrar CR, Prime MB, Shevitz DW (1996). Damage identification and health monitoring of structural and mechanical systems from changes in their vibration characteristics: a literature review. Las Alamos National Lab., NM (United States).
- Doebing SW, Farrar CR & Prime MB. A summary review of vibration based damage identification method.

- Duek E, Zavaglia C, Belangero W (1999). In vitro study of poly(lactic acid) pin degradation. *Polymer*, 40:6465-6473.
- Fan W, Qiao P (2011). Vibration-based damage identification methods: a review and comparative study. *Structural Health Monitoring*, 10:83-111.
- Gao P, Fagerness PE (1995). Diffusion in HPMC Cels. I. Determination of Drug and Water Diffusivity by pulsed-Field-Gradient Spin-Echo NMR. *Pharmaceutical Research*, 12(7):995-964.
- Gleadall A (2015). Modelling degradation of biodegradable polymers and their mechanical properties (PhD thesis). University of Leicester.
- Gleadall A, Pan J and Atkinson H (2012). A simplified theory of crystallisation induced by polymer chain scission for biodegradable polymers. *Polymer Degradation and Stability*, 97:1616-1620.
- Gleadall A, Pan J, Krufft M (2015). An atomic finite element model for biodegradable polymer. Part 2. A model for change in Young's modulus due to polymer chain scission. *Journal of the Mechanical Behaviour of Biomedical Materials*, 51:237-247.
- Gleadall A, Pan J, Krufft MA and Kellomake M (2014) Degradation mechanisms of bioresorbable polymers, Part 1: effects of random scission, end scission and autocatalysis. *Acta Biomaterial*, 10:2223-2232.
- Gomez-Lara J, Garcia-Garcia H.M, Onuma Y et al., (2010). A comparison of the conformability of everolimus-elution bioresorbable vascular scaffolds to metal platform coronary stents. *JACC: Cardiovasc. Interv.*, 3(11):1190-1198.
- Grizzi I, Garreau H, Li S, Vert M (1995). Hydrolytic degradation of devices based on poly [DL-lactic acid] size dependence. *Biomaterials*, 16:305-311.
- Han X and Pan J (2009). A model for simultaneous degradation and crystallization in biodegradable polymers. *Biomaterials*, 30:423-430
- Han X and Pan J (2011). Polymer chain scission, oligomer production and diffusion – a two scale model for degradation of bioresorbable polyesters. *Acta Biomaterialia* 7:538-547.

- Han X, (2011). Degradation Models for Polyesters and their composites: Chapter three, a multiscale model for polymer degradation, pp. 57
- Han X, Pan J (2009). A model for simultaneous crystallisation and biodegradation of biodegradable polymers. *Biomaterials*, 30:423-30.
- Han X, Pan J, Buchanan F, Weir N, Farrar D (2010). Analysis of degradation data of poly(l-lactide-co-l, d-lactide) and poly(l-lactide) obtained at elevated and physiological temperatures using mathematical models. *Acta Biomaterialia*, 6:3882-9.
- Han X, Pan J, Buchannan F, Weir N and Farrar D (2010). Analysis of degradation data of bioresorbable polymers obtained at elevated and physiological temperatures using mathematical models. *Acta Biomaterialia*, 6:3882-3889.
- Jingzhe Pan (2013), Chapter 4, Degradation of amorphous biodegradable polyesters – Modelling degradation of semi-crystalline biodegradable polyesters, edited by Jingzhe Pan, Woodhead Publishing Ltd, Cambridge, UK.
- Jingzhe Pan and Xinpu Chen (2013), Chapter 2, Degradation of amorphous biodegradable polyesters – the basic model, "Modelling Degradation of Bioresorbable and Polymeric Medical Devices", edited by Jingzhe Pan, Woodhead Publishing Ltd, Cambridge, UK.
- Jingzhe Pan and Xinpu Chen (2013), Chapter 3, Degradation of amorphous biodegradable polyesters – advanced models , "Modelling Degradation of Bioresorbable and Polymeric Medical Devices", edited by Jingzhe Pan, Woodhead Publishing Ltd, Cambridge, UK.
- Jingzhe Pan and Xinpu Chen (2013), Chapter 6, Degradation of amorphous biodegradable polyesters – Modelling heterogeneous degradation of polymeric devices due to short chain diffusion, edited by Jingzhe Pan, Woodhead Publishing Ltd, Cambridge, UK.
- Joshi A, Himmelstein KJ (1991). Dynamics of controlled release from bioerodible matrices. *Journal of Controlled Release*, 15:95-104.

- Karst D, Yang Y. (2006) Molecular modelling study of the resistance of PLA to hydrolysis based on the blending of PLLA and PDLA. *Polymer*, 47(13):4845-4850.
- Lam K, Nieuwenhuis P, Molenaar I, Esselbrugge H, Feijen J, Dijkstra P, Schakenraad J (1994). Biodegradation of porous versus non-porous poly(L-lactic acid) films. *J. Mater. Sci.-Mater. Med.*, 5:181-189.
- Li S, Vert M, In: Scott G, Gilead D, editors (1995). *Biodegradable Polymers, Principles & Applications*. London: Chapman and Hall, 43-87.
- Li SM, Tenon M, Garreau H, Braud C, Vert M (2000). Enzymatic degradation of stereocopolymers derived from L-, DL- and meso-lactides. *Polymer Degradation and Stability*, 67(1):85-90.
- Lobodzinski S (2008). Bioabsorbable coronary stents. *Cardiol. J.*, 15:569-571.
- Lyu S, Schley J, Loy B, Lind D, Hobot C, Sparer R, et al (2007). Kinetics and time-Temperature Equivalence of Polymer Degradation. *Biomacromolecules*, 8:2301-10.
- Miller RA, Brady JM, Cutright DE. (1997). Degradation rates of oral resorbable implants (polylactates and polyglycolates): Rate modification with changes in PLA/PGA copolymer ratios. *Journal of Biomedical Materials Research*, 11(5):711-719.
- O'brien B, Carroll W (2009). The evolution of cardiovascular stent materials and surfaces in response to clinical drivers: a review. *Acta Biomater.*, 5:945-958.
- Omiston J.A, Serruys P.W (2009). Bioabsorbable coronary stents. *Circ. Cardiovasc. Interv.*, 2:255-260.
- Pandey AK, Biswas M, Samman MM (1991). Damage detection from changes in curvature mode shapes. *Journal of Sound and Vibration*, 145:321-332.
- Peral G, Arosio P, Moscatelli D (2009). A new model of resorbable device degradation and drug release: Transient 1-dimension diffusion model. *Journal of Controlled Release*, 136:196-205.

- Pitt CG, Chasalow F, Hibionada Y, Klimas D, Schindler A (1981). Aliphatic polyesters. I. the degradation of poly(ϵ -caprolactone) in vivo. *JAppl Polym Sci*, 26:2279-87.
- Pitt CG, Gratzl MM, Kimmel GL, Surles J, Schindler A (1981). Aliphatic polymers II. The degradation of poly(DL-lactide), poly(ϵ -caprolactone), and their copolymers in vivo. *Biomaterials*, 2:215-20.
- Pitt CG, Zhong-wei G (1987). Modification of the rates of chain cleavage of poly(ϵ -caprolactone) and related polyesters on the solid state. *Journal of Controlled Release*, 4:283-92.
- Salawu O (1997). Detection of structural damage through changes in frequency: a review. *Engineering Structure*, 19:718-723.
- Samami H, Pan J (2016). A constitutive law for degrading bioresorbable polymers. *Mechanical Behaviour of Biomedical Materials*.
- Samami H, Pan J (2016). Detection degradation in degrading polymeric implants using dynamic analysis.
- Schwach G, Vert M (1998). In vitro and in vivo degradation of lactic acid-based interference screws used in cruciate ligament reconstruction. *Biological Macromolecules*, 25:283-291.
- Siparsky GL, Voorhees KJ, Miao F (1998). Hydrolysis of polylactic acid (PLA) polycaprolactone (PLC) in aqueous acetonitrile solutions: Autocatalysis. *Journal of Environmental Polymer degradation*, 6:31-41.
- Tsuji H, Mizuno A, Ikada Y (2000). Properties and morphology of poly(L-lactide). III. Effects of initial crystallinity on long-term in vitro hydrolysis of high molecular weight poly(L-lactide) film in phosphate-buffered solution. *J. Appl. Polym. Sci.* 77:1452-1464.
- Tsuji H, Muramatsu H (2001). Blends of aliphatic polyesters: V Non-enzymatic and enzymatic hydrolysis of blends from hydrophobic poly(L-lactide) and hydrophilic poly(vinyl alcohol). *Polymer Degradation and stability*, 71:403-413

- Wang Y, Han X, Pan J, Sinka C (2010). An entropy spring model for the Young's modulus change of biodegradable polymers during biodegradation. *J. Mech. Behav. Biomed. Mater.* 3:14-21.
- Wang Y, Pan J, Han X, Sinka C, Ding L (2008). A phenomenological model for the degradation of biodegradable polymers. *Biomaterials*, 29:3393-401.
- Weir N, Buchanan F, Orr J, Dickson G (2004). Degradation of poly-L-lactide. Part 1: In vitro and in vivo physiological temperature degradation. *Proc. Inst. Mech. Eng. Part H J. Eng. Med.* 218:307-319.
- Yang A.S, Jow K, Morrison A.D, Limon T.A (2013). Polymeric stent. Google Patents.
- Yuen MM (1985). A numerical study of the eigenparameters of a damaged cantilever. *Journal of Sound and Vibration*, 103:301-310.

Appendix

The C++ programme

```
#include <stdio.h> #include <math.h> #include <stdlib.h>    //(call C++ libraries)
double function_of_Rs_bar(double, double, double, double, double, double, double);
double calculate_Mn_bar(double, double);
//(give function prototype of two subroutines function_of_Rs_bar and calculate_Mn_bar, which will
be used afterwards to calculate  $f(\overline{R_s})$  and  $\overline{M_n}$  respectively.)
int main ()      //(set main function)
{  double t=0.0, delta_t=0.0; //(arguments)
  double k1, k2_bar, n, alpha, beta, m, Rs_bar_Max, Ce0, Cchain0;
  int N;
  printf("Input initial m value: "); scanf("%lf", &m);
  printf("Input Rs_bar_Max: "); scanf("%lf", &Rs_bar_Max);
  printf("Input number N: "); scanf("%d", &N);
  printf("Input parameters, n: "); scanf("%lf", &n);
  printf("Input parameters, alpha: "); scanf("%lf", &alpha);
  printf("Input parameters, bata: "); scanf("%lf", &beta);
  printf("Input parameters, k1: "); scanf("%lf", &k1);
  printf("Input parameters, k2_bar: "); scanf("%lf", &k2_bar);
  printf("Input parameters, Ce0: "); scanf("%lf", &Ce0);
  printf("Input parameters, Cchain0: "); scanf("%lf", &Cchain0);
  double Ndp0;
  int read_data;
  Ndp0=Ce0/Cchain0;      //(calculate Ndp0.)
  read_data=N/5000;     //(select maximum 5000 sets of data)
  FILE *output; output = fopen("output.txt", "w"); //(open file "output")
  double Rs_bar=0.0, Rol_bar=0.0, Mn_bar=1.0; //(set initial value for outputs)
  int count=0;          //(set initial value of count.)
  double f_Rs_bar =0.0; //(use to call function_of_Rs_bar later)
  fprintf(output, " t  \tRs_bar  \tMn_bar  \tRol_bar\n"); //(print out the title of outputs in file)
  while (Rs_bar<=Rs_bar_Max) //(set up a while loop to do the reporting calculation)
  {  if (t==0) fprintf(output, "%.8lf  \t%.8lf  \t%.8lf  \t%.8lf\n", t, Rs_bar, Mn_bar, Rol_bar);
  //(print out initial output values in file)
  if (count == read_data) //(write data to file)
  {  fprintf(output, "%.8lf  \t%.8lf  \t%.8lf  \t%.8lf\n", t, Rs_bar, Mn_bar, Rol_bar);
  count = 0; }
  else { count = count+1; }
```

```

f_Rs_bar= function_of_Rs_bar(alpha, beta, k1, k2_bar, Ndp0, Rs_bar, n);
//(call subroutine function_of_Rs_bar)
delta_t = (Rs_bar_Max/N)/f_Rs_bar;      //(calculat delta_t)
t = t+delta_t;          //(update time t)
Rs_bar=Rs_bar+f_of_Rs_bar*delta_t;      //(calculate Rs_bar using equation (2.34))
Rol_bar=alpha*pow(Rs_bar, beta);    //(calculate Rol_bar using equation (2.9))
Mn_bar=calculate_Mn_bar(Ndp0, Rs_bar); //(call subroutine ) calculate_Mn_bar to calculate
Mn_bar
    if (Mn_bar<0.1) break;  }
fclose(output);          //(close file "output")
system ("pause");      }

double function_of_Rs_bar(double alpha, double beta, double k1, double k2_bar, double Ndp0,
double Rs_bar, double n)
{
    return (1-alpha*pow(Rs_bar, beta))*(k1+k2_bar*pow((1/Ndp0+Rs_bar),n));
}      //(a subroutine to calculate  $f(R_s)$  use equation (2.15))

double calculate_Mn_bar(double Ndp0, double Rs_bar)
{
    return 1/(1+Ndp0*Rs_bar);
}      //(a subroutine to calculate  $M_n$  use equation (2.18))

```